Par **Hongliang LIU**

Contribution for integrating urban wind turbine into electrical microgrid: modeling and control

Thèse présentée
pour l'obtention du grade
de Docteur de l'UTC

Soutenue le 27 janvier 2017
Spécialité : Génie Électrique : Laboratoire Avenues - GSU (EA-7284)

D2331

UNIVERSITE DE TECHNOLOGIE DE COMPIEGNE

THESE

Pour obtenir le grade de

DOCTEUR

Spécialité : Génie Electrique

Par

Hongliang LIU

Contribution for integrating urban wind turbine into electrical microgrid: modeling and control

Laboratoire AVENUES, EA 7284

Soutenue le 27 janvier 2017 devant le jury composé de :

Rapporteurs :	Raphaël ROMARY	LSEE, Béthune
	Christophe SAUDEMONT	L2EP, Lille
Examinateurs :	Franck BETIN	LTI, Amiens
	Christine PRELLE	ROBERVAL, Compiègne
Directeurs de thèse :	Fabrice LOCMENT	AVENUES, Compiègne
	Manuela SECHILARIU	AVENUES, Compiègne

Abstract

The integration of the wind power, which is one mostly used renewable resource, is always one challenger for urban microgrid. In this thesis, one urban wind turbine based on a permanent magnet synchronous machine (PMSM) is studied in order to be integrated into a DC urban microgrid. A state of the art concerning the renewable energies, DC microgrid, and control strategies of wind power generation is done.

Based on a model of urban wind turbine fitting the demand of urban electric system, which consists of an emulator of wind speed and blades, a PMSM and a DC/DC converter, this thesis proposes the maximum power point tracking (MPPT) methods satisfying the requirement of producing energy as much as possible, and power limited control (PLC) strategies answering the demand of flexible energy production. From simple to complex, four MPPT algorithms including Perturbation and Observation (P&O) fixed step-size method, P&O with improved Newton-Raphson method, P&O with fuzzy logic method and lookup table method are studied and implemented to be compared with each other using three wind velocity profiles. According to the experience about MPPT subject, four PLC algorithms are introduced and implemented to be analyzed and compared with each other with one power demand profile calculated randomly.

Summarizing all experimental results, the lookup table method can handle all requirement of MPPT operating mode supplying the best performance, however, in the condition of more flexible power demand operating mode, the combination of P&O and fuzzy logic method presents the best performance and potential which can be achieved in future works.

Key words

Wind power generation, DC microgrid, urban wind turbine, permanent magnets synchronous machine (PMSM), Maximum power point tracking (MPPT), Power limited control (PLC).

Résumé

L’intégration de l’énergie éolienne, qui est une ressource renouvelable très utilisée, n’est pas toujours facile pour le micro-réseau urbain. Dans cette thèse, une éolienne urbaine basée sur une machine synchrone à aimants permanents (MSAP) est étudiée pour être intégrée dans un micro-réseau urbain à courant continu. Un état de l'art concernant les énergies renouvelables, les micro-réseaux à courant continu et les stratégies de contrôle de la production d'énergie éolienne, est réalisée.

Basé sur un modèle d’éolienne urbaine répondant à la demande du système électrique, qui se compose d’un émulateur de vent et de pales, un MSAP et un convertisseur DC/DC, cette thèse propose des méthodes de poursuite du point de puissance maximale satisfaisant à l’obligation de produire de l’énergie dans la mesure du possible. Une stratégie de contrôle à puissance limitée répond correctement.

De simples à complexes, quatre algorithmes MPPT, P&O à pas fixe, P&O à pas variable avec la méthode Newton-Raphson améliorée, P&O à pas variable à base de logique floue et une méthode indirecte de type *lookup table*, sont étudiés et implémentés pour être comparés à l’aide de trois profils de vitesse du vent.

Par expérimentation, les algorithmes MPPT et PLC sont comparés, analysés et discutés.

Résumant tous les résultats expérimentaux, la méthode *lookup table* peut gérer toutes les exigences du mode de fonctionnement MPPT en présentant la meilleure performance, mais, dans le mode de fonctionnement PLC, la P&O à base de logique floue présente les meilleures performances.

Mots-clé

Production éolienne, micro-réseau DC, éolienne urbaine, machine synchrone à aimants permanents (MSAP), suivi du point de puissance maximale, commande en puissance limitée.

Acknowledgments

First of all, I would like to express my sincere gratitude to my supervisors, Dr. Fabrice LOCMENT and Dr. Manuela SECHILARIU, for the good guidance and great efforts throughout the research and the writing of the thesis. Thanks to this teamwork and their well-organized working mode, this thesis has advanced well according planning, which has permitted the thesis work can be published in each phase of progressing.

I also express my very gratitude to Professor Raphaël ROMARY and Professor Christophe SAUDEMONT, who have made detailed reports and remarks on my thesis, which helps a lot in improving the quality of my thesis for both research content and presentation. Thanks also to Professor Franck BETIN, chairman of the thesis committee, and Professor Christine PRELLE for their interest in my work.

In addition, I would like to thank all colleagues of the laboratory AVENUES for the good ambiance during my PhD studies in France.

I also thank my friends from the different countries in AVENUS: Hossam AL-GHOSSINI, Leonardo TRIGUEIRO DOS SANTOS, Walid BOUCHENAFA, Hongwei WU, Changjie YIN and Raphael ROLIN for sharing the PhD and life experience, for discussions on culture and customs, as well as on the study.

I would like to thank my friends Wenxiang ZHANG, Hongjuan BAI, Yongjiang LI, Liqi SUI and Kang YANG for their help during the PhD studies. I would like to thank the China Scholarship Council for offering the opportunity to support my PhD study in France. I will treasure the experiences both academic and personal in my life.

Finally, a special bunch of thanks goes to Miss Yun CAI and my mother for their love and encouragement to support me in finishing the PhD studies.

Table of contents

Figure List

Table List

Abbreviations

WT	Wind turbine
PV	Photovoltaic
AC	Alternating current
DC	Direct current
MPPT	Maximum power point tracking
PLC	Power limited control
HAWT	Horizontal axis wind turbine
TSR	Tip speed ratio
P&O-F	Perturbation and observation method with fixed step-size
P&O-INR	Perturbation and observation method with variable step-size calculated by improved Newton-Raphson method
P&O-FL	Perturbation and observation method with variable step-size calculated by fuzzy logic method
LT	Lookup table method
P&O	Perturbation and observation
HCS	Hill-climb searching
MPP	Maximum power point
OT	Optimal torque method
PSF	Power signal feedback method
MPSO	Modified particle swarm optimization
PSO	Particle swarm optimization
PI	Proportional integral
PMSM	Permanent magnet synchronous motor
IGBT	Insulated gate bipolar transistor
PEL	Programmable electronic load

Nomenclature

λ	Tip speed ration
v	Wind speed
ω	Rotational speed
c_p	Power co-efficient
R	Blade radius
p_{AERO}	Harvested aerodynamic power
ρ	Air density
V_{cut-in}	Cut-in speed of wind turbine
$V_{cut-out}$	Cut-out speed of wind turbine
V_{rated}	Rated speed of wind turbine
ω^*	Optimal rotational speed
$d(k)$	Duty cycle of the converter
α	Coefficient of variable perturbation in ref
k	Perturbation step
$u(k)$	Electrical voltage
$p(k)$	Electrical power
$\Delta p(k)$	Change of electrical power
$\Delta u(k)$	Change of electrical voltage
$slope(k)$	Ratio between the change of electrical power and the change of voltage
$\Delta slope(k)$	Change of $slope(k)$
Δu	Perturbation step-size
$u_{ref}(k)$	Reference of electrical voltage
λ_{opt}	Optimal tip speed ratio
c_{p-opt}	Optimal power co-efficient

ω_{opt}	Optimal rotational speed
$p_{AERO-opt}$	Optimal aerodynamic power
K_{opt}	Integrated optimal coefficient
T_{opt}	Optimal torque
p_{li}	Demanded power value for power limited control
p_{diff}	Difference between the actual and demanded power
$\lvert p_{diff} \rvert$	Absolute value of p_{diff}
$\lvert slope \rvert$	Absolute value of $slope$
α_K	Polynomial parameters of coefficient c_p
J	Equivalent inertia of blades and hub
F	Viscous damping coefficient
P_{EM}	Electromagnetic power
u_A, u_B, u_C	Three-phase voltages
i_A, i_B, i_C	Three-phase currents
C_{BUS}	Capacitor at DC BUS
L	Inductor at DC BUS
C_{PEL}	Capacitor to emulate the power demand
u_{PEL}	Output voltage
p_{BUS}	Electrical DC BUS power of experimental platform
u_{BUS}	Electrical DC BUS voltage of experimental platform
i_{BUS}	Electrical DC BUS current of experimental platform
u_{BUS}^*	Reference of DC BUS voltage of experimental platform
n	Rotational speed using the unit rpm
p_{BUS}^*	Potential electrical power for experimental test validating P&O-INR method
p_{BUS-F}	Experimental electrical power for P&O-F method in experimental test validating P&O-INR method

p_{BUS-V}	Experimental electrical power for classic P&O variable step-size method calculated by Newton-Raphson method in experimental test validating P&O-INR method
P_{BUS-V1}	Experimental electrical power for classic P&O variable step-size method calculated by Newton-Raphson method with a "kick It Out" trigger in experimental test validating P&O-INR method
$P_{BUS-Vart}$	Experimental electrical power for P&O-INR method in experimental test validating P&O-INR method
K_p	Gain for normalizing power input of fuzzy logic
K_u	Gain for normalizing voltage input of fuzzy logic
K_S	Gain for anti-normalizing output of fuzzy logic
p_{BUS-p}	Potential electrical power in comparative experimental tests
P_{BUS-f}	Electrical power for P&O-F in comparative experimental tests
P_{BUS-v}	Electrical power for P&O-INR in comparative experimental tests
$P_{BUS-lf-}$	Electrical power for P&O-FL in comparative experimental tests
P_{BUS-lt}	Electrical power for LT in comparative experimental tests
u_{BUS-p}	Potential electrical voltage in comparative experimental tests
u_{BUS-f}	Electrical voltage for P&O-F in comparative experimental tests
u_{BUS-v}	Electrical voltage for P&O-INR in comparative experimental tests
$u_{BUS-lf-}$	Electrical voltage for P&O-FL in comparative experimental tests
u_{BUS-lt}	Electrical voltage for LT in comparative experimental tests
Δu_{-f}	Actual perturbation step-size of P&O-F in comparative experimental tests
Δu_{-v}	Actual perturbation step-size of P&O-INR in comparative experimental tests
Δu_{-lf-}	Actual perturbation step-size of P&O-FL in comparative experimental tests
n_{-p}	Potential rotational speed in comparative experimental tests
n_{-f}	Rotational speed for P&O-F in comparative experimental tests
n_{-v}	Rotational speed for P&O-INR in comparative experimental tests

$n_{\_lf\_}$	Rotational speed for P&O-FL in comparative experimental tests
$n_{\_lt}$	Rotational speed for LT in comparative experimental tests
K_1	Gain for normalizing the first input of fuzzy logic for PLC condition
K_2	Gain for normalizing the second input of fuzzy logic for PLC condition

Publications associated with this PhD thesis

The works presented in thesis are validated by several publications which have been accepted or submitted in journals and conferences. The details of them are listed as below:

Article in international refereed journal:

H. Liu, F. Locment, and M. Sechilariu. "Experimental analysis of impact of Maximum Power Point Tracking methods on energy efficiency for small-scale wind energy conversion system." IET Renewable Power Generation, 2016.

Article in the process of submission for international refereed journal:

H. Liu, F. Locment, and M. Sechilariu. "Integrated power control method for small scale wind generator." Renewable Energy, 2017.

Articles in proceedings at international conferences:

H. Liu, F. Locment and M. Sechilariu, "Maximum power point tracking method for small scale wind generator experimental validation." 2015 54th Annual Conference of the Society of Instrument and Control Engineers of Japan (SICE), China, pp. 864-869, 2015.

H. Al-Ghossini, H. Liu, F. Locment, and M. Sechilariu. "Estimation of speed rotation for MPPT used by small scale wind generator integrated in DC microgrid experimental validation." In IECON 2014-40th Annual Conference of the IEEE Industrial Electronics Society, USA, pp. 2082-2088. IEEE, 2014.

General introduction

In recent decades, the research and the implementation of the renewable energy sources have increased since the traditional fuel utilization has reduced. This pressure for a clean and environmental friendly energy, along with the liberalized electricity market, demands efficient, reliable and diversified energy sources [1]. Renewable energy sources such as the wind turbine (WT), photovoltaic (PV) panel and biomass have received more and more attention inasmuch as its high efficiency, reliability, easy installation, less environmental impact and political factors [1]. Thus, the energy transition is an important concern in the various strata of society in near future to almost the entire world. Human beings' activities, such as industry, lighting, transport, etc. will be more and more powered by renewable energy sources.

Highlighted by the World Energy Council, providing the sustainable energy policies, the three following dimensions are important to be considered: the energy security; the energy equity and the environmental sustainability. Today, the utility power grid is confronting the requirements about high reliability, low costs, high efficiency, integration of renewable energy sources and electric vehicles into power grid. Producing more and more energy from renewable sources like wind, solar, biomass and geothermal sources is the priority of electricity production. But, integration of power from renewable resources into the utility power grid is a huge challenge while it is one huge opportunity. Even though the application of the decentralized electricity generation, for which the commonly use of renewable energy sources is widely spreading, the intermittent and random production of renewable sources is still an issue for public power grid that is unable to bypass. The power quality of the wind or solar source is influenced by their seasonal and unpredictable nature, including the problem of fluctuations of voltage and/or frequency, harmonic pollution, etc.

Facing the environmental challenges, urban areas are key players to achieve the energy transition given their strong potential of intensive development of renewable sources. The main strategy is to find solutions reducing energy consumption and increasing the share of renewable resources, while reducing the environmental impact of existing and future urban areas. It means that the urban areas are going to have more authority to manipulate the distribution of energy as well as the production. Thus, many projects are launched for creating positive energy buildings and territories achieving the balance between consumption and production of energy at the local scale.

1. Decentralized electricity production

Recently, the distributed energy generation system presents a rapid growth and reveals an increasing complexity for grid managers. This distributed generation requires grid management and the consumption must be optimized. Renewable energy sources are simple to realize distributed generation, that is the reason why renewable energy generation leads to new path for balancing of production and consumption, especially for large scale implementation.

What is the best power grid technical regulation to integrate renewable energy to accommodate the utility grid in real time? Centralized regulation? Local regulation? Or both? To make full use of distributed generation, requirements from both utility grid and terminal user and the communication among them are must to be considered. This demand results in the appearance of smart grid, which is a power grid fulfilled by communication and information technology. Becoming a 'smart grid', the problem of peak consumption, optimal energy and demand response should be solved to increase the integration level of renewable energy sources and its own robustness. The smart grid has high level of surveillance about bidirectional power and information flows, providing flexible option to terminal users and better services to electricity producers and distributors. Aiming to reduce power losses and peak energy demand, supplying ancillary services, smart grid leads to the concept of microgrid. The definition of a microgrid is a set of renewable and traditional sources, storage, utility grid connection and controllable loads. Microgrid is more suitable to manage and optimize local energy sources respecting the requirement of utility grid. It can better deal with the power grid and terminal users and improve the reliability of power supply.

The main research issues on microgrid include following aspects: power converter (components, topology, and power quality), power balancing (droop control), protection, and energy management. The main challenge is the energy management. There are two kinds of energy management approaches. The rule based approach, built on sets of logic rules, is robust but cannot guarantee the optimal performance for any condition. The second approach is the optimization based on advanced control tools. However, implementing this optimization approach is hard in real-time condition. Usually, optimization methods involve prediction of environment variables, which naturally has bias degrading operation even leading failure. For assuring safety, the microgrid has to introduce bidirectional power flow and flexible structure. Thus, new protection device or method are demanded to deal with this complex environment. In a word, ensuring reliable distribution of electricity based on microgrid, it is not easy to integrate itself into centralized large production of the power grid.

2. *Microgrid research project of AVENUES EA 7284*

Our laboratory has been working for more than eight years on the urban micro grid as the main body of the advanced local energy management and smart grid communications. The focus of our research project is to design a micro grid control strategy to optimize the local area of energy demand, based on local information, and can participate in the global smart grid interaction through communication. The smart grid topology presented in Figure 1 shows the vision of the smart grid concept and the role of microgrid, using general concepts.

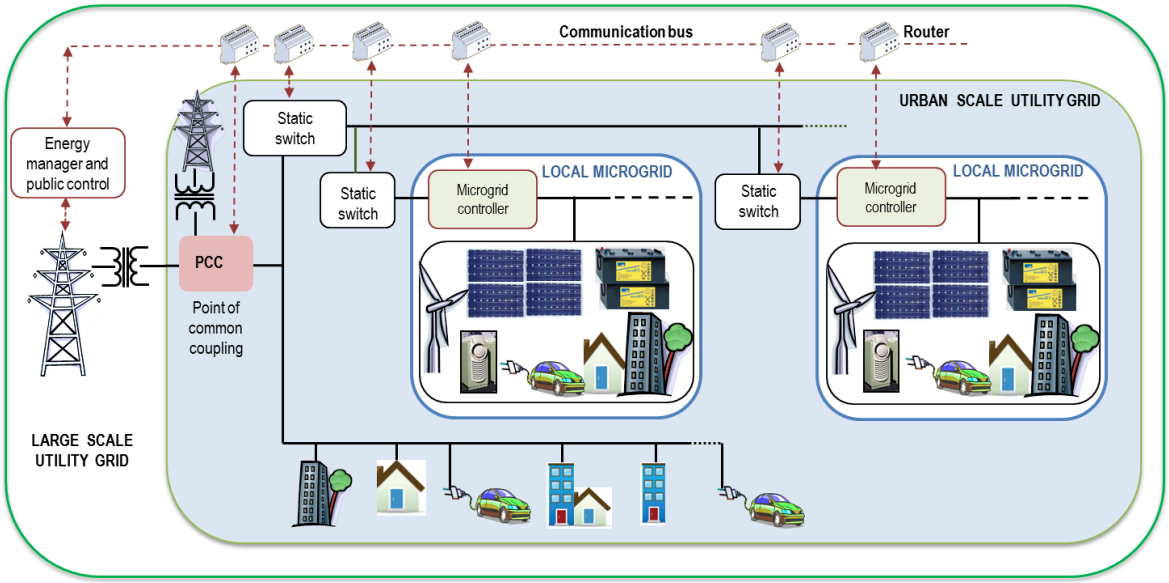

Figure 1: Smart grid topology [2].

The microgrid can be integrated into a city's infrastructure at the local level, and is connected to the main power grid through a dedicated adaptive controller. At urban scale, there are several microgrids and parts of traditional utility grid connected together to the grid through common connection point. Microgrid is allowed to be connected and isolated by intelligent switches.

The urban microgrid developed by AVENUES laboratory is connected to the smart grid by a controller which must supply the interface between the utility grid and the loads, in order to realize an optimal power management. Figure 2 displays the principle of power management interface using the main data exchanged between the microgrid and the utility grid.

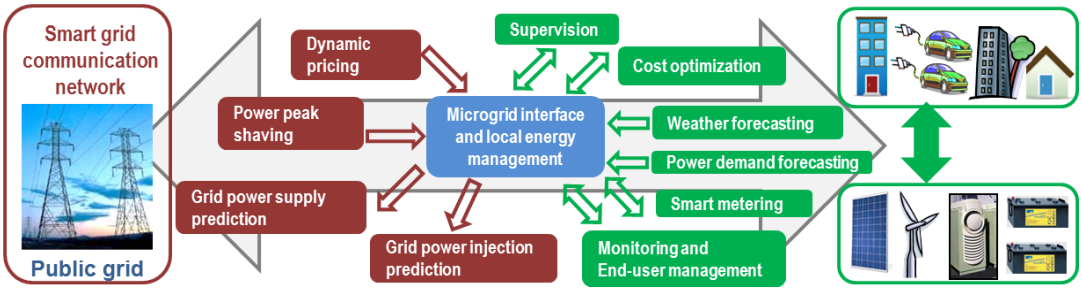

Figure 2: Power management interface principle [3].

The microgrid controller must collect information about the availability and dynamic pricing of the public grid, must send information about the smart grid on injection intentions and power demand forecast, match the terminal users' requirements under all physical and technical limits, and operate at the condition with the lowest energy costs. The specific interface associated with the urban microgrid [3] aiming to meet those objectives, was designed as given in Figure 3.

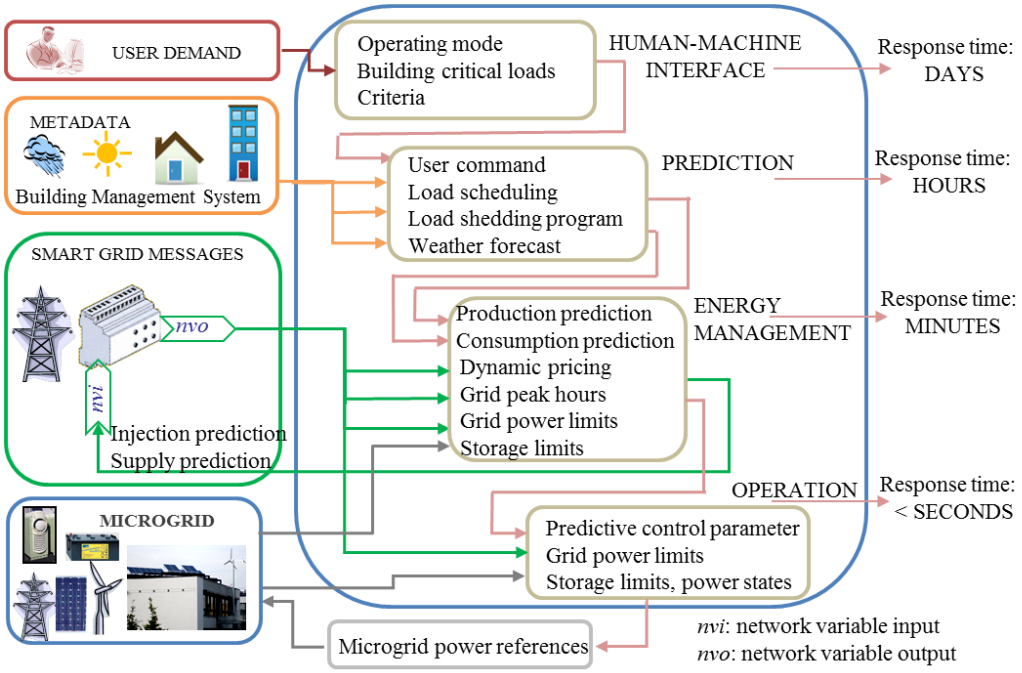

Figure 3: Microgrid controller [3].

The microgrid controller designed by AVENUES laboratory is a multilayer and multiscale design able to provide flexibility with the necessary algorithms [4]. It can be sorted into four layers, the operating time scale of which is different and ranges from days to less than seconds.

Human-machine interface allow counting the terminal users' options or building critical loads, or load shedding limits, or other specific criteria.

Prediction layer considers the terminal users' options, forecast data for several variables and calculated two power variables: the predictions of renewable energy production and the energy demand.

The optimization of energy costs is calculated in the energy management layer given two power variables mentioned above. According to the previously calculated predictions and the operating constraints such dynamic pricing, storage capacity, etc., the optimization is solved by mixed integer linear programming and the used solver is CPLEX [4]. The main challenge in scientific point of view are the difficulties of global optimization, due to the error introduced by the mismatch between predictions and the real time operating conditions, and the limitation resulted from the constraints imposed by the utility grid. This layer is the most important intelligent layer.

For urban microgrids, several operating strategies are developed based on its resources, such as photovoltaic, wind turbine, storage, public grid connection, micro-turbine or biodiesel generator, and loads. Figure 4 presents the main possible strategies.

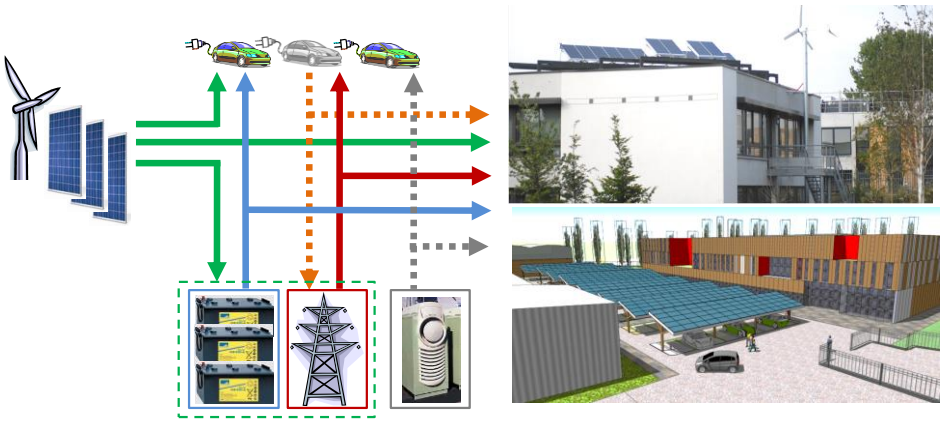

Figure 4: Energy management strategies for urban microgrid [2].

Renewable sources supply the consumption of building and charge the electric vehicles. Extra energy could be stored in storage or injected into the utility grid. However, the utility grid is regarded as the back-up source for the building and electric vehicles, if it is available. Since the utility grid is not available and there is any lack of power, the micro-turbine works. Information given by the smart grid commands the microgrid working mode, in order to compliance the actual availability of the utility grid.

3. *Small scale wind turbine integration in urban DC microgrid*

Focusing on the wind generation system, the appliances generally are sorted by the productivity of power, into the large, medium and small scales [5]. Comparing with large wind generation system, which is widely used for wind farm, the medium and small scale wind turbine can be implemented in more flexible environment, especially small scale wind turbine system which is commonly used in urban distributed energy system. Using different electrical conversion structures, the small scale wind turbine, which is our research interest, can supply alternating current (AC) or direct current (DC) loads.

In the urban microgrid environment developed by AVENUES laboratory, presented in Figure 5, all elements are coupled on the same DC bus. It can operate in the grid-connected mode and in isolated mode.

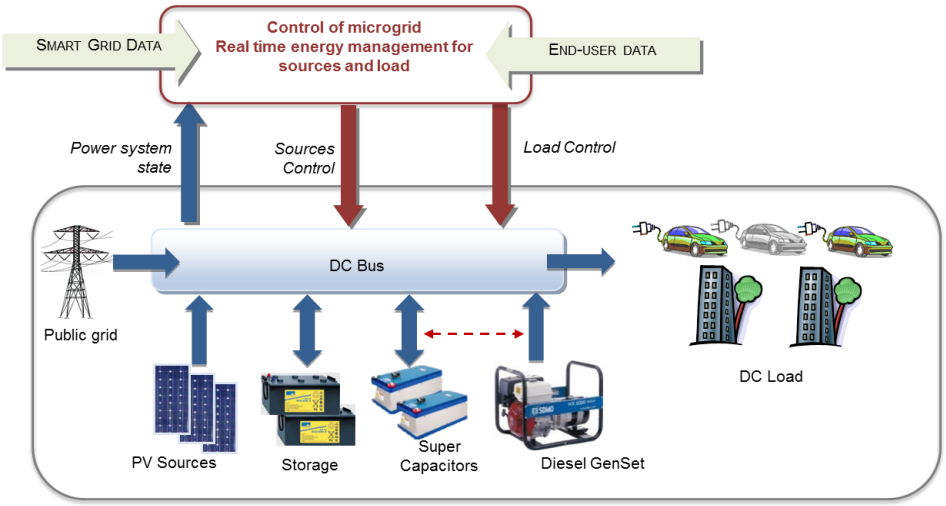

Figure 5: DC microgrid overview [3].

This microgrid used the DC bus link efficiently integrating renewable sources and storage. Since, there isn't the problem of phase synchronization which is related with AC bus, and there is only one control objective, voltage at DC bus, the overall performance can be improved by removing multiple energy conversions [6]. The DC bus can directly supply almost main part of building appliances, for example lighting, ventilation and air conditioning, office devices, etc., with less power losses. The microgrids research project of AVENUES laboratory considers a small-scale wind generator that has to be integrated to the described DC microgrid. Comparing with PV sources, the small-scale wind generator is seen as a complementary renewable energy source. However, the energy potential and dynamic characteristics of the wind generator are very different from PV generators.

4. *Main objectives of the thesis*

Being different from wind farm, wind resource in urban environment is intermittent and influenced by the season and the spatial structure of the installation location. According to the fact that wind power urban DC microgrid integrated is usually consumed at the place of production, it askes a more flexible power control strategy to deal with the user requirements which cannot be completely forecasted before the installation. Theoretically, wind turbine might be demanded to extract as much power as possible following the variation of wind velocity, or to product the demanded power value following the variation of user's requirements. Otherwise, the switching effect between these two power control strategies influences the power quality and safety of electrical system. To meet these requirements, the study of the integration of small scale wind turbine into electric urban microgrid system is proposed in this thesis.

This thesis is expected to reach the following achievements:

-Modeling a small scale wind turbine system consisting of the generator, the electrical conversion structure and wind and blades emulator using Matlab®/Simulink® model. Aiming to study small scale wind turbines in urban areas, a mathematics model of wind and blades indicating 1 kW rated power was chosen to be implemented in Matlab®/Simulink®. According to advantages and disadvantages of different kinds of used generator, the Permanent Magnet Synchronous Machine (PMSM) stands out from among the double-fed asynchronous machine and the asynchronous machine with squirrel cage. With respect to conversion mechanical energy in to the electrical form for small scale wind generator, the passive structure, *i.e.* non-controllable convertor and the active structure with controllable convertor are probably used. Even though the passive structure has the advantages of robustness and attractive price, the energy flow cannot be optimized. The active structure allows this energy optimization. Due to less financial cost and energy loss, the active structure of the diode bridge and one chopper was implemented to realize the proposed power control strategies. Based on this platform, several experiments were introduced to reveal the steady-state and dynamic characteristics of the studied small scale wind energy conversion system, in order to make a contribution for application of power control strategies.

-Implementing maximum power point tracking (MPPT) algorithms including different types and advanced control methods, to extract power as much as possible; then exploring and comparing characteristics of those proposed MPPT algorithms in the modeled experimental platform. Aiming to extract the power from air flow as much as possible, four MPPT methods were studied and installed in our platform. Three direct MPPT methods based on perturbation and observation principle integrated different ways of step-size calculating to improve the performance. And, one indirect MPPT method using relationship between optimal mechanical rotational speeds and optimal DC bus voltages was chosen as the contrast. Two designed wind profiles and one measured real wind data in France are implemented into our platform to explore overall performance of all four MPPT methods and to enable the next research topic—the power limited control.

-Implementing power limited control (PLC) algorithms tending to integrate MPPT condition together in order to avoid the switching effect between controlling modes; and comparing characteristics of those proposed PLC algorithms in the modeled experimental platform. On the basis of MPPT research achievements, four power control methods integrated MPPT and PLC, which were extended from implemented four MPPT methods, are installed and studied with the measured real wind data mentioned before combining with a randomly calculated power demand profile. All power control methods are designed without requirement of the operating mode identification that tends to avoid the switching effect between different operating modes and reduce the complex of application. In the experimental validation, obtained experiences would help us to developed the integration work of small scale wind turbine into the electrical microgrid which is the main research subject of our lab AVENUES.

This thesis is organized as follow: Chapter I generally introduces the concept of eolic system positing the research presented in this thesis. Chapter II and III respectively describe the principle of proposed MPPT algorithms and PLC algorithms. The detail of experimental platform and its steady and dynamic characteristics are presented in Chapter IV. Based on the experimental platform, sets of experimental tests are designed and actualized to validate the proposed MPPT and PLC algorithms and compare them in Chapter V. Finally, the conclusions and further works are given in Chapter VI.

Chapter I. Eolic generation system

All energies were almost extracted from renewable sources before the first industrial revolution and made the reputation of fossil resources rise in the 19th century. The usage of renewable energy is associated with the wind in order to drive ships over water. This practice can be traced back some 7000 years, to ships on the Nile. Moving into the time of recorded history, the primary sources of "traditional" renewable energy were human labor, animal power, water power, wind, in grain crushing windmills, and firewood, a traditional biomass.

There are many definitions that characterize a renewable energy:

- Energy that can be reconstituted or is recovering faster than it is used;
- Energy natural renewal is fast enough for it to be considered as inexhaustible at the human time scale;
- An inexhaustible primary energy in the very long term, as it is directly come from natural phenomena.

From 2012 to present, renewable energies markets share over one-quarter of global power capacity with an increase of 8% based on 2011. From electricity viewpoint, renewable energies provide over 21% of global demand; but the most part is based on hydraulic power.

As one of the main options of renewable resources, the wind power is the utilization of air flow through wind turbines to mechanically power generators for electricity. The emergence of the wind power, regarded as a significant source of the world's energy, must be ranked as one of the significant developments of the late 20th century [5]. The emerging awareness of the finiteness of the earth's fossil fuel reserves, as well as the adverse effects of burning those fuels for energy, gave the need of seeking alternatives. Wind exists everywhere all over the world, and in some places with considerable energy density. Certainly, it is conceivable to be used again, since wind had been widely used in the past for mechanical power as well as transportation.

This Chapter will briefly describe the eolic generation system, while pointing out different scales and different energy conversion structures of eolic generation systems.

I.1. Wind turbine framework

A wind turbine is described as a machine which converts the power of the wind into electricity. As an alternative of fossil fuels, wind power is plentiful, renewable, widely distributed, clean, produces no greenhouse gas emissions during operating, does not use water, and occupies little land [7]. The net effects on the environment are far less problematic than those of nonrenewable power sources. In modern wind turbines, the actual conversion process uses the basic aerodynamic force of blades to produce a net positive torque on a rotating shaft, resulting first in the production of mechanical power and then in its transformation to electricity within a generator. According to this mechanism, it is not possible to store the wind and use it a later time. The power output of a wind turbine is thus inherently fluctuating and non-dispatchable. Thus, the most common solution is to limit the production below what the wind could produce [5]. In the viewpoint of application, in larger networks, the use of wind turbine results in a decrease in either the number of conventional generators being used or in the fuel use of those that are running. Conversely, in smaller networks, there may be energy storage, backup generators, and some specialized control systems.

The most common design of wind turbine, which is also adopted for study in this thesis, is the horizontal axis wind turbine (HAWT) whose axis of rotation is parallel to the ground. This design has been widely used (Figure 6 (a)) for the large wind turbine in wind farm [8], small scale wind turbine such as in urban areas, and off-shore environment [9]. Beside this concept, there is other topology named vertical axis wind turbine (VAWT) [10, 11] (Figure 6 (a)). An example of HAWT is presented in Figure 6 (b).

a

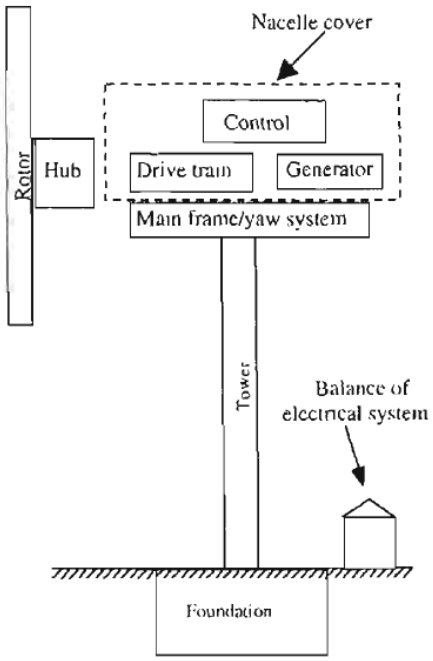

b

Figure 6: (a) Large scale, small scale, off-shore and vertical axis wind turbine; (b) Major components of a typical horizontal axis wind turbine.

Based on this Figure, the principal subsystems of a typical horizontal axis wind turbine are displayed [5]:

- The rotor consisting of the blades and the hub;
- The drive train , which includes the rotating parts of the wind turbine (exclusive of the rotor), usually consists of shafts, gearbox, coupling, a mechanical brake, and the generator;
- The nacelle and main frame, including wind turbine housing, bedplate, and the yaw system;

- The tower and the foundation;
- The machine controls;
- The electrical system, including cables, switchgear, transformers, and possibly electronic power converters.

The short introduction over of some of the most important components of wind turbine system follows. Nevertheless, since the detailed discussion of the overall design aspects of these components are not research focuses of this thesis, there will be no more information about them besides follows.

The rotor consists of the hub and blades of the wind turbine. These are usually considered to be the most important components in the point of view of the performance and the overall cost. Generally, concerning the number of blades, the three blades design is the most common choice. Regarding the structure of the hub, the most of intermediate sized and small sized turbines have used fixed blade pitch and stall control, meanwhile, the general trend now seems to be an increased use of pitch control, especially in larger turbine such as those used in wind farm. From the material point of view, blades on the majority of turbines are made from composites, primarily fiberglass reinforced plastics, but sometimes wood/epoxy laminates are used.

The drive train shown in Figure 6, usually consisting of the rotating parts of the wind turbine, typically includes a low-speed shaft, a gearbox, and high-speed shaft. Sometimes, these components could have the support bearings, one or more couplings, a brake and the rotating parts of the generator. The aim of using the gearbox is to regulate speed to a rate suitable for driving a standard generator. To larger wind turbines (over approximately 500kW [5]), planetary gearboxes became more pronounced because of the weight and size advantages, comparing with the parallel shaft structure. Some wind turbine designs use specially designed low-speed generators demanding no gearbox.

Nearly all wind turbines use either induction or synchronous generators [5, 12, 13]. Both of these designs entail a constant or near-constant rotational speed of the generator when the generator is directly connected to the utility network. The main advantage of induction generators is that they are rugged, inexpensive, and easy to connect to an electrical network. The variable speed wind turbine becomes more and more popular having a number of benefits including the reduction of wear and tear on the wind turbine and potential operation of the wind turbine at maximum efficiency over a wind range of wind speed, yielding increased energy capture.

The control system for a wind turbine is important with respect to both machine operation and power production. Generally, a wind turbine control system includes the following components:

- Sensors—speed, position, flow, temperature, current, voltage, etc.;
- Controllers—mechanical mechanisms, electrical circuits, and computers;
- Power amplifiers—switches, electrical amplifiers, hydraulic pumps and valves;
- Actuators—motors, pistons, magnets, and solenoids.

The design process of control systems for wind turbine application follows traditional control engineering practices; however, many aspects are quite specific to wind turbine, which will be detailed with our studied system in following chapters.

In order to highlight the research work presented in this thesis, we will talk about different scales of wind turbine. Large scale, big scale or utility-scale wind turbine is used to describe those wind turbines applied for economic wind farm which can produce no less than 1 MW power [14]. Another side, those wind turbines whose capacities are no more than 50 kW (the standard in Europe [15]) or 100 kW (according to the criterion of the United States of America [14]), are named as the small scale wind turbine.

I.1.1. Basic aerodynamic characteristic of wind turbine

Whatever the big scale or small scale wind turbine, there is a basic expression for its mechanism, which is presented in this subchapter.

Above all, original models of wind turbines were fixed speed turbines. This means that the rotor speed was a constant for all wind speeds. The tip-speed ratio (TSR) for a wind turbine is given by the following formula:

$$\lambda = \frac{\text{Tip speed of blade}}{\text{Wind speed}} \qquad (1)$$

The definition of TSR is the ratio between the tangential speed of the tip of a blade and the actual speed of the wind v. The tip-speed ratio is related to efficiency, with the optimum varying with blade design. Higher tip speeds result in higher noise levels and require stronger blades due to large centrifugal forces. The equation (1) can be presented as in (2), calculating the tip speed of the blade by the rotor rotational speed ω in radians/second and R the blade radius in meters.

$$\lambda = \frac{\omega R}{v} \qquad (2)$$

Thus, for a fixed-speed wind turbine, the value of the tip-speed ration is only changed by wind speed variations. In reference to a $c_p - \lambda$ graph, that illustrates the relationship between TSR and the efficiency, it is evident that only one value of λ yields the highest efficiency. Therefore, the fixed speed wind turbine is not operating at peak efficiency across a range of wind speeds. This was a motivator for the development of variable speed wind turbines. The research in this thesis focuses on the variable speed wind turbine.

The typical curve of power co-efficient c_p and tip-speed ration λ is presented below:

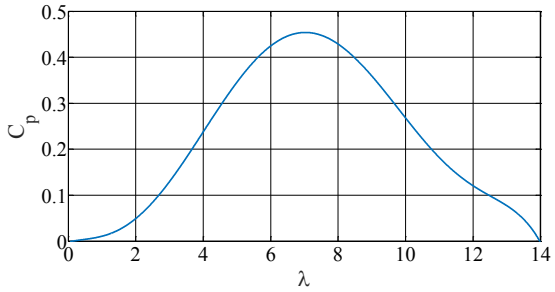

Figure 7: $C_p - \lambda$ graph [5].

According to all physic mentioned above, the harvested power p_{AERO} is given by the following formula:

$$p_{AERO} = \frac{1}{2}\rho\pi R^2 v^3 c_p \qquad (3)$$

in which, ρ is the air density.

Maintaining these concepts, the description of the large scale wind turbine and the small scale wind turbine are introduced in the next paragraph.

I.1.2. Large scale wind turbine

As mentioned above, the U.S. Department of Energy's National Renewable Energy Laboratory defines utility-scale wind projects—both land-based and offshore—as turbines larger than 1 MW, and utility-scale wind turbines also come in a multi-megawatt scale. The world's largest wind turbine has a rated power output of 8 MW. This kind of wind turbine is widely used, for example, in United States, in 2012, the utility-scale systems account for the majority of installed distributed wind capacity and comprised nearly 79% of distributed wind capacity additions.

I.1.3. Small scale wind turbine

As presented above, although definitions of small scale wind turbine in Europe and in United States are not the same, the majority of small scale wind system is suitable for a variety of applications including on- or off-grid residences; telecom towers, offshore platforms, rural schools and clinics, remote monitoring and other purposes that require energy where there is no electric grid, or where the grid is unstable. Associated with microgeneration, as opposed to large wind turbines, small scale wind turbines are applied for traffic signage, particularly in rural locations, as they avoid the need to lay long cables from the nearest mains grid connection point [16]. These small units often have direct drive generators; direct current output, aeroelastic blades, lifetime bearing and use a vane to point into the wind. As an important reference, the small scale wind turbine's capacity of producing is less than or equal to 30 kW (in Europe) or 100 kW (in USA) of electrical power.

Although vertical axis wind turbines are a growing type of wind turbine in the small-wind market, the majority of small wind turbines are traditional horizontal axis wind turbines [17]. One notes that the small scale wind turbine in the form of horizontal axis is exactly the research objective in this thesis.

Naturally, wind turbines are controlled to operate only in a specified range of wind speeds bounded by cut-in (V_{cut-in}) and cut-out ($V_{cut-out}$) speeds. When the operating conditions are out of those limits, the whole generation system should be stopped to protect both the generator and mechanic structure of the turbine. Figure 8 shows the typical power curve of a wind turbine [18, 19]. From the figure, it can be observed that there are three different operational regions.

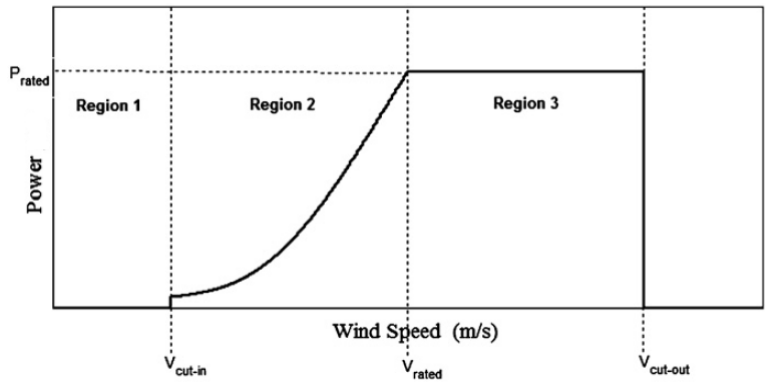

Figure 8: Ideal power curve of a wind turbine.

The first is the low-speed region, in which the turbine should be stopped and disconnected from the grid or its load to prevent it from being driven by the generator. The second is the moderate-speed region that is bounded by the cut-in speed at which the turbine starts working and the rated speed (V_{rated}), at which the turbine produces its rated power. The turbine produces maximum power in this region, as it is controlled to extract the available power from the wind. In the high speed region (i.e. between V_{rated} and $V_{cut-out}$), the turbine power is limited so that the turbine and generator are not overloaded and dynamic loads do not result in mechanical failure [18]. It is noteworthy that to protect the turbine from structural overload, it should be shut down above the cut-out speed.

To different application environment, wind turbine could be demanded operate in different modes in the wind speed range, such as constant rotational speed of turbine's blades or variable rotational speed of turbine's blades. The used generator and the power conversion structure of wind generation system limit this operating mode, which are discussed in next parts.

I.1.3.1. Different types of machines

After the extraction of aerodynamic power from air flow by turbine's blades, energy is transformed into the electrical form via the generator. Different types of electrical machines may be chosen as an option for the small scale wind generator. Among these all alternatives, the permanent magnet synchronous machine (PMSM) is the one used most commonly; however, one note that the induction machine may also be used [12]. Since its efficiency reliability, energy density, small size and light weight, PMSM is popular than other alternatives. For the research in this thesis, the selected machine is a classical radial flux PMSM, even though there are new topologies of PMSM developed, such as axial flux type. The reason is that the excellent axial flux PMSM has large manufacturing constraints [13].

I.1.3.1.1. Asynchronous machines

The advantages of asynchronous electrical machines are that they are easy to manufacture and cheap. Generally this type of machines can be sort into two main categories: squirreled cage machine and doubly-fed machine.

The squirreled cage asynchronous machine is simple to be standardized and manufacture in large quantities and very large power scale, with a high reliability, requiring a low cost of maintenance. However, limited by the physical structure, the squirreled cage asynchronous machine is hard to realize the modification of rotational speed. Consequently the main application of this type machine in wind power, are in constant rotation speed and direct connection to the grid. They can be simply used in large wind turbines because of the demand of the blades rotational speed and possibility of direct-drive. But, comparing with variable frequency system, the squirreled cage asynchronous machine has weak points such as: lower energy efficiency, the problem of sudden power changes and the grid problem in case of wind drop.

Double-fed asynchronous machine is currently one of two competing solutions in variable speed wind applications. For this machine, its stator is directly coupled to the grid commonly by a transformer. The wind turbine thus allows the rotor set of variable speed operation working over a range of speed depending on the type and size of the wind turbine rotor [20]. Coupling the generator rotor to double-fed rotor through two three-phase converters, one as rectifier mode and another as an inverter, can obtain a variation in the rotation speed about 30% of the synchronous speed. In application, the wind turbine rotor is designed with the limitation to 25% of the rated power of the electrical machine stator, which supplies a sufficient change of speed up to 30% of the speed range. This is the advantage of double-fed asynchronous machine; meanwhile it maintains the drawback of interactions with the utility grid especially over current resulted from voltage drops of the grid [20].

I.1.3.1.2. Synchronous machines

In past several decades, the DC motor has been used in the industry since its main advantage of being easy to be controlled through the natural decoupling of lux and torque. However, the collector brush system introduces a big engine problem limiting the power rating and maximum speed. Furthermore, difficulties of continuous operating maintained by predicted interruptions appear which limit its application more and more. Based on these drawbacks above and thanks to advances in power electronics, the industry's interest has switched to the use of AC machines taking advantage from benefits of the flexibility of speed change rate and operation stability. As mentioned above, the PMSM has several strengths, low inertia, no losses to the rotor, and higher mass torque than asynchronous machine and classic synchronous machine. The PMSM supplies rapid current and torque response because of its relatively small inductance. Hence, from technical viewpoint, this type of machine has tighter configuration and less energy losses than those machines excited separately. Generally, it has a low inertial time constant and high massif torque presenting robust and reliable, meanwhile its weak points are the lack of adjustment in the amplitude of the magnetic moment and high cost [21].

In this thesis, the PMSM is chosen for its significant advantages, then, there are various types of control allow connection between the generator and electrical grid which is presented in next part.

I.1.3.2. Converter types and structures

Generally, the wind turbine is demanded to extract power as much as possible, which means that a MPPT algorithm is involved, in Region 2 presented in Figure 8, and to export constant power amount in Region 3 presented in Figure 8. But, this thesis just focuses on the Region 2 to realize the MPPT and the limited power amount control topics. Although the speed of the wind turbine could be fixed or variable, maximization of the extracted energy only is achievable with variable speed wind turbines. Aiming to operate in variable speed conditions, a power electronic converter is necessary to convert the variable—voltage—variable—frequency of the generator in to a fixed—voltage—fixed—frequency which is suitable for the load [22, 23, 24]. In [22, 25, 26, 27], researchers have analyzed different possible

configurations of power converters and electrical generators for variable-speed wind turbine systems, which cover both the AC and DC application environment.

For the research in this thesis, based on the power level of small scale wind turbine and application conditions in which the output of the small scale wind turbine is connected to one DC BUS [28, 29, 30, 31, 32, 33], specific implementations about the electrical structure of power conversion can be passive and active types (as presented in Figure 9) for converting mechanical energy into electrical form.

Passive structure, which is robust and economical, uses an uncontrollable three-phase AC/DC converter (three-phase diode bridge) [12] (Figure 9 (a)).

The active structure given in Figure 9 (b) has a controllable DC/DC converter and a three-phase diode bridge [34], or, as shown in Figure 9 (c) uses a three-phase AC/DC converter based on passive structure.

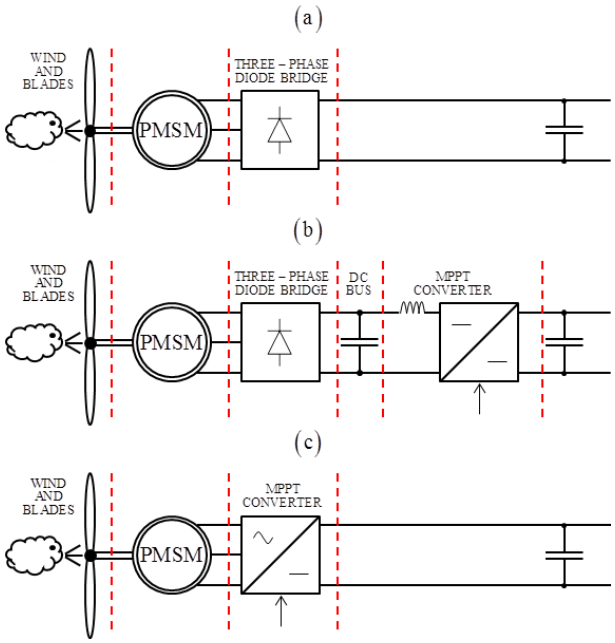

Figure 9: Electrical structures of power conversion.

The topologies of static converters are designed for application in medium and high power scale, while our study is for small scale. For the small scale system the fully controlled components are too expensive. In order to reduce costs, the diode bridge is attractive, since it is cheap and provides the energy performance not too degraded. To match the requirements of load, additional power electronic devices are asked because PMSM produces a variable frequency and amplitude voltage. In this research, the three-phase diode bridge is used to rectify the voltage generated by the PMSM. The diodes in the circuit of the diode bridge are considered as the ideal switches and the output current of the rectifier circuit is continuous. A topology of this passive diode rectifier can be found as shown in Figure 9 (a).

The essential elements of the wind energy conversion system with variable speed is the static converter, which allows the system operating at variable speed and extracting the maximum power produced by the wind turbine. Output power at the DC side can be optimized by a voltage control (similarly, the rotational speed control at the generator) using a rectifier of three-phase diode bridge associated with a controlled converter (buck of boost, such as presented in Figure 9 (b)) or a controlled PWM rectifier (presented in Figure 9 (c)). As described in [31, 33], the achievement of AVENUES laboratory, the application of the fully controlled rectifier demands complex control method such as the vector control based on PMSM model to realize the modification of output power, and the process of designing this vector control requires researchers having rich application experiences. And, this kind of application usually arouses the development of sensorless technology about information of PMSM, such as achievements [31, 33], the work of H. Al-Ghossini of AVENUES laboratory. Furthermore, expensive equipment is asked to realize this structure offering a good performance. Contrary to the fully controlled structure, the active structure displayed in Figure 9 (b) requires a simple and less expensive control system. The control method for DC/DC converter is simpler and more robust than those used for the controlled rectifier, and the power loss of the three-phase diode bridge is less than the controlled rectifier.

I.2. Conclusion

Brief description about renewable energies has been introduced in this chapter, especially the important concepts of wind energy generation technology: basic characteristics of power generation, architectures, used generators, etc. Works in this thesis focuses on the small scale wind turbine which has to be integrated into an urban DC microgrid and, therefore, concerns the urban environment. Wind turbine studied in our research is small scale horizontal axis wind turbine. PMSM is the used type of the generator according to its known advantages. The power conversion structure is composed of a three-phase diode bridge and a boost DC-DC convertor that was chosen after discussion about different structures and respectively control laws. Based on the system composed of the chosen architecture, generator and power conversion structure, the power control strategies, such as MPPT and PLC, are studied and then implemented. The theory of proposed MPPT methods will be introduced in next chapter focusing on extracting the power as much as possible

Chapter II. Maximum power point tracking

The control of power output of small scale wind turbine almost is the most important topic to it. As mentioned above, realizing MPPT algorithm is one fundamental subject of power controlling about small scale wind turbine. MPPT methods can be sorted into direct method and indirect method according to whether the method lies on the mathematic model of the studied system. Inasmuch as our research target is to compare and analyze the regulating effect of both direct and indirect MPPT methods, the selected four MPPT methods are: Perturbation and Observation method fixed step-size (P&O-F); Perturbation and Observation method variable step-size with improved Newton-Raphson method (P&O-INR); Perturbation and Observation method variable step-size with Fuzzy Logic method (P&O-FL); Lookup table method based on rotational speed and DC voltage (LT). In this chapter, the theories of four MPPT methods will be presented with the summary of published applications [12, 35--71], and their advantages and disadvantages are also analyzed and compared to prepare the experimental implement in our platform, which will be presented and discussed in detail in Chapter V.

II.1. Perturbation and observation with fixed step-size

Summarizing the vast majority of achievements, MPPT methods can be sorted in to direct and indirect methods as summarized in [12, 35, 37, 38]. The direct MPPT method is used to describe the algorithm which theoretically doesn't require the math information of studied system's steady-state operating points. This type of MPPT method presents more robustness, simplicity and flexibility. These methods almost lie on the principle of the perturbation and observation (P&O), or hill-climb searching (HCS), which is a mathematical optimization technique used to search for the local optimum point of a given function. These methods are based on perturbing a control variable in small step-size and observing the resulting changes in the target function until the slope becomes zero. The basic operating process of this method is presented as in Figure 10.

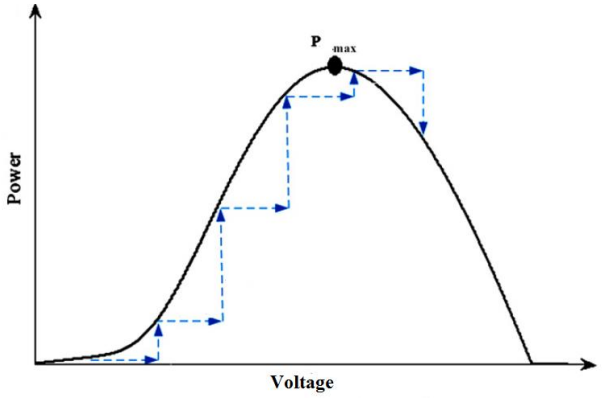

Figure 10: P&O control process.

The process of the perturbation and observation method's operating, describes the movement of steady-state operating point of system; the perturb step-size and the observe time step-size are the only parameters to be selected. As displayed in Figure 10, using the DC voltage and the power output as an example, each perturbation of the voltage introduces a variation of power output. If the variation of power output is positive which means the system is getting close to the maximum power point (MPP), so, the next step of perturb will follow the varying direction of the last step; and if the value of difference of power output is negative meaning that the system is moving in a direction away from the maximum power operating point, the next step of perturbing has to change the direction.

The perturbation and observation method with fixed step-size (P&O-F) is one basic direct MPPT method. So, it was selected to be implemented into our platform as the first step. In the available literature, some authors perturbed the rotational speed and observed the mechanical power [35, 39, 40], while others monitored the output power of the generator and perturbed the inverter input voltage [41] or one of the converter variables, such as duty cycle [42, 43, 44]; input current [45]; or input voltage [32, 46]. Comparing with mechanical sensors, apparently measuring electrical power and other variables are more reliable and low-cost.

In this work, the chosen variable of perturbation is the local DC bus voltage, which is exactly the output voltage of the diode bridge, and the output power is directly selected as the observe parameter. In the Matlab®/Simulink® software environment, this P&O-F method was implemented following the flowchart displayed in Figure 11.

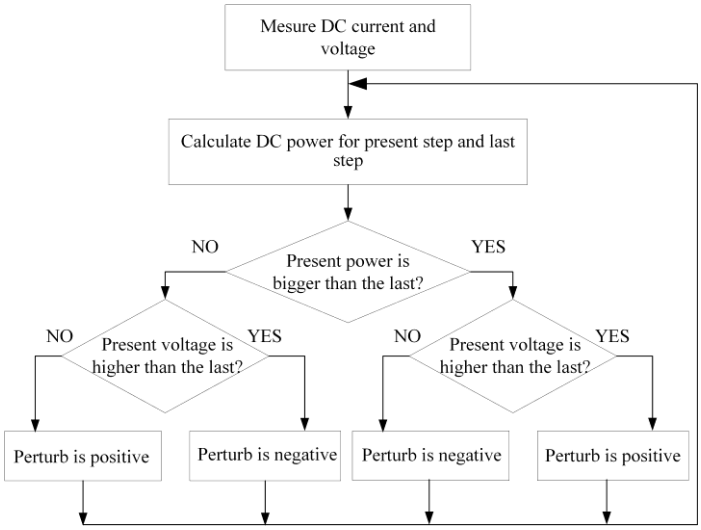

Figure 11: Principle of P&O-F method.

On the basis of the mechanism in Figure 11, it is obvious that the perturb step-size and the observe time interval are the only two parameters that can be modified, which make the P&O-F independent, simple and flexible, and strong adaptable. However, it has the possibility to fail under rapid wind variations if the P&O-F is used into the Eolic system with medium and large inertia wind turbines. Furthermore, for applying the P&O-F method, there is one trade-off about choosing an appropriate perturbation step-size and the observation interval, especially in noisy systems: a larger step-size enables a faster response but induces more power oscillations, which means less efficiency; a smaller step-size improves the efficiency but reduces the convergence speed at the same time [47, 48, 49, 50, 51]. In addition, the initialization of these parameters affects the performance of this algorithm.

Furthermore, another major drawback, which can lead to the failure of the tracking process, is apparent, the lack of distinction between the power differences resulting from the change in the wind with those resulting from the change in the previous perturbation [35]. The reason, why indistinct differences in power can result in a wrong determination the direction of the next perturbation step, is presented in Figure 12.

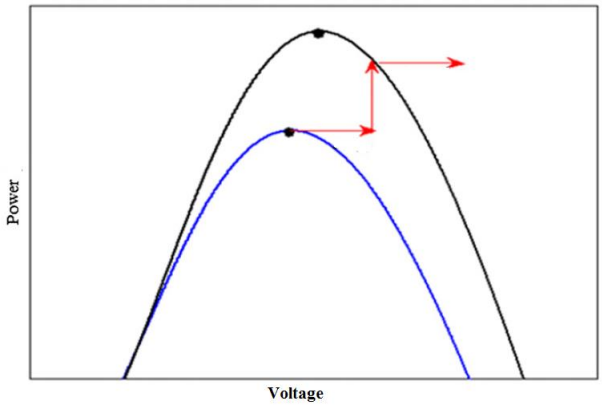

Figure 12: Tracking error of P&O method [35].

Since the wind speed changes, the actual difference of power is positive, furthermore, the actual determination of next perturb is also positive. However, in theory, the operating point has been the right side of the maximum power point, so the determination of perturbing direction should be negative. For P&O-F method, this moving, which is away from the peak, apparently decreases the efficiency to tracking the MPP, especially with a big fixed perturb step-size.

II.2. Perturbation and observation with variable step-size

As discussed before, the classic P&O method with fixed step-size apparently has drawbacks. Thus, concerning the direct methods, improving the efficiency and the accuracy promotes the development of modified variable step-size algorithms [32, 42, 46, 49]. In those adaptive step-size methods, the perturb step-size is automatically updated according to the actual operating point. Ideally, if the actual operating point is far away from the potential MPP, the step-size should be increased to accelerate the process for getting close; conversely the determination is reversed to decrease the step-size when the actual operating point is close to the MPP. Continually, the variable step-size decreases until it approaches zero in order to drive the operating point to settle down exactly at the MPP [35]. This principle reduces the oscillation of steady-state operating point of the system which occurs in the conventional P&O method, accelerates the speed to reach the maximum, and lowers the time needed for tracking.

In the study [49], the difference between the actual rotational speed ω and the optimal rotational speed ω^* is used to adjust the step-size of variable perturbation periodically at the end of the each iteration as following:

$$d(k+1) = d(k) + \alpha\left(\omega - \omega^*\right) \quad (4)$$

in which, the $d(k)$ is the duty cycle of the converter used in [49], and the α is a coefficient needed to be determined. The value of α is determined according to the optimal power curve, which means that the way for varying perturb step-size used in [49] actually removes the advantage of independence of P&O method. To each different wind turbine system, this optimal rotational speed ω^* needs to be re-confirmed, and there is one coefficient α requiring experienced users.

However the perturb step-size can also be chosen according to the scaled measure of the slope of power output, respecting the converter's duty ratio [42, 52]:

$$\text{Duty cycle}(k+1) = \text{Duty cycle}(k) + \alpha \frac{\Delta\text{power}(k)}{\Delta\text{Duty cycle}(k)} \quad (5)$$

in which, there still exits one coefficient α needed to be determined by designers.

Furthermore, some research presented the way using a piecewise function [53], or calculating the slope value between the power and the rotational speed to determine the variable step-size [35]. However, the piecewise function method cannot converge the actual perturb step-size to zeros. And both of them are not independent enough, since they used several numeral parameters need to be determine.

The first way to calculate variable step-size used in this thesis is based on the Newton-Raphson method [46], which doesn't have other numeral parameters besides the maximum limit of perturbation step-size and the observe time interval. Another approach is based on fuzzy logic.

II.2.1. Improved Newton-Raphson method

Essentially, P&O variable step-size calculated by Newton-Raphson method still is one mathematic way to adapt the perturb step-size [46]. In numerical analysis, Newton-Raphson method, named after Isaac Newton and joseph Raphson, is a method for finding successively better approximations to the roots (or zeros) of a real-valued function.

$$x : f(x) = 0 \quad (6)$$

The Newton-Raphson method in one variable is implemented as follows:

The method starts with a function f defined over the real numbers x, the function's derivative f', and an initial guess x_0 for a root of the function. If the function satisfies the assumptions made in the derivation of the formula and the initial guess is close, than a better approximation x_1 is

$$x_1 = x_0 - \frac{f(x_0)}{f'(x_0)} \tag{7}$$

Geometrically, (x_1, 0) is the intersection of the *x*-axis and the tangent of the graph of f at $(x_0, f(x_0))$.

The process is repeated as

$$x_{n+1} = x_n - \frac{f(x_n)}{f'(x_n)} \tag{8}$$

until a sufficiently accurate value is reached.

For MPPT application, using the voltage u as the x, and the ratio between the change of electrical power p and the change of voltage u (the variable *slope* in (9)) as the function $f(x)$, the practical application process is repeated at each step k, as presented in (9) [46].

$$\begin{aligned} \Delta p(k) &= p(k) - p(k-1) \\ \Delta u(k) &= u(k) - u(k-1) \\ slope(k) &= \frac{\Delta p(k)}{\Delta u(k)} \\ \Delta slope(k) &= slope(k) - slope(k-1) \\ \Delta u &= \frac{\Delta p(\mathrm{k})}{\Delta slope(k)} \\ u_{ref}(k+1) &= u_{ref}(k) + \Delta u \end{aligned} \tag{9}$$

During experiments on the platform, this variable step-size P&O method with Newton-Raphson method, demonstrated one kind of overly strong convergence capability of perturb step-size Δu. In several statistics for MPPT experiments, this algorithm could not respond to the rapid changes of the wind speed with small amplitude. The experimental results will be presented and discussed in detail in Chapter V.1.

According to those drawbacks, one improved method was introduced in this thesis, whose calculated process is iterated as follows:

$$\begin{aligned} \Delta p(k) &= p(k) - p(k-1) \\ \Delta u(k) &= u(k) - u(k-1) \\ slope(k) &= \frac{\Delta u(k)}{\Delta p(k)} \\ \Delta slope(k) &= slope(k) - slope(k-1) \\ \Delta u &= \frac{\Delta u(\mathrm{k})}{\Delta slope(k)} \\ u_{ref}(k+1) &= u_{ref}(k) + \Delta u \end{aligned} \qquad (10)$$

The difference of this improvement will be explained in the Chapter V.1, with one experimental validation.

II.2.2. Fuzzy logic method

Many of the problems associated with the aforementioned methods have been solved by artificial intelligence control and hybrid methods. According to one study [54, 55, 56, 57, 58], fuzzy logic method can be utilized to calculate an optimal perturb step-size for the conventional P&O method. Ref. [54] used fuzzy logic method based on two integrated variables mixed by several mechanical variables to determine the perturb step-size to the Duty Cycle of converter used in their system. In [55], used inputs of fuzzy logic method directly were the output power and the Duty Cycle of the converter, and the perturbed variable also was the converter's Duty Cycle. In comparison, [56] used the rotational speed and the output power as the inputs of fuzzy logic reasoning to modify the rotational speed. Being consistent with P&O-F and P&O-INR methods, this thesis used the DC voltage and the output power as the inputs of fuzzy logic method.

Theoretically, fuzzy logic method can handle with robust and nonlinear control requirements, although it needs thorough knowledge about the studied system. In general, the fuzzy logic consists of mapping the input space and the output space through logical operations. The application process is divided into three steps: the fuzzification, the fuzzy reasoning and the defuzzification.

The numerical values of inputs or outputs are transformed into fuzzy sets in the process of fuzzification. Every point of input space will be transformed into the "code" in form of the degree of membership for a set of membership functions, as the example shown in Figure 13. And this degree can take all the values between 0 and 1, which means it is not a Boolean logic. Furthermore, the result of fuzzy reasoning is converted to a quantifiable result based on its membership function in the defuzzification process.

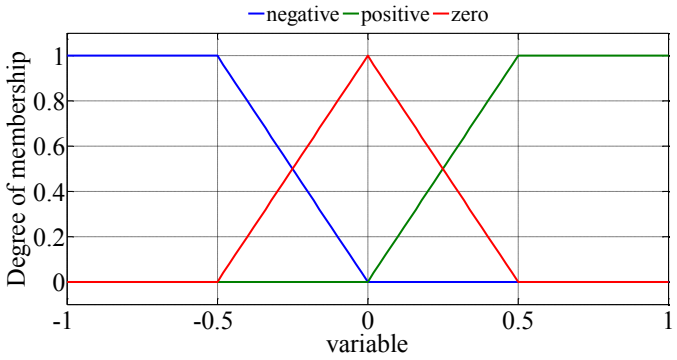

Figure 13: Membership function example.

As presented in Figure 13, concepts named “negative”, “positive” and “zero” compose the fuzzy set. Each concept has its own membership function which represents the degree of truth as an extension of valuation. Degrees of truth are often confused with probabilities, although they are conceptually distinct. Fuzzy truth represents membership in vaguely defined sets, not likelihood of some event or condition.

Generally, the range of variable at x-axis equals the real operating range of this physic variable. The determination of this range influences the performance of applying fuzzy logic for MPPT methods. In this thesis, in order to simplify the process of applying the fuzzy logic and optimizing its parameters, all inputs are normalized before the process of fuzzification, and the result of defuzzification needs to be anti-normalized to become real output of the variable step-size P&O MPPT method. Modifying those coefficients of normalization and anti-normalization can optimize the performance of fuzzy logic application in MPPT topic.

The process of fuzzy reasoning usually can be explained by the fuzzy rules (as an example given in Table 1) or the reasoning surface as presented in Figure 14.

Table 1 – Fuzzy rule table

Output		**Input 1**		
		negative	**zero**	**positive**
Input 2	**negative**	+	0	-
	zero	-	0	+
	positive	-	0	+

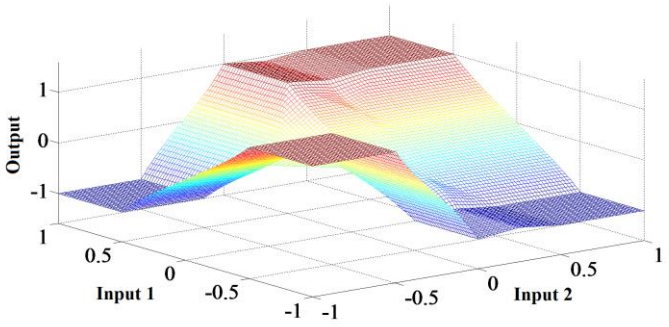

Figure 14: Fuzzy reasoning surface.

Figure 14 presents the fuzzy reasoning surface of the proposed fuzzy logic, and the Table 1 explains the "if-then" reasoning role. The step of "if" defines a fuzzy region in the input space while the "then" step specifies the output in the fuzzy region. With a logical operator, membership functions values evaluating the degree of each activated rule express that how the "if" step of each rule is satisfied. Subsequently, the fuzzy set in the "then" step of each rule is determined. Finally outputs of each rule are combined to form one fuzzy set. In this thesis, the Mamdani fuzzy inference system fuzzy toolbox is used. The main goal of defuzzification is to interpret the fuzzy set resulted from the fuzzy reasoning into a numerical value between 0 and 1. Several defuzzification operators are mentioned in [59], but the most used one is the centroid, or center of gravity, which is chosen in this article also. The determination of these coefficients about normalizing for fuzzification and anti-normalizing for defuzzification will be presented in Chapter V. This selection influences the performances of fuzzy logic algorithm calculating variable step-size, so, it is usually optimized by another optimization algorithm such as particle swarm optimization method. However, in this thesis, physical means of those coefficients are simple and direct, so, values of these coefficients applied in Chapter V are chosen by the enumeration method. Detail information and the explanation can also be found in Chapter V.

II.3. Lookup table method

Aiming to compare as many different types of MPPT methods as possible, the second type of MPPT method rightfully will be implemented in our platform, since three direct MPPT methods have been chosen, as mentioned above. The indirect MPPT method, always indicates that it relies on precise mathematic model of the studied system, such as, the Tip Speed Ratio (TSR) method presented in [35], the optimal torque (OT) method used in [60, 61], the power signal feedback (PSF) method applied in [41, 62], or methods based on relationship among several parameters of system [63, 64, 65, 66, 67]. Based on mathematic information between several variables of the studied system, the lookup table tool is usually chosen as the realizing approach. Advantages of the indirect method are clear: high accuracy and fast reaction, but they also have drawbacks such as lots of preliminary work, being sensitive to system parameter drift and requirements about sensors with high precision.

One indirect method relied on the most used parameter, i.e. the TSR, introduced in [35], is based on the identification of the optimal value of TSR pre-measured. The optimal point of the TSR can be determined experimentally or theoretically and stored as a reference. Although this method seems simple as wind speed is directly and continuously measured, a precise measurement for wind speed is impossible in reality and increases the cost of the system [68]. The block diagram of the TSR control method is presented in Figure 15.

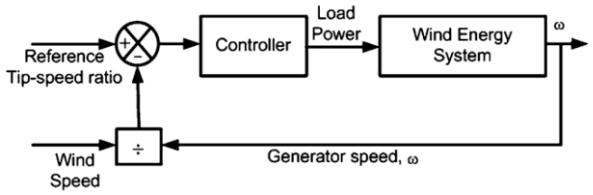

Figure 15: The block diagram of the tip speed ratio control [60].

Another basic indirect method is the optimal torque (OT) method. As mentioned previously, upholding the system operating at optimal points of the TSR can guarantees the conversion of available wind energy into mechanical form. As presented in Figure 16, the principle of OT method is to adjust the generator torque according to a maximum power reference torque of the wind turbine at a given wind speed.

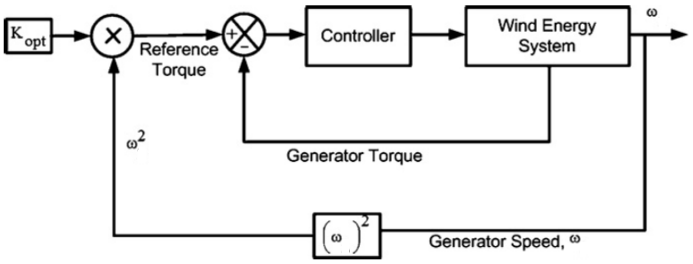

Figure 16: the block diagram of optimal torque control MPPT method [60].

Regarding the turbine power as a function of λ and ω, (3) is rewritten in the form in order to obtain the wind speed [35, 61]:

$$p_{AERO} = \frac{1}{2}\rho\pi R^5 \frac{\omega^3}{\lambda^3} c_p \qquad (11)$$

Assuming that the wind turbine is operating at optimal point of TSR, values of TSR and c_p can be marked as λ_{opt} and c_{p-opt}. Consequently, (11) can be transformed into the following expression:

$$p_{AERO-opt} = \frac{1}{2}\rho\pi R^5 \frac{\omega_{opt}^3}{\lambda_{opt}^3} c_{p-opt} = K_{opt}\omega_{opt}^3 \qquad (12)$$

Considering that $p_{AERO-opt} = \omega_{opt} T_{opt}$, T_{opt} can be rearranged as presented in (13):

$$T_{opt} = \frac{1}{2} \rho \pi R^5 \frac{\omega_{opt}^2}{\lambda_{opt}^3} c_{p-opt} = K_{opt} \omega_{opt}^2 \quad (13)$$

It is a torque-control-based method, where the analytical expression of the optimum torque curve, represented (13) is given as a reference torque for the controller that is connected to the wind turbine.

Inside the scope of the concept of the indirect method, one straight way is the power signal feedback (PSF) control method shown in Figure 17. Unlike the optimal TSR method or OT method, in this method the reference optimum power curve of the wind turbine should be obtained first from the experimental results. Then, the data points for maximum output power and the corresponding wind turbine speed must be recorded in a lookup table. Rather than using the wind turbine's maximum power versus shaft speed curve to populate the lookup table, the maximum DC output power and the DC-link voltage were taken as input and output of the lookup table in Quincy and Liuchen [41]. According to Raza Kazmi et al. [62], there is no difference between the PSF and the OT methods in terms of performance and the complexity of implementation.

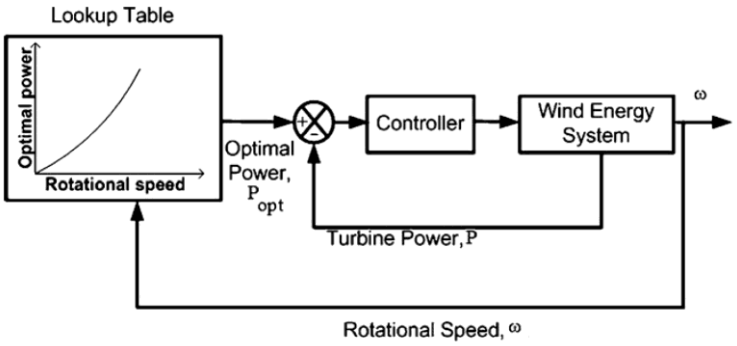

Figure 17: The block diagram of a wind energy system with the power signal feedback control technique.

The indirect method used in this thesis is based on the optimal relationship between the rotational speed and the DC bus voltage. This optimal curve was obtained via prior measurement about the studied system's steady state operating points. Obviously, for each fixed wind velocity, there is just one operating point extracting the most amount of power. So, forcing the system operating along this optimal curve can satisfy MPPT topic. The process of establishing this lookup table method is presented as in Figure 18.

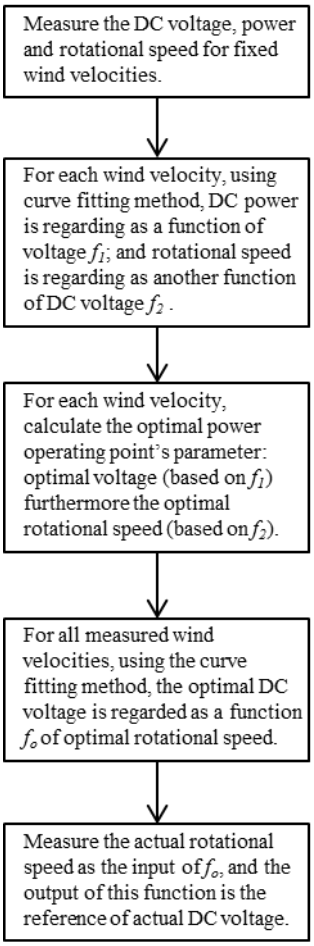

Figure 18: Process of establishing lookup table for MPPT.

There are also several combination applications of artificial intelligence method such as fuzzy logic or neural networks with indirect MPPT methods, such as [36, 39, 69, 70, 71]. [69] presents a radial basis function neural networks trained by the modified particle swarm optimization (MPSO) algorithm to be used as a control algorithm. The used way to realize MPPT topic was still to use the optimal TSR value pre-measured to calculate the reference of rotational speed based on measuring actual wind velocity. In this article, the fuzzy logic method saw also used to control the system follow the reference of rotational speed based on the pre-measured optimal TSR and actual wind velocity measured during operation. In [39], one neural network was used as the estimator of wind velocity to reduce the economic cost for MPPT. In addition, also in [39], another neural network, optimized by the particle swarm optimization (PSO) algorithm, was applied to calculate the reference of DC voltage according to the wind velocity value estimated by the first neural network, whose inputs were the actual rotational speed and output power. Furthermore, in [70] the authors show that the fuzzy logic algorithm can be used to estimate wind speed based on the mechanical power. Or, one growing neural gas network [36], which could be e-learning (i.e. trained by itself), was implemented to give the reference of optimal rotational speed. Applications of those artificial intelligence algorithms performed well, as discussed in those references. However, little few of these articles explained how to validate the training of neural networks finished during the application.

II.4. Conclusion

In this chapter, theories of four proposed MPPT methods, which belong to two different sorts, are described in detail, summering the state of art of each sort of MPPT methods. Follow the principle of perturb and observe, the methods P&O-F, P&O-INR and P&O-FL repeatedly disturb the key parameter of system's operation to determine the modification of working condition. From fixed perturb step-size to the variable step-size calculated by different methods the performances of these MPPT method tend to solve the problem of step-size's convergence. Since this principle requires few knowledge of system's specificity, those three direct MPPT methods maintain strong robustness and flexible applicability. As a representative of indirect MPPT method, the proposed lookup table algorithm based on the mathematic relationship of symbolic parameters was introduced and analyzed. Due to the utilization of precise information about studied system, this method naturally presents high precision while naturally be sensitive about the drift of system's parameters. In this chapter, only basic logic of each proposed methods are presented. The parameters setting of each method will be discussed in Chapter V when all of them are going to be implemented into the test bench. With the explicit application objective, all proposed MPPT methods will be tested by several chosen wind velocity profiles and compared with each other. Experimental validation obtained during the study of this topic will make a contribution to the design of PLC methods, which is going to be described in next chapter.

Chapter III. Power limited control

The small scale wind generation system right now is more and more used as one common source of distributed energy forms. Consequently, the small scale wind turbine has a strong possibility to be asked to output the electrical power for a certain variable value required by the load. Different from the fixed given power demands, the power limited control (PLC) demand can ask the system operating at any potential operating point including maximum power point. So, the optimal option is to integrate the MPPT method into the power limited control strategy to avoid the switching effect between different mode and the requirement of identifying for operating mode.

In this chapter, four different PLC methods respectively based on those four MPPT methods presented in Chapter II are described with principle analysis. Each PLC method integrates the corresponding MPPT method avoiding the requirement of identification of operating mode. The advantages and disadvantages in theory are also discussed in this chapter, preparing the experimental comparison presented in Chapter V.

III.1. Perturbation and observation with fixed step-size

The integrated power control strategy of MPPT and PLC has several approaches. In [72] the authors used the variable step-size P&O method based on the change rate of the current output to disturb the duty cycle of DC/DC converter of their system; also, the authors used a PI (proportinal integral) controller to realize tracking the limited power defined by load. This article introduced a complex mechanism switching between MPPT mode, limited power tracking mode and over wind speed protection mode in which the wind speed is over than the rated value. So, an additional dynamic characteristic about switching effect is inevitable. In [73], a modified P&O method is selected for MPPT regulation, but, to this article, power limited control just means the constant power output when wind velocity is over the rated value of the studied system, and a double loop PI control with a voltage inner loop and a power outer loop is implemented to achieve this objective. The sliding model control used in [74, 75], which dedicates to demand the system to meet a relatively logical relationship between the actual electrical power and the mechanical torque (regarded as the 'sliding surface') is independent on the mathematic information about the studied system. Thus, sliding model control applied for the integrated power control maintains strong robustness. But, similar as P&O's principle, the sliding model control also just describes the movement of steady operating points of the wind generation system. At the same time, the determination of parameters of sliding model control requires experienced designers. Ref. [76] selected TSR as the feedback parameter of P&O method, then compare the actual value of TSR with ideal value calculated by mathematic model of studied system. Therefore, even it used the principle of P&O, the method still performed weak robustness.

The first PLC regulating method introduced in this thesis is based on the P&O-F method used for MPPT presented in Chapter II.1. Comparing with P&O-F for MPPT, PLC demands to focus on the absolute value of the difference between the required power value and the actual output power assuming that the required value always can be known. Figure 19 presents the difference between MPPT condition and PLC condition in generally way.

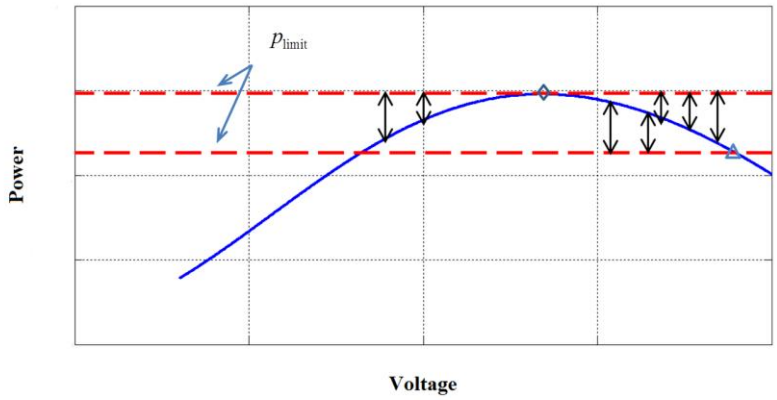

Figure 19: Power control strategies.

For a given wind velocity (the blue curve in Figure 19), if the demanded power value p_{limit} (the dash line) equals the potential maximum, there is only one operating point, as illustrated by the upper red dotted line in Figure 19. If the demanded power value is lower than the potential maximum value, in theory, there are two operating points supplying the same power value as displayed by the below red dotted line in Figure 19. Considering the transfer of operating points, if the steady component of operating currents is close to equipment's physical limitations, the dynamic components of current resulting from the transfer between operating points has great risk for damaging devices. So, in this study, the system will be forced to operate at the "low current—high voltage" side for PLC condition.

Following the logic of presenting the MPPT approaches in Chapter II, the first algorithm to be extended is the P&O-F method. As described above, when the demanded power value is lower than the potential maximum power value, the whole operating region can be divided into four sub regions by the MPP and two limited power operating points, as shown in Figure 20.

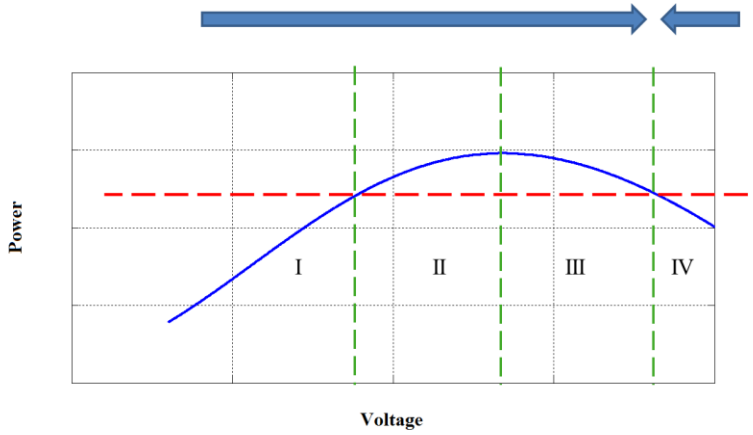

Figure 20: Four operating regions for PLC condition.

In order to distinguish these different regions, the identification based on the change of three variables during the P&O process is introduced. At first, is has to be mentioned that, the goal of P&O-F PLC method is to minimize the difference between actual power and demanded power value (marked as

$p_{diff} = p_{\text{limit}} - p$). Hence, the change of the difference is the prioritized variable for P&O-F PLC method. Aiming to explain the logic easy, using the actual power as p and the actual voltage as u, the four regions (marked as I, II, III and IV in Figure 20) can be indicated by the change of $|p_{diff}|$, p and u, as in Table 2.

Table 2 – Definition of four operating regions for PLC condition

	I		II		III		IV	
$\Delta u(k)$	↑	↓	↑	↓	↑	↓	↑	↓
$\Delta p(k)$	↑	↓	↑	↓	↓	↑	↓	↑
$\Delta\|p_{diff}\|(k)$	↓	↑	↑	↓	↓	↑	↑	↓

Based on the rules presented in Figure 20 and Table 2, when the system is operating in the regions I, II, or III, the perturb direction should be positive; if in regions IV, the perturbation must decrease the voltage. Aiming to assure the rules' adaptability for MPPT condition, Figure 21 and Table 3 are presented following.

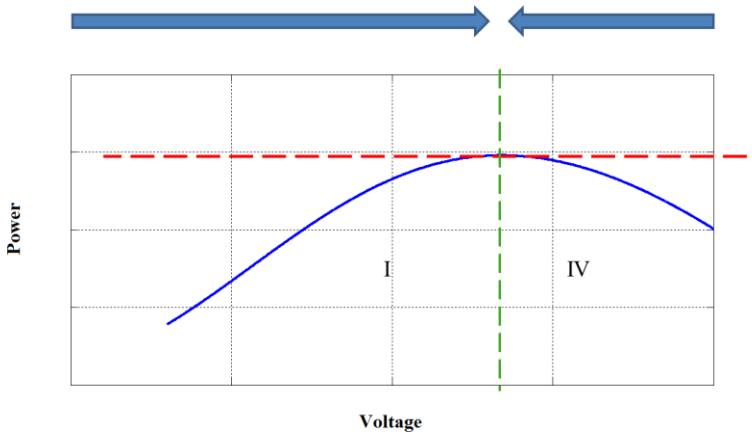

Figure 21: Operating regions for MPPT condition.

Table 3 – Definition of operating regions for MPPT condition

	I		IV	
$\Delta u(k)$	↑	↓	↑	↓
$\Delta p(k)$	↑	↓	↓	↑
$\Delta\|p_{diff}\|(k)$	↓	↑	↑	↓

According to the Figure 21 and Table 3, using the same way to indicate the operating regions for MPPT, the determination of perturbation is same as the for PLC condition. The difference between these two operating conditions is that the operating regions II and III for PLC condition don't exist in the MPPT case. So, it can be claimed that this kind of identification based on the change of $\left|p_{diff}\right|$, p and u can integrate the MPPT and PLC power control demands without recognition of operating condition.

Obviously, similar as MPPT condition, P&O-F method for PLC condition also has the drawback such as the problem about the convergence of perturbation step-size around the target operating point. Thus, the variable step-size P&O method for PCL is logical to be developed based on the same principle presented in Chapter II. 2.

III.2. Perturbation and observation with variable step-size

In order to integrate the P&O-INR and P&O-FL MPPT methods into PLC condition, the determination of perturbation direction is separated from the calculation of variable step-size. Similar as P&O-F method for PLC condition, the determination of perturbation direction is based on the logic presented in Table 2 and Figure 20. However, the calculation of variable step-size is also different from the MPPT condition: as presented in Figure 20, for the PLC condition, there is one "low voltage—high current" operating point supplying the same amount of power. If the calculation of variable step-size works for all four regions, the moving speed will be decreased around this operating point which is opposite to the principle of variable step-size application. So, the variable step-size calculation will just works at regions III and IV, for both of Newton-Raphson method and fuzzy logic method.

III.2.1. Newton-Raphson method

Since the regulating target of P&O PLC method is to minimize the difference between the required power and the actual power, based on (8), the x variable is still the DC bus voltage u_{BUS}, but the function $f(x)$ is the p_{diff}. Thus, the iterative methodology is organized as follow:

$$\begin{aligned} \Delta p_{diff}(k) &= \left|p_{diff}(k)\right| - \left|p_{diff}(k-1)\right| \\ \Delta u(k) &= u(k) - u(k-1) \\ \Delta u &= sign \bullet \left\| p_{diff}(k) \right| / \left(\Delta p_{diff}(k) / \Delta u(k) \right) \Big| \\ u_{ref}(k+1) &= u_{ref}(k) + \Delta u \end{aligned} \qquad (14)$$

The value of variable "*Sign*" is determined by the identification of operating region, what means using the Table 2. If system is operating at region I, II, or III, "*Sign*" is positive one; if it works at region IV, "*Sign*" equals negative one.

In (14) it is shown the iterative approach following the principle of Newton-Raphson method, but according to several experimental results, which will be explained in Chapter V, this approach cannot decrease the step-size significantly for both MPPT and PLC conditions. Essentially, the root is that, based on the power distribution of wind generation system, the same perturb amount of voltage introduces different change of power for MPPT and PLC conditions. In detail, the gradient, seen as the change of power respect to the change of voltage, at the maximum power operating point is almost zero. However, at other operating points, this gradient has a positive or negative value.

With those reasons mentioned above, in this thesis, one improved P&O-NR method for PLC is introduced as follow:

$$slope(k) = \frac{p(k) - p(k-1)}{u(k) - u(k-1)}$$

$$\begin{cases} \Delta u = sign \bullet \left\| p_{diff}(k) \right| / \left(\Delta p_{diff}(k) / \Delta u(k) \right) \Big|, if \left| slope(k) \right| \le 1 \\ \Delta u = sign \bullet \dfrac{\left\| p_{diff}(k) \right| / \left(\Delta p_{diff}(k) / \Delta u(k) \right) \Big|}{\left| slope(k) \right|}, if \left| slope(k) \right| > 1 \end{cases} \qquad (15)$$

$$u_{ref}(k+1) = u_{ref}(k) + \Delta u$$

The mechanism is that: when demanded power value is far away from the potential maximum power, value of $\left| slope(k) \right|$ is bigger than 1. So the calculated perturb step-size will divided by this value to make sure the convergence is significant; when the demanded power value is close to the potential maximum power where the $\left| slope(k) \right|$ is not bigger than 1, the result of perturb step-size calculated by (14) converges well enough. So, the result calculated by (14) can be accepted.

Taking into account the above considerations, it can be stated that with this variable step-size algorithm, the P&O-INR method can deal with the convergence of variable step-size for both conditions of MPPT and PLC.

III.2.2. Fuzzy Logic method

Following the logic of P&O applications for PLC condition, the used fuzzy logic will chose new input variables and new fuzzy reasoning rules. As similar as application of Newton-Raphson method for PLC condition which has been presented in Chapter III.2.1, the proposed fuzzy logic application for PLC condition selects the $slope(k)$ (calculated by (14)) and $\left| p_{diff}(k) \right|$ as input variables, while the output of fuzzy logic method is still the perturb step-size for DC voltage.

At the process of fuzzification, the fuzzy set for $slope(k)$ consists of five membership functions: they are "big negative", "negative", "zero", "positive" and "big positive", respectively marked as $\{\text{bn,n,z,p,bp}\}$; but the fuzzy set for $|p_{diff}(k)|$ are still "negative", "zero", and "positive" which marked as $\{n, z, p\}$. Similar as the design for P&O-FL MPPT method, both of two inputs will be normalized ($slope(k) \to e_1$ and $|p_{diff}(k)| \to e_2$) before transformed into the form of the degree of membership whose value is between 0 and 1. Detail shapes of membership functions are displayed as in Figure 22. All the shapes of proposed membership functions are chosen based on experimental experiences.

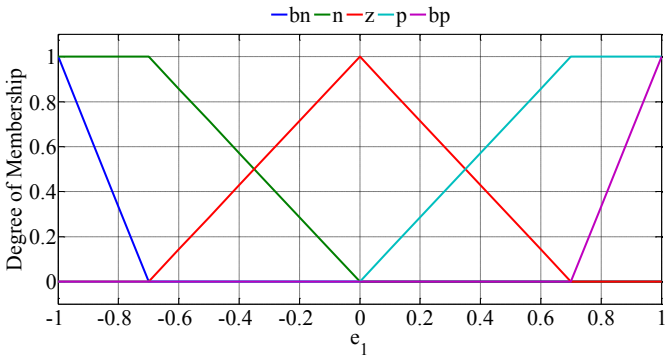

a

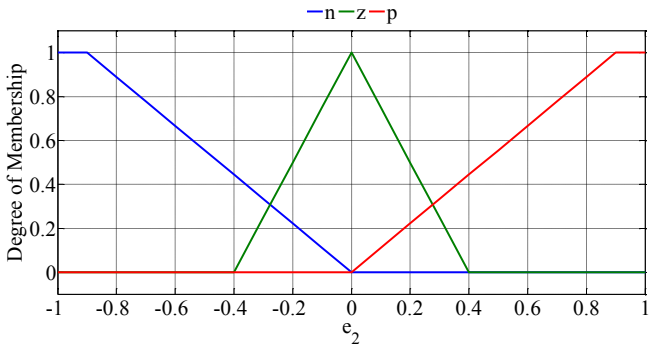

b

Figure 22: Membership functions for inputs: (a) e_1 ; (b) e_2

The fuzzy reasoning rules are described as in Table 4.

Table 4 – Fuzzy rules for PLC

Output S		e_2		
		n	**z**	**p**
e_1	**bn**	0	0	0
	n	+	0	-
	z	+	0	-
	p	+	0	-
	bp	0	0	0

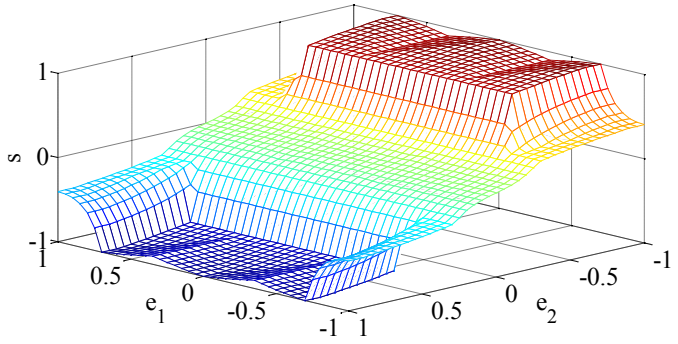

Figure 23: Fuzzy reasoning surface.

Figure 23 shows the fuzzy reasoning surface of the proposed fuzzy logic, and the Table 4 explains the "if-then" reasoning role. The step of "if" defines a fuzzy region in the input space while the "then" step specifies the output in the fuzzy region. With a logical operator, membership functions values evaluating the degree of each activated rule express that how the "if" step of each rule is satisfied. Subsequently, the fuzzy set in the "then" step of each rule is determined. Finally outputs of each rule are combined to form one fuzzy set. In this work, the Mamdani fuzzy inference system fuzzy toolbox is used.

After the fuzzy reasoning process, given output s is defuzzified using the membership function presented in Figure 24. Several defuzzification operators are mentioned in [59], but the most used one is the centroid, or center of gravity, which is also selected by this thesis. Then, the result will be anti-normalized into the real perturb step-size by one coefficient determined based on experience.

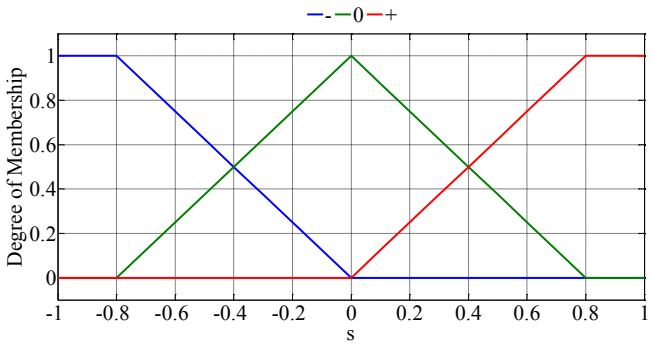

Figure 24: Membership function for s.

III.3. Online update lookup table method

This approach follows the principle of the lookup table method presented in Chapter II.3. The selected input of this method is not just the rotational speed, but also the demanded power value. Output variable of this method is still the DC bus voltage.

In theory, measuring and storing information about all operating points matching the PLC condition can establish one binary function, which is easy to fulfil requirements. However, according to devices used in our experimental platform, fixing the power value is not easy to be guaranteed during whole pre-measuring work.

In order to reduce the uncertainty in the process of measuring operating points' information, the pre-measured data about studied system is still sorted by different wind speed while varying the DC bus voltage. Then, data for each wind speed is used to fit one function, so that there are several curves indicating different wind speeds.

Different from MPPT condition, since PLC method should help the system producing demanded power amount, the actual curve for calculating reference of DC bus voltage in the fact is updating with the vary of demanded power value. In this method, using just the operating points at the "low current – high voltage" side could match our design mentioned in Chapter III.1. In experiments, it can be claimed that calculation time is short enough to avoid introducing additional time delay, which will be presented in Chapter V.

Based on this mechanism, the proposed PLC method can be marked as online update lookup table method. The flowchart describing the principle in general way is displayed in Figure 25.

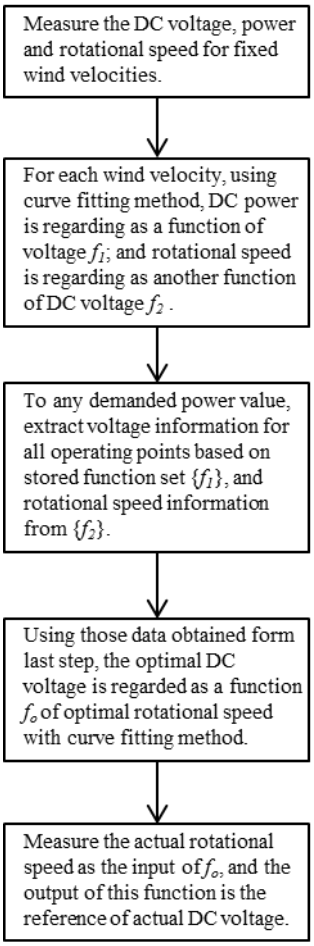

Figure 25: Flowchart about online update lookup table method.

III.4. Conclusion

Chapter III elaborates the theories of each proposed PLC method, which are designed to deal with the demand of operating either at the potential maximum power level or following the power level asked by load. According to description of presented methods, all of them, in fact, were designed to cope with the integrated power control issue that mixed MPPT goal and PLC goal together avoiding the switching effect between these two operating modes.

Three direct methods are also based on the principle of perturb and observe logic, but the difference with pure MPPT condition is that the rule to determine the direction of system operating point's movement is composed by three variables of system: the change of DC bus voltage, the change of actual DC bus power and the change of difference value of actual DC bus power and the demanded value. Adding just one variable into the logic of determination of P&O can extend the MPPT method covering PLC control topic. This is the contribution of this thesis. Since the objective variable has changed, the way of calculating variable step-size for P&O-INR and P&O-FL method are relatively varied. All three

direct methods don’t need the alternative identification about that whether the system is asked to extract power as much as possible or response the power demand from load side.

The proposed indirect method also naturally integrates the control strategy of MPPT and PLC, automatically updating mathematic relationship between chosen parameters of system respecting the change of demanded power value. So, as long as the given power value is reasonable, this method also need no information of identification about system’s operating mode. Inevitably, this method requires precise information of studied system, such as working points’ distribution, to supply good performance. The more data about system has been collected before implementation, the better performance can be achieved, while the sensitivity of the parameters drifts also increase theoretically. Determination of all parameters about each method are presented and discussed in Chapter V. Contrast experiments are also displayed in that Chapter.

Chapter IV. Experimental Platform

The detail information of experimental platform emulating the small scale wind generation system is presented in this Chapter. The approach of emulating wind speed and blades of one existing small scale wind turbine is in traduced at first. The model and operating condition for each device, such as the chosen PMSG and other electrical equipment, also can be found.

The power distribution and dynamic characteristics of the studied system are revealed and analyzed subsequently. Based on the steady state and dynamic characteristics, several fundamental experimental tests are presented to explain how to assist those proposed MPPT and PLC algorithms realize their due features, preparing the comparing experimental tests described in Chapter V.

IV.1. Emulator wind speed and blades and generator

According to discussion presented in Chapter I, the structure of studied system must include the blades and the hub of wind turbine, a generator and the electrical energy conversion structure. Since supplying a real controllable air flow makes whole platform difficult to maintain constant operating condition, the wind speed and the mechanical characteristic of blades and hub are decided to be emulated by a mathematic model in the Matlab®/Simulink® environment.

According to the Chapter I.1.1, the power harvested by the wind turbine is given as in (3). The most important parameter needs to be identified is the power coefficient c_p. The most used way to emulate fitted equation for c_p is based on the following [35]:

$$\begin{aligned} c_p(\lambda,\beta) &= 0.5\left(116\frac{1}{\lambda_i} - 0.4\beta - 5\right)e^{-(21/\lambda_i)} \\ \frac{1}{\lambda_i} &= \frac{1}{\lambda + 0.08\beta} - \frac{0.035}{1+\beta^3} \end{aligned} \qquad (16)$$

For the present work in this thesis, the pitch of the blades of the small scale wind turbine is fixed, the pitch angle β in (16) is set to zero. So, there are other researches using polynomial function to fit the curve, such as in [46], a 5th order polynomial function.

In this thesis, considering the rated power level defined by the user, a 7th order polynomial function was selected because this function was obtained from one 1 kW HAWT product fabricated by Bergey Excel 1 [77], whose blade radius is $R = 1.25\text{m}$. This 7th order polynomial function is described as follow:

$$\begin{aligned} c_p(\lambda) &= \sum_{K=0}^{7} a_K \lambda^K \\ a_7 &= -4.1\times10^{-8}; \quad a_6 = -4.2\times10^{-6}; \\ a_5 &= 2.1\times10^{-4}; \quad a_4 = -4.2\times10^{-3}; \\ a_3 &= 1.65\times10^{-2}; \quad a_2 = -1.9\times10^{-2}; \\ a_1 &= 1.7\times10^{-2}; \quad a_0 = -1.9\times10^{-3} \end{aligned} \qquad (17)$$

Based on (3) and (17), assuming that the air density ρ is constant and equal to 1.225kg/m^3, the distribution of harvested power p_{AERO}, which is regarded as the function of rotational speed, can be illustrated as in Figure 26.

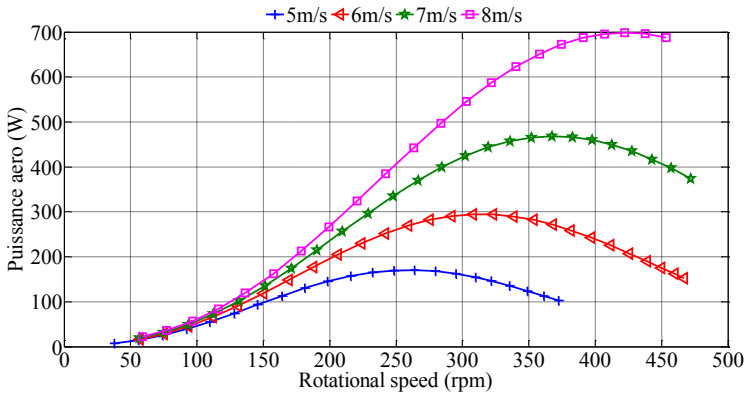

Figure 26: Power distribution for p_{AERO}.

In experimental platform, this emulator consists of a control board for rapid control prototyping (dSPACE DS1103) a three-phase industrial driver (C3S063V2F10 from Parker) commanded by the dSPACE, and a three-phase permanent magnet synchronous motor (PMSM) (NX430E -AJR7000 from Parker). The PMSM is driven to supply the rotational speed and mechanical torque calculated by (3), (17) and function following:

$$\frac{1}{\omega}\left(p_{AERO}-p_{EM}\right)=J\frac{d\omega}{dt}+F\omega \qquad (18)$$

With the equivalent inertia of blades and hub $J=1.5\text{kg}\cdot\text{m}^2$, the viscous damping coefficient $F=0.06\text{Nm/rad}$, and the electromagnetic power p_{EM}, which is calculated by (19).

$$p_{EM}=u_A i_A+u_B i_B+u_C i_C \qquad (19)$$

In which, $\{u_A,u_B,u_C\}$ and $\{i_A,i_B,i_C\}$ separately are the three-phase voltages and currents of the generator in this platform, another PMSM as the same type as the one used for emulator of wind and blades. Parameters of this PMSM are: the number of pole pairs is 5; the measured phase resistance is 1.46 ohms; the measured flux linkage of the magnets is 0.393 Wb; the self and mutual inductance in average are 0.0051 H and 0.0005 H; and the inertia of rotor is 42.6×10^{-5} kg×m^2.

IV.2. Electrical conversion structure

Following the output of generator of the studied system, a three-phase diode-bridge, whose type is SEMIKRON SKD 51/14, is used to transform the AC power into DC form. As presented in Figure 27, after this diode-bridge, one capacitor C_{BUS} of 1 mF and one inductor L of 50 mH (with resistance 267.5 milliohms) constitute the DC BUS keeping an acceptable balance between filtering and system dynamics. Driving by dSPACE DS1103 (sample time set as 100 µs), an insulated gate bipolar transistor (IGBT) module (SEMIKRON SKM100GB063D) and another driver (SEMIKRON SKHI22A) realize the MPPT

and PLC commands. The DC/DC boost converter, constituted by the used inductor and IGBT, operates with approximately 0-300V input for a constant 400V output voltage. One programmable electronic load (PEL, PL-6000-A Puissance+) and a 1.1 mF capacitor C_{PEL} are used to emulate the power demand. For all operating points of the studied system, the PEL maintains the output voltage u_{PEL} of boost converter at 400 V [31, 32,33].

Gathering information of all equipment, the schema of experimental platform is illustrated in Figure 27 and the photo of real system is presented in Figure 28.

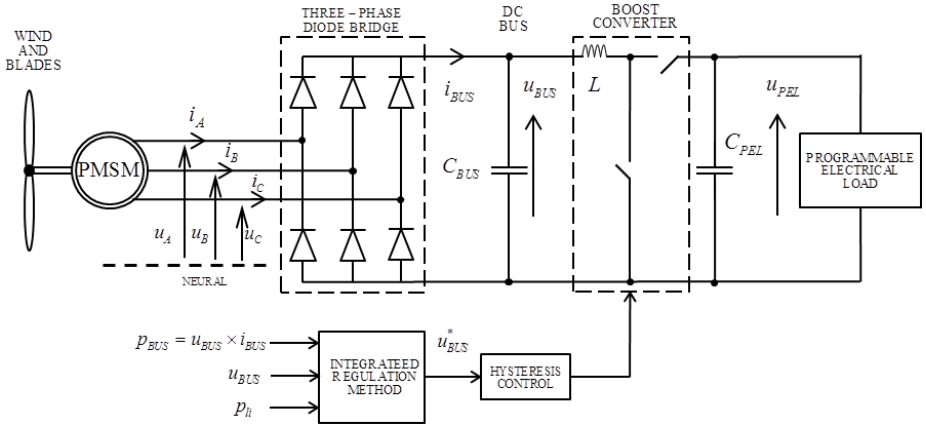

Figure 27: Schema of experimental platform.

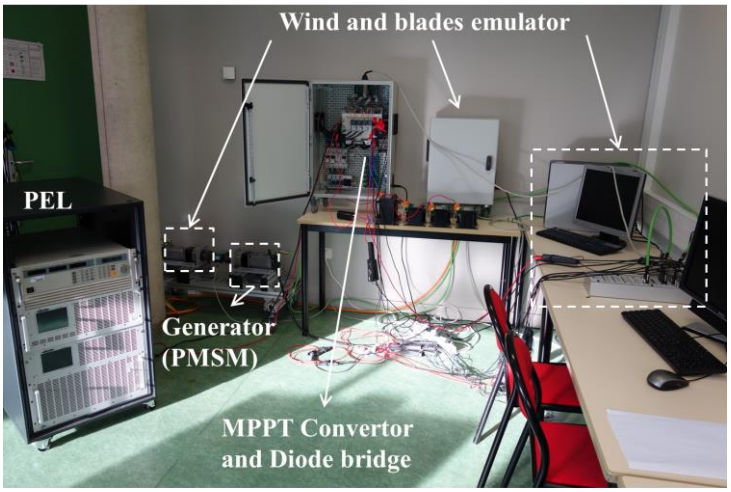

Figure 28: Test bench photo.

Based on the experimental platform stated in the previous paragraph, the distributions of the harvested power p_{AERO} and the DC form electrical power p_{BUS} are separately revealed regarding as the function of DC voltage u_{BUS} and DC current i_{BUS}, in Figure 29 and Figure 30.

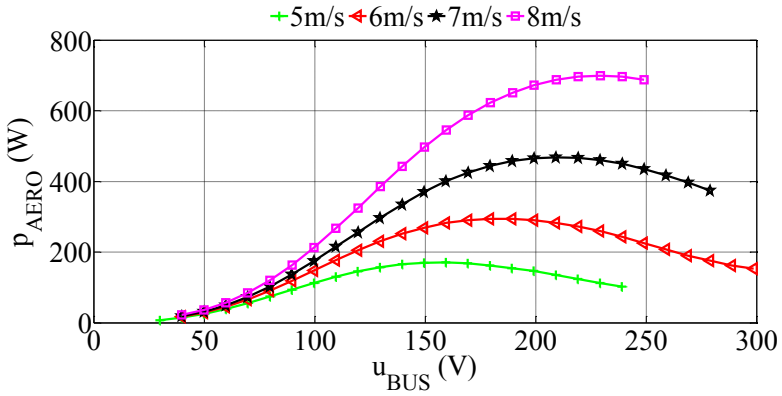

a

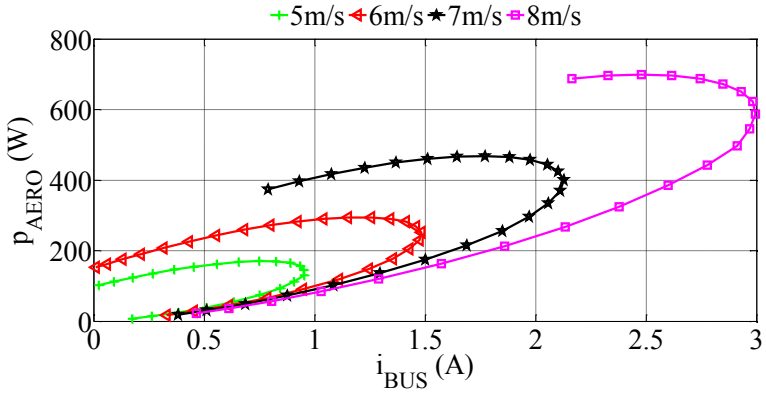

b

Figure 29: Experimental evolution of aerodynamic power p_{AERO}.

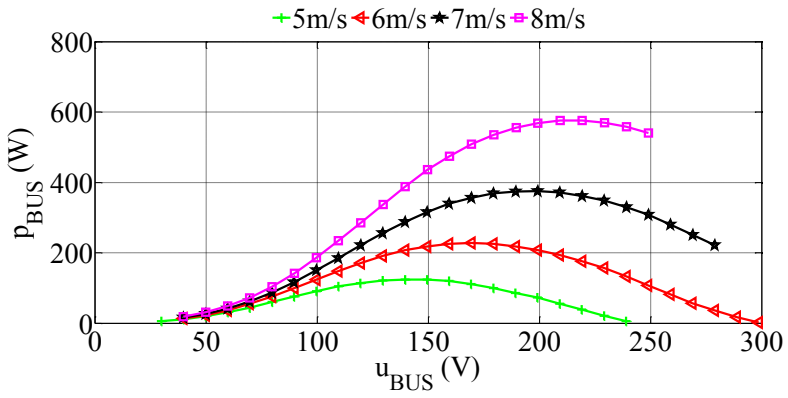

a

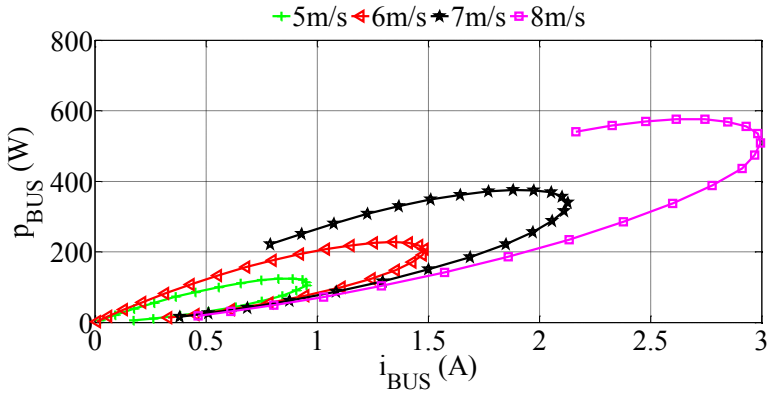

b

Figure 30: Experimental evolution of electrical power p_{BUS}.

According to these experimental results shown in Figure 29 and Figure 30, it can be noted that: first, resulting from losses of power from the input side of PMSM to the output side of three-phase diode bridge, operating MPPs of electrical power curves are not the same operating MPPs of aerodynamic power ones; then, for limited power demand, aerodynamic power curves supply operating points different from electrical power curves. So, for both MPPT and PLC operating conditions, aerodynamic power curves are useless even as indirect references. This preliminary conclusion is important to the control strategy and the MPPT and PLC algorithm application. Based on the characteristics of electrical power curves, the DC bus voltage u_{BUS} is chosen as the variable to realize the modification of system's operating point. It is axiomatic that, for each wind speed, one value of i_{BUS} indicates two different working points within the operating range. So, comparing with i_{BUS}, u_{BUS} is more suitable to be regarded as the reference variable, since each value of u_{BUS} indicates one unique operating state, at the beginning of research.

IV.3. Control loop

In Chapter IV.2, the steady-state characteristics of experimental platform has been revealed and analyzed. The controlled variable also has been determined based on these steady-state characteristics. As stated in the previous paragraph, in order to simply the comparison of MPPT or PLC algorithms, we tried to decouple the effect of MPPT and PLC algorithms from control loop, by using a fixed and simple controller, hysteresis controller. For the control loop, the commanding goal is to drive the system following the reference of DC bus voltage, which can be calculated by MPPT algorithm or PLC algorithm. The hysteresis was chosen based on its advantage of high dynamic performance and low implementation difficulty [32, 78].

A set of step inputs experiments of DC bus voltage u_{BUS} has been implemented to investigate the dynamic of the system response. The operation conditions are: wind speed is 8 m/s, based on two initial DC voltages: 150 V and 200 V, the step input is 10 V. These selected two initial DC bus voltages indicate low power and high power operating point for 8 m/s wind velocity. The actual response of DC bus voltage has been presented in Figure 31 and Figure 32.

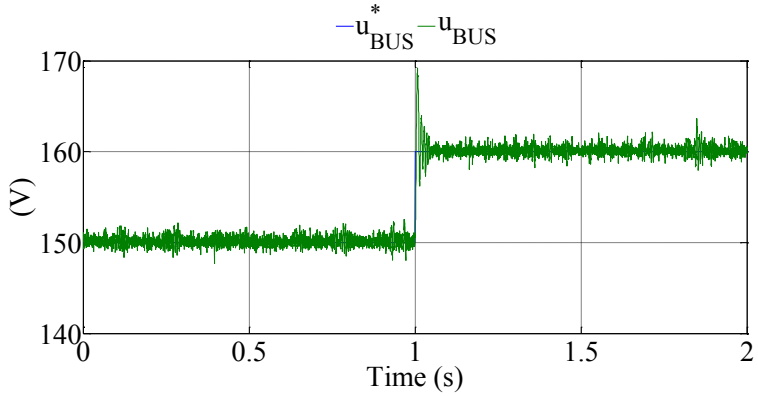

Figure 31: Experimental response of DC voltage at low power operating point.

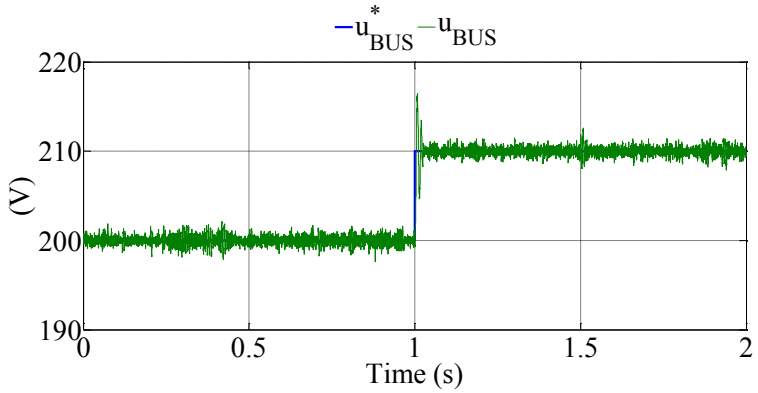

Figure 32: Experimental response of DC voltage at high power operating point.

In both of these two figures, u_{BUS}^{*} is the reference of DC bus voltage. Beside the actual DC bus voltage response, the dynamic of three-phase voltages and currents are also analyzed (Figure 33 and Figure 34). In order to analyze the system's electrical operating mode during the operating process of hysteresis controller, the enlarged experimental evolution of three-phase voltages and currents for both cases are presented in Figure 35 and Figure 36.

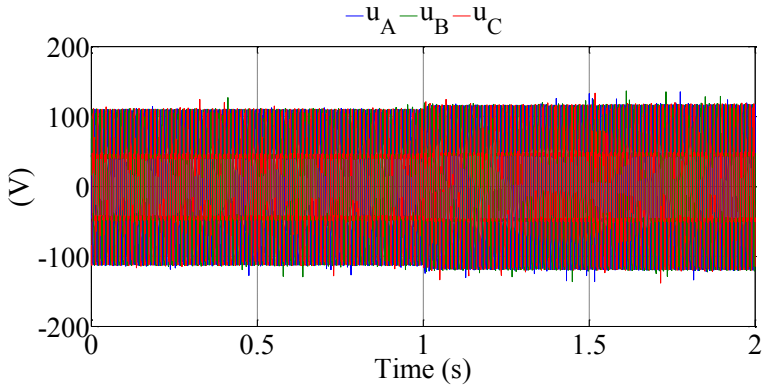

a

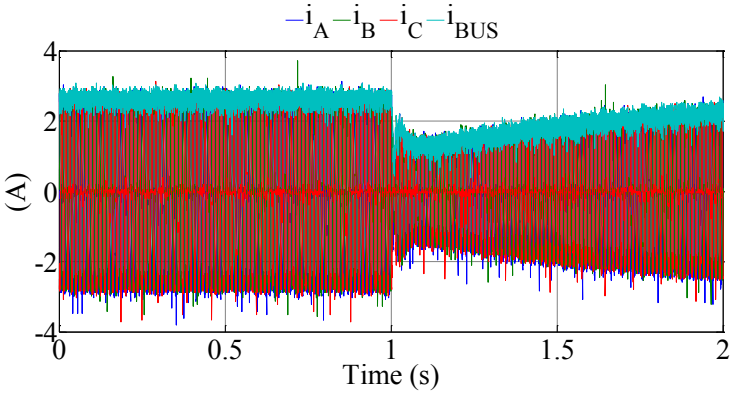

b

Figure 33: Response of three-phase voltages and currents at low power operating point.

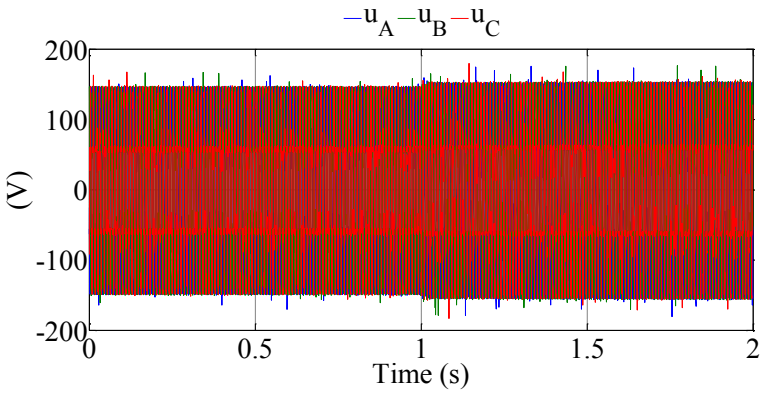

a

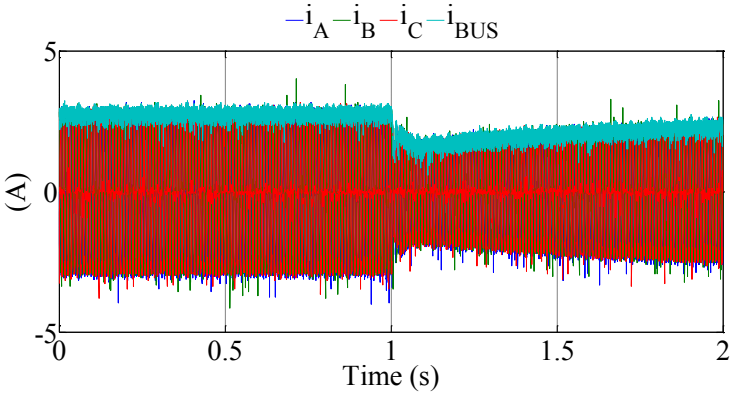

b

Figure 34: Response of three-phase voltages and currents at high power operating point.

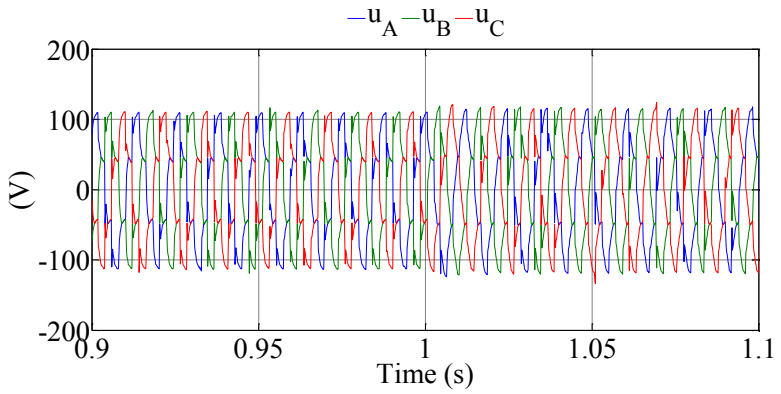

a

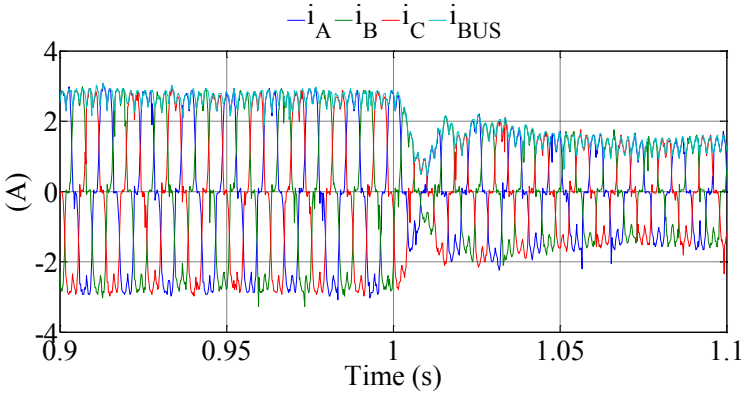

b

Figure 35: Enlarged response of three-phase voltages and currents at low power operating point.

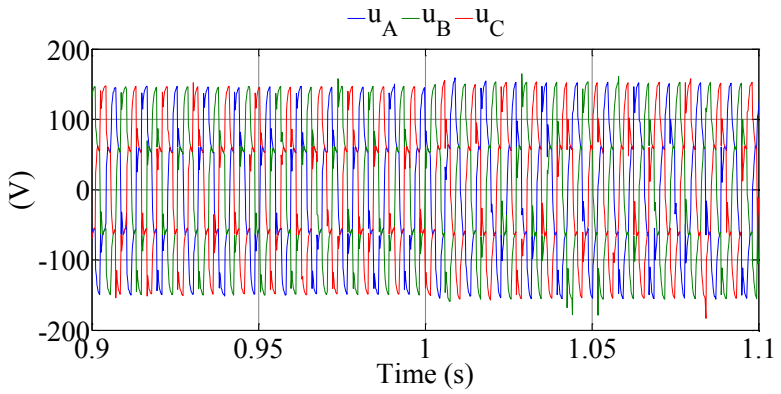

a

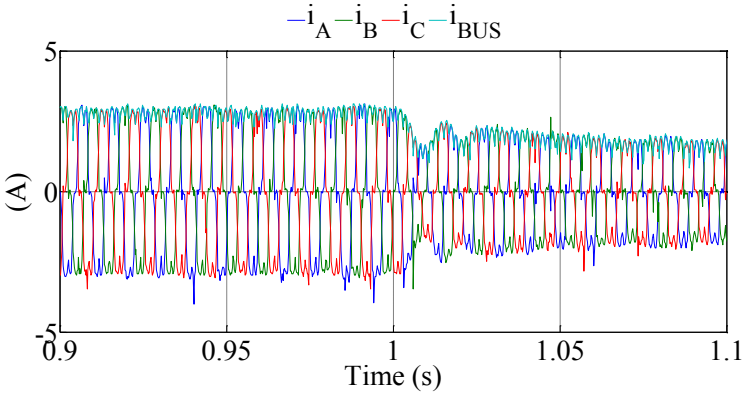

b

Figure 36: Enlarged response of three-phase voltages and currents at high power operating point.

Based on information from these figures, it can be said with certainty that the hysteresis controller suffices the requirement of rapid response, without the distortion of system operating mode, since wave forms of three-phase voltages and currents do not transform significantly. Since the hysteresis controller is simple and robust control method, it is suitable to be used to compare different MPPT or PLC algorithms.

After studying the control loop itself, the cooperation between the hysteresis controller and the MPPT or PLC algorithms needs to be analyzed. Thus, for both of 150 V and 200 V initial voltages, one set of step input with different amplitudes were introduced to observe the electrical power's response respect to the varying of DC voltage.

This set of step input is {0.5 V, 2.5 V, 5 V, 7.5 V, and 10 V}. The experimental evolutions of the actual DC voltage are illustrated in Figure 37 and Figure 38.

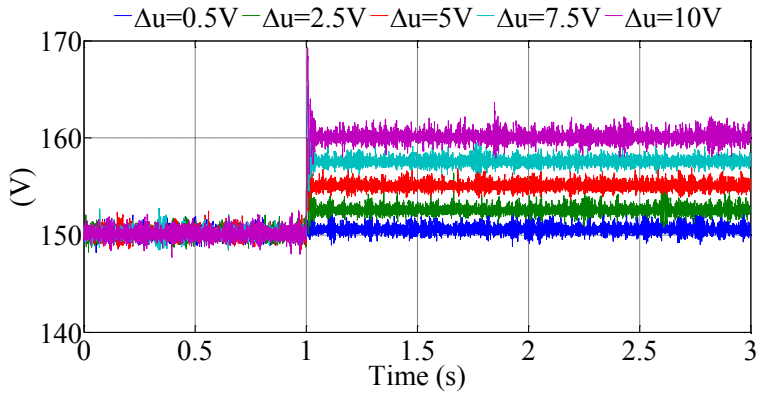

Figure 37: Experimental evolution of DC voltage at low power condition.

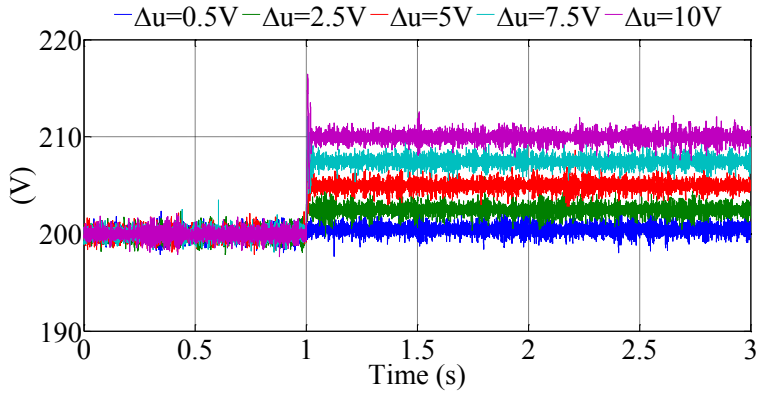

Figure 38: Experimental evolution of DC voltage at high power condition.

With this set of step input, the responses of electrical power p_{BUS} are presented in Figure 39 and Figure 40. According to those figure, it can be seen that the power response contains the high order dynamic characteristic, which can also be found in the dynamic responses of the three-phase currents and DC current shown in Figure 33, Figure 34, Figure 35 and Figure 36. Considering our proposed MPPT and PLC algorithms based on the principle of P&O, information about the dynamic process of power response should not be observed by those mentioned algorithms. Otherwise, experimental evolutions of p_{BUS} presented in Figure 39 and Figure 40 are the measured raw data. It is clear that those signals contain the high frequency noise, which is not good for extracting the precise information about operating condition. Consequently, one low-pass filter has been added with the cut-off frequency 30 Hz to give prominence to the regulation time of power response. The experimental evolutions with this low-pass filter are displayed in Figure 41 and Figure 42.

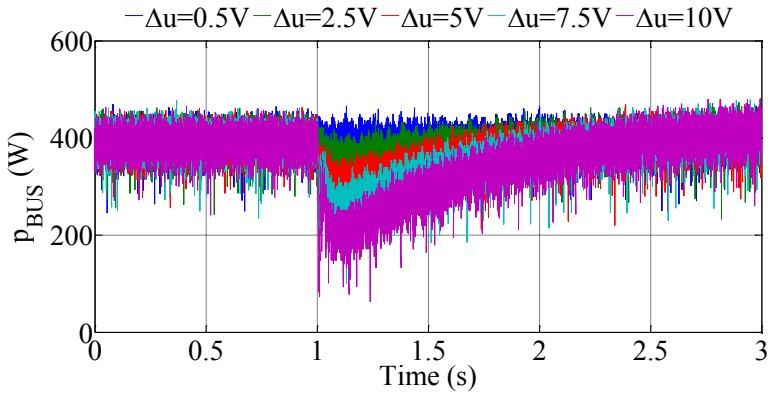

Figure 39: Experimental evolution of electrical response at low power condition.

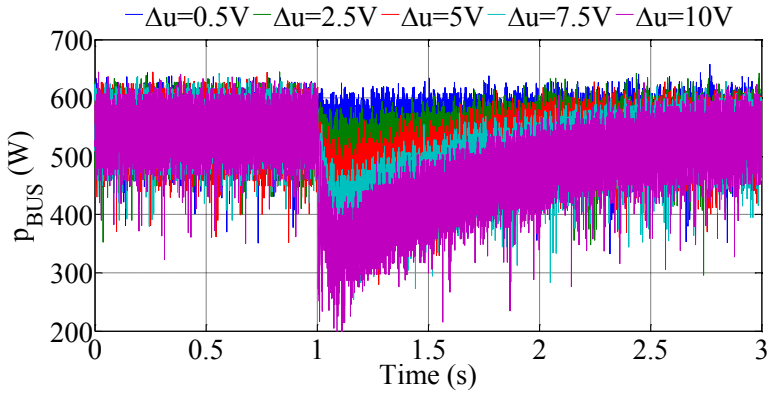

Figure 40: Experimental evolution of electrical response at high power condition.

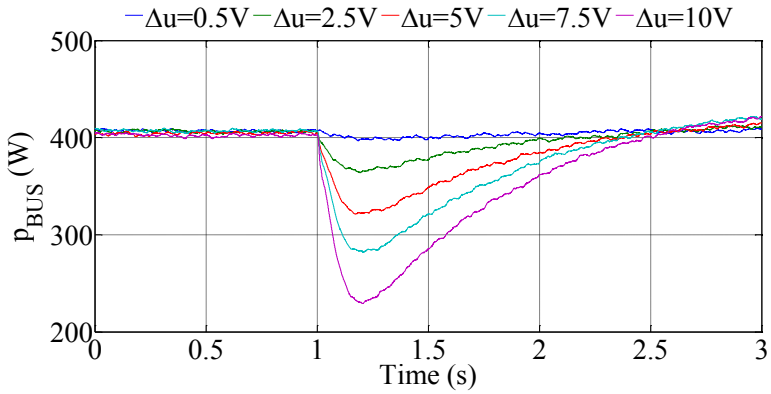

Figure 41: Experimental evolution of electrical response at low power condition with low pass filter.

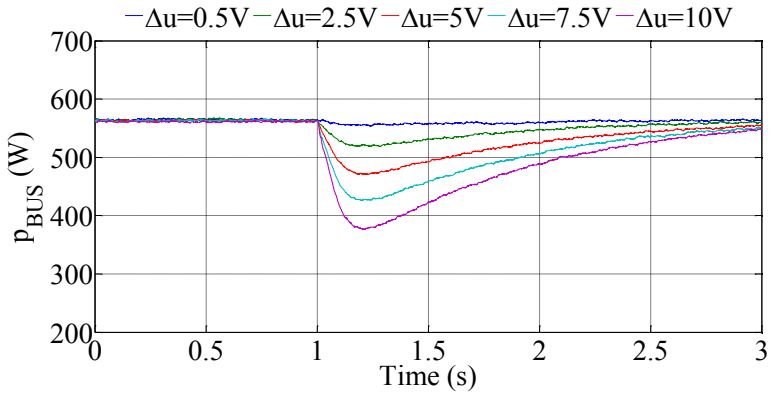

Figure 42: Experimental evolution of electrical response at high power condition with low pass filter.

According to the results from Figure 39 to Figure 42, under the control effect of hysteresis controller, the DC bus power p_{BUS} responds the step input of the DC voltage u_{BUS} with high order dynamic characteristic. If the observation action operated continually (in fact, if it operated each calculation time of Matlab®/Simulink® model), all the MPPT and PLC algorithms using P&O principle would made the wrong determination of perturbing direction. Thus, one important parameter to applying all P&O-class MPPT and PLC algorithms, the observation time interval was chosen as 2 seconds to make sure that whatever the perturb step-size is big or small, the determination of next perturbation's direction will just be calculated based on the information of steady- state operating points about the studied system.

By contrast, the lookup table algorithms for MPPT and PLC condition used the rotational speed n (using the unit rpm) as the input variable instead of actual DC electrical power p_{BUS}. Therefore, the response characteristic of rotational speed respect to the varying of the DC voltage also needs to be analyzed.

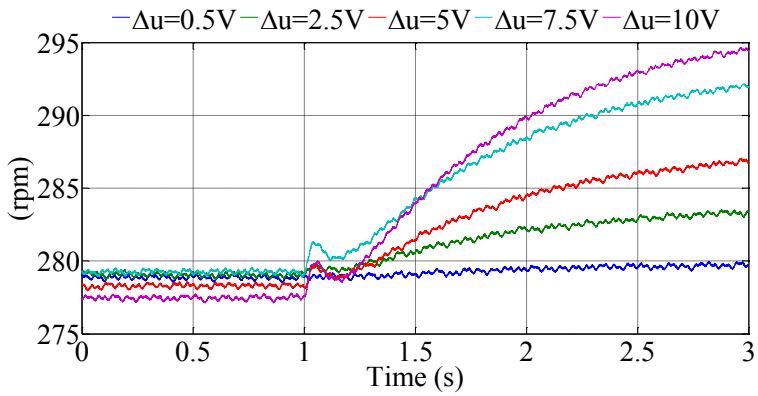

Figure 43: Experimental evolution of rotational speed at low power condition.

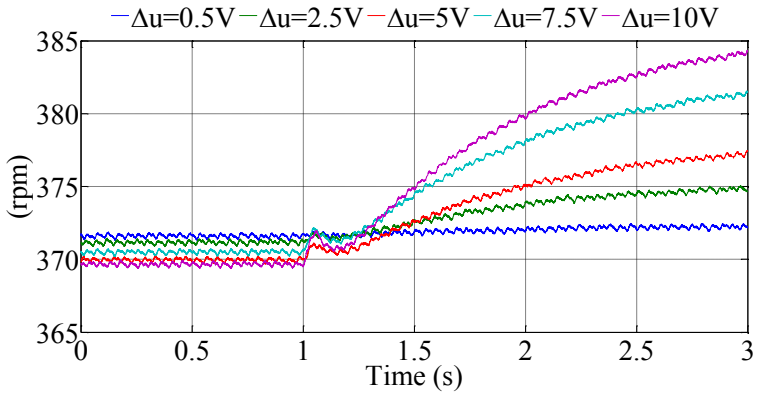

Figure 44: Experimental evolution of rotational speed at high power condition.

The Figure 43 and Figure 44 can support the following conclusion: even the rotational speed response respect to the DC voltage varying also presents the complex and high order behavior, but this part of information will not confuse the determination of proposed lookup table algorithms. So, for used experimental platform, lookup table algorithm for MPPT and PLC condition can operate continually (as mentioned above, in fact, it operates with the Matlab®/Simulink® model calculating time step).

IV.4. Conclusion

In this Chapter, details of the used test bench are presented. Types and parameters of all devices, structure of whole system are displayed at first. The emulator of wind velocity and mechanism of blades modeled in Matlab®/Simulink® indicates one small scale wind generation system whose rated power is 1000 W. Based on the distribution of operating points of system limits, the choice of the control variable whatever for MPPT or PLC. Thus, several experiments were planned to decide the parameter used to modify the operating point. According to these results, the DC bus voltage is more suitable to be the modifying parameter than the DC bus current. Also, the design of control loop has been presented after this determination to ensure when the output of MPPT or PLC method arrives, the actual operating condition can rapidly respond. Results of some experiments proved that using the hysteresis control law the DC bus voltage can rapidly respond reference from MPPT or PLC methods, without introducing alternative distortion of electrical variables. Then, with respect to each implemented MPPT method and PLC method, dynamic characteristics of system were revealed by experimental tests introducing sets of DC bus voltage step-input, to observe the response of the actual power and mechanical rotational speed. These results helped to determine parameters of each MPPT and PLC method, which will be described in the next chapter.

Chapter V. Experimental results and analysis

In this Chapter, several groups of experimental test will be displayed.

The first group of experiments is used to supply the necessity of the P&O-INR algorithms for MPPT operating condition. The results for this set of experiments prove that the P&O variable step-size calculated by classical Newton-Raphson method cannot work properly with the small scale wind generation system. And, they also supply our improvement about this algorithm.

The second group of experiments contains three sets of comparison experiments for MPPT operating condition. They used three different wind velocity profiles: two designed profile and one recorded real wind speed data in Compiegne, France, on January 15, 2015, to give prominence to different characteristics of all proposed MPPT algorithms.

The last group of experiments only used one limited power profile calculated randomly based on the recorded real wind velocity profile mentioned above. All four proposed PLC algorithms were compared and analyzed together.

V.1. Experimental verify of P&O-INR algorithm

V.1.1. MPPT condition

As stated in the previous paragraph, Chapter II.2.1, P&O variable step-size method calculated by classical Newton-Raphson method, which follows the iteration presented in (9), cannot respond properly. It demonstrated one kind of overly strong convergence capability about the perturb step-size. Aiming to verify the mentioned drawback and the improvement of P&O-INR method, one step jumping wind profile was chosen to highlight rapid change of real wind. It can be easy to see that each step vary of wind velocity is big enough to introduce a huge difference of electrical power between. This huge difference of electrical should results in a big step-size starting to move the operating point of system. However, as presented in Figure 46, the actual power at that time point cannot respond this significantly difference in electrical power. As a comparison, the power response of P&O-F method and the classical Newton-Raphson P&O method with a “Kick It Out” trigger, which forces the MPPT output using the maximum value of step-size based on the amplitude of measured change of electrical power, are presented. At the same time, the P&O-INR method’s power response is also presented in Figure 46. And, the Figure 47 and Figure 48 show the evolution of voltage and actual step-size.

In Figure 46, Figure 47 and Figure 48:

p_{BUS}^{*} is the potential electrical power based on the wind speed profile;

p_{BUS-F} marks experimental electrical power following P&O MPPT with fixed step-size (5Volts);

p_{BUS-V} indicates experimental electrical power following P&O MPPT with variable step-size based on classical Newton-Raphson method, which is calculated by (9).

p_{BUS-V1} is the power response of classical Newton-Raphson variable step-size P&O method with "Kick It Out" trigger.

$p_{BUS-Vart}$ is the result of P&O-INR method.

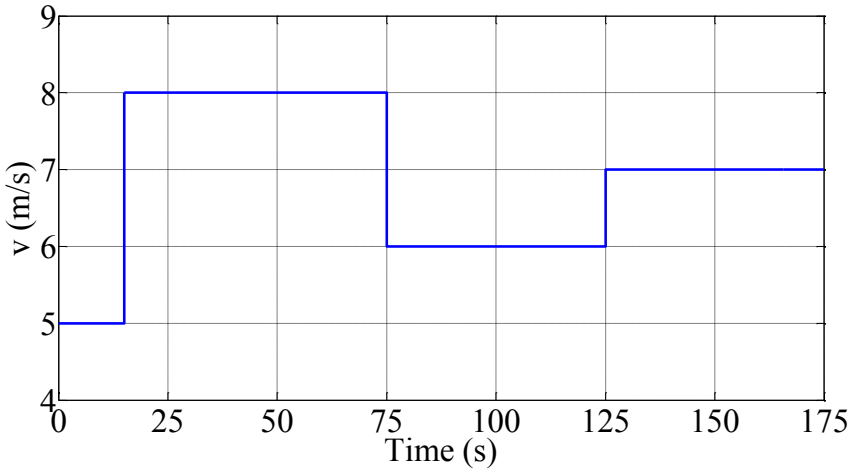

Figure 45: Profile of wind velocity.

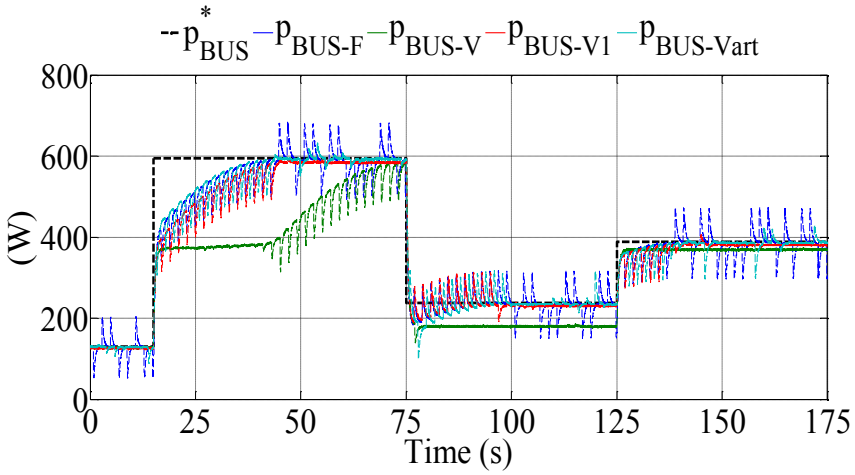

Figure 46: Power responses.

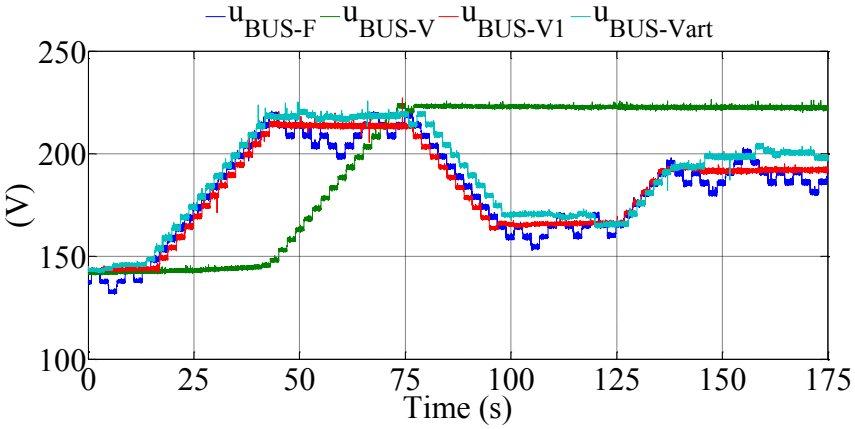

Figure 47: Evolution of DC voltage.

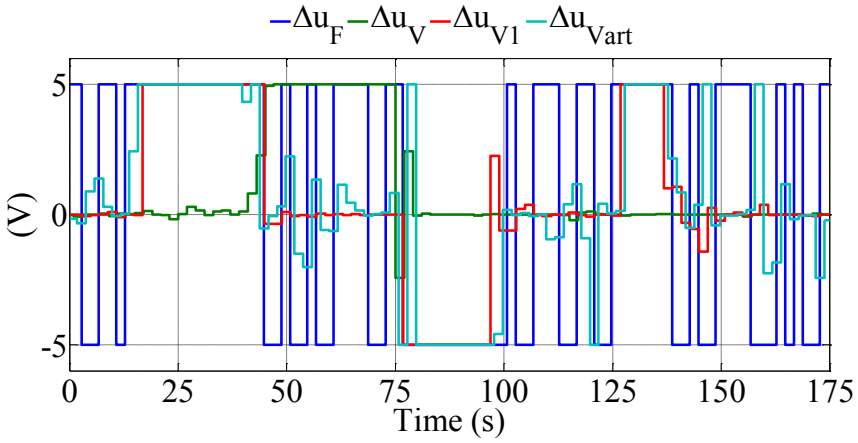

Figure 48: Experimental evolution of actual step-size.

As stated in the previous paragraph, classical Newton-Raphson method (remarked with "-V") failed to respond the rapid change of wind velocity. From the power response and the actual variable perturb step-size, it is clear that the classical way needs long time to start the movement of operating point which should occurs just after the vary of wind velocity.

Otherwise, the P&O variable step-size method using the "Kick It Out" trigger (remarked with"-V1") also has its drawback. Since it used the amplitude as the threshold of this trigger, there exists a numerical parameter demand to be determined by the experiences of designers. This weakens the general applicability of the algorithm. Moreover, focusing at the power evolutions around MPP, this algorithm stabilized at a power value lower than the P&O-F and P&O-INR algorithms.

All things considered, it can be safely said that the proposed P&O-INR MPPT algorithm sensitively respond to the change of wind speed supplying the effective convergence around MPP without setting any numerical parameters.

V.2. Maximum power point tracking

In this section, two designed wind velocity profiles and one real wind velocity data measured in Compiegne, France, on January 15, 2015 are introduced to compare all proposed four MPPT algorithms. Not only the fundamental functions to being a MPPT algorithm, but also the global dynamic process and extracted energy are going to be analyzed.

V.2.1. Experiment design

- Case 1 Figure 49: a wind profile about 200 seconds is designed to highlight the MPPT capability converging to MPP after wind speed jumps to a new steady value. This case is used to validate the principle of each MPPT algorithm: when wind speed changes, the used MPPT algorithm can drive the system operating at right operating point or not.

- Case 2 Figure 50: reveals the dynamic characteristics of each MPPT algorithm for rapid wind speed changes.

- Case 3 Figure 51: a real wind speed profile is extracted from the recorded real wind speed data in Compiegne, France, on January 15, 2015. The wind speed profile highlights a strained condition with rapid changes. According to the power level of studied system, the cut-in speed value is fixed at 5 m/s.

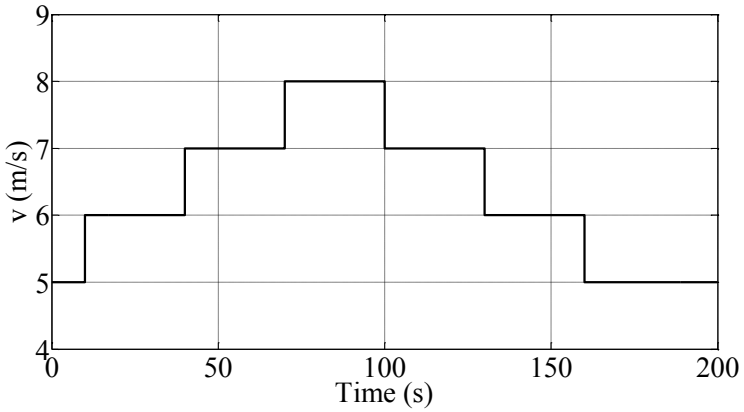

Figure 49: Step input profile of wind velocity.

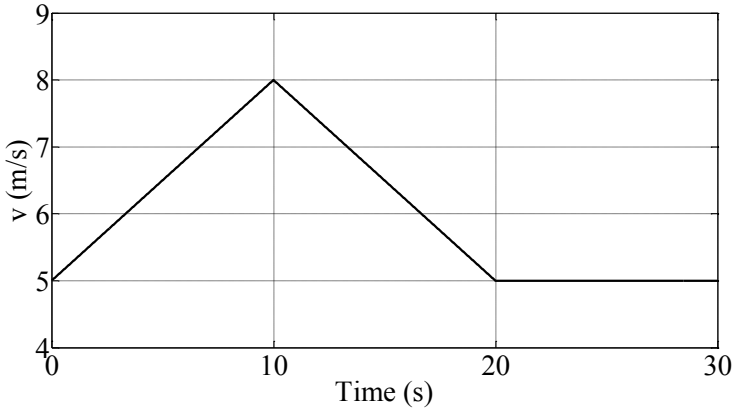

Figure 50: Triangle input profile of wind speed.

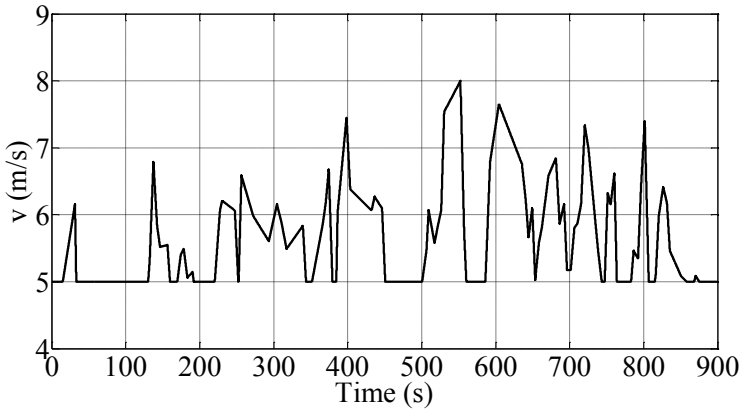

Figure 51: Profile of wind speed based on measured data.

For each experiment case, there are 16 tests were implemented:

To P&O-F algorithm, experimental test with fixed step-size 2.5 V; fixed step-size 5 V and fixed step-size 10 V.

To P&O-INR algorithm, experimental test with maximum limit of variable step-size 2.5 V; maximum limit of variable step-size 5 V and maximum limit of variable step-size 10 V.

To P&O-FL algorithm, the way to realize the modification of its parameters is shown as follow.

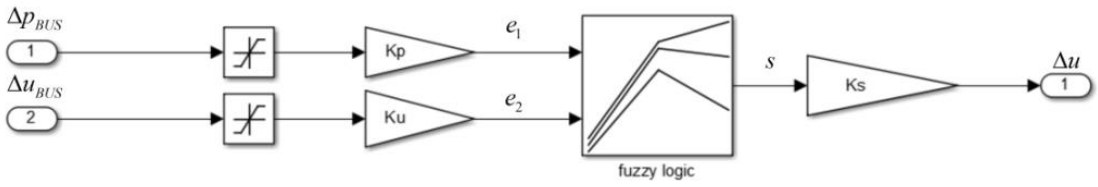

Figure 52: Structure used in Matlab®/Simulink® for normalization and anti-normalization.

Figure 52 shows that input variables, Δp_{BUS} and Δu_{BUS}, are respectively normalized into e_1 and e_2 by the gains K_p and K_u before the process of fuzzification. After the defuzzification of the output s, it is anti-normalized by K_s into the actual perturb step-size Δu. In this thesis, generally, it is acceptable that $K_u \bullet K_s = 1$. Consequently, the determination of values of $\{K_p, K_u, K_s\}$ is the way to optimize the Fuzzy logic method used for MPPT application. And, the implemented combinations in all three experimental cases are cross combination of $1/K_p \in \{2.5,\ 5,\ 10\}$ and $1/K_u = K_s \in \{2.5,\ 5,\ 10\}$.

The last implemented MPPT algorithm is the proposed LT method.

V.2.2. Evolution experimental and analysis

The experimental results are presented in this order: for proposed three direct algorithms, they can be sorted by the fixed perturb step-size or maximum limit of variable step-size, so, the experimental results of three direct MPPT algorithms using the same value as the fixed or maximum limit of variable perturb step-size are presented together. At the end, the results of proposed lookup table algorithm are presented separately.

In each group of results sorted by the value of perturb step-size, subscript '-f' means P&O-F method;

Subscript '-v' means P&-INR method;

Subscript '-lf-2.5' means P&O-FL method with the gain $K_p = 2.5$, remaining numbers are similar;

Subscript '-lt' means lookup table method;

Subscript '-p' means the theoretical reference value for optimal condition.

As an important indicator of investigation, and in order to avoid the effect of huge noise, power evolutions are the results obtained with low-pass filter, whose cross-frequency is 30 Hz.

V.2.2.1. Case 1: step input of wind velocity

Direct MPPT algorithms with 2.5 V fixed step-size or maximum limit of variable step-size:

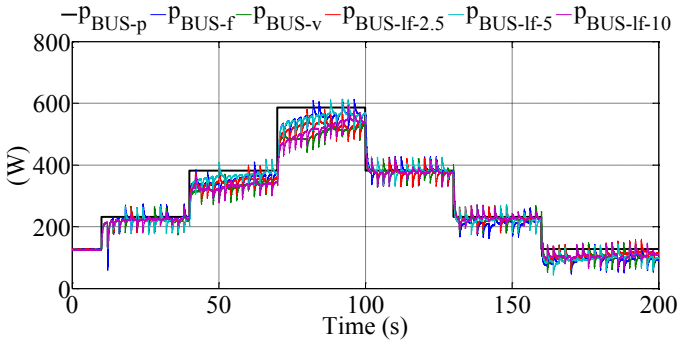

Figure 53: Experimental evolution of electrical powers with step-size maximum 2.5 V.

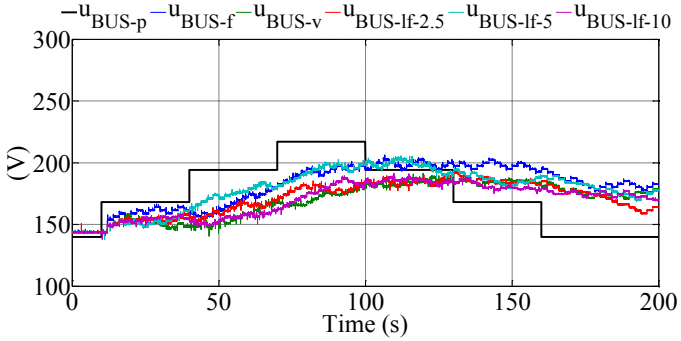

Figure 54: Experimental evolution of DC voltages with step-size maximum 2.5 V.

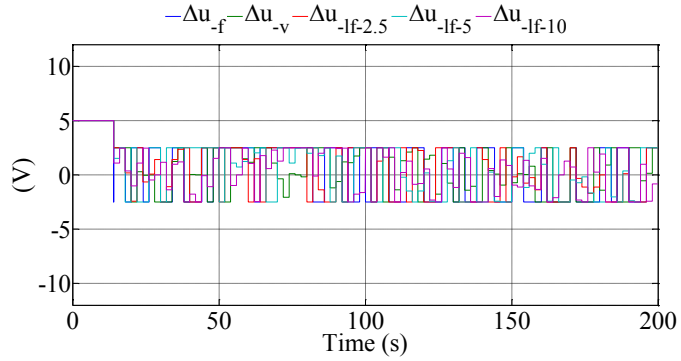

Figure 55: Experimental evolution of actual step size with maximum 2.5 V.

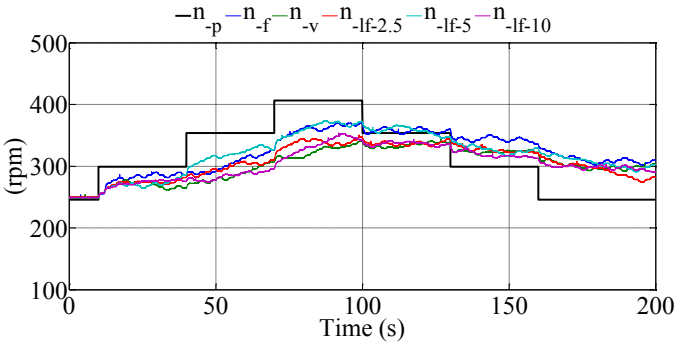

Figure 56: Experimental evolution of rotational speed with step-size maximum 2.5 V.

Direct MPPT algorithms with 5 V fixed step-size or maximum limit of variable step-size:

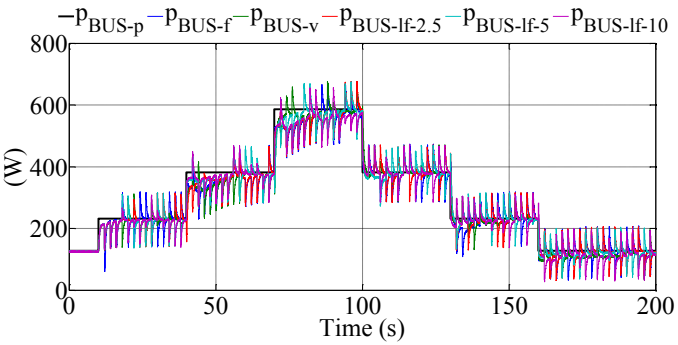

Figure 57: Experimental evolution of electrical powers with step-size maximum 5 V.

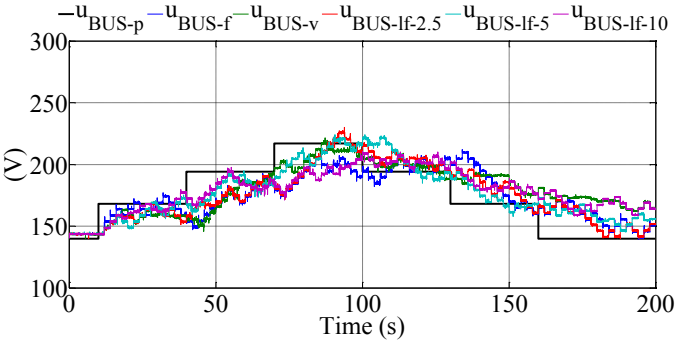

Figure 58: Experimental evolution of DC voltages with step-size maximum 5 V.

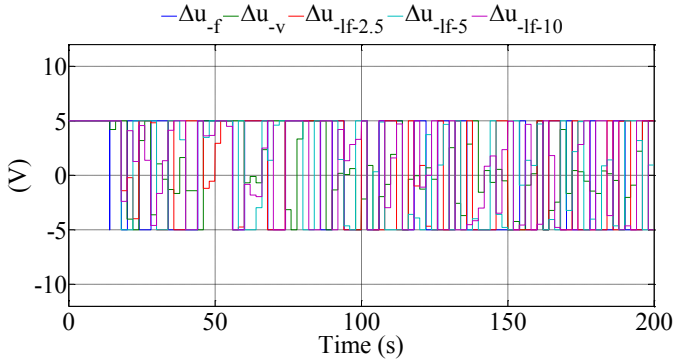

Figure 59: Experimental evolution of actual step size with maximum 5 V.

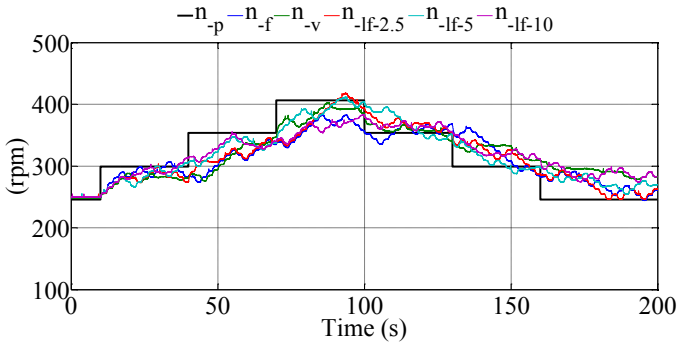

Figure 60: Experimental evolution of rotational speed with step-size maximum 5 V.

Direct MPPT algorithms with 10 V fixed step-size or maximum limit of variable step-size:

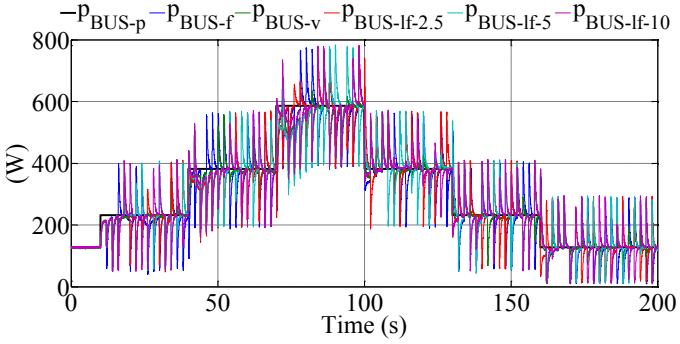

Figure 61: Experimental evolution of electrical powers with step-size maximum 10 V.

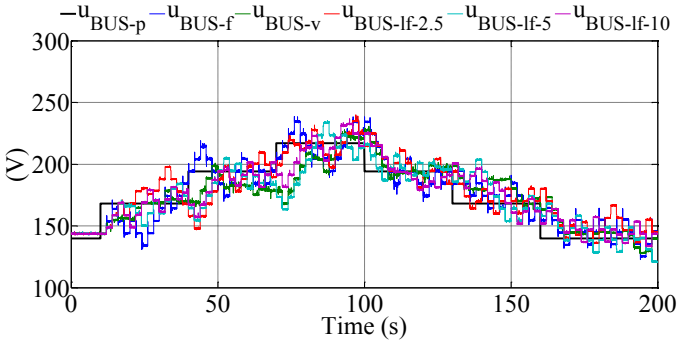

Figure 62: Experimental evolution of DC voltages with step-size maximum 10 V.

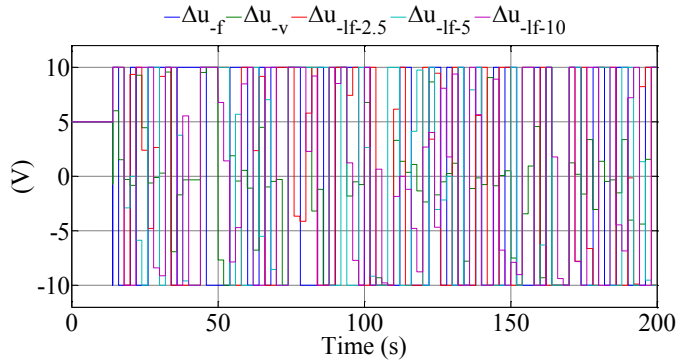

Figure 63: Experimental evolution of actual step size with maximum 10 V.

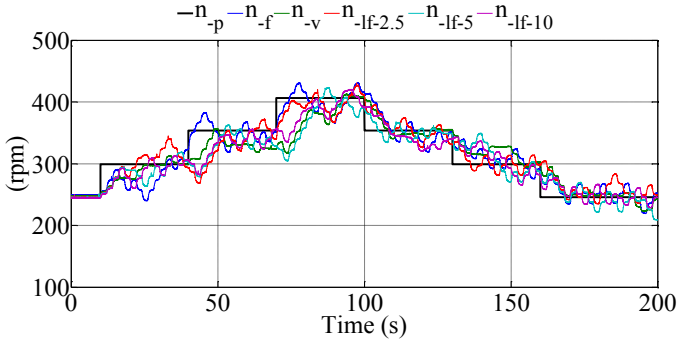

Figure 64: Experimental evolution of rotational speed with step-size maximum 10 V.

The proposed LT algorithm:

As discussed in Chapter II, the proposed lookup table algorithm works continually, there isn't the experimental evolution of perturbation step-size presented.

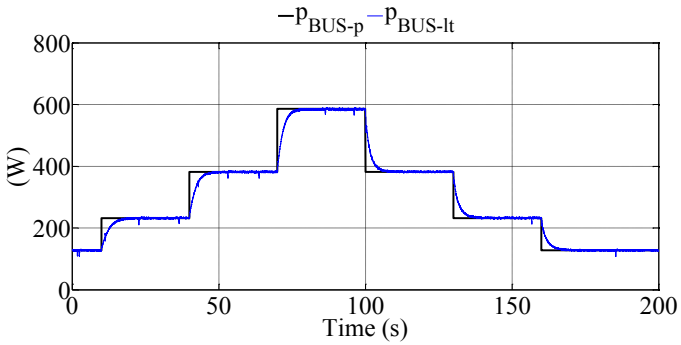

Figure 65: Experimental evolution of electrical power for LT algorithm.

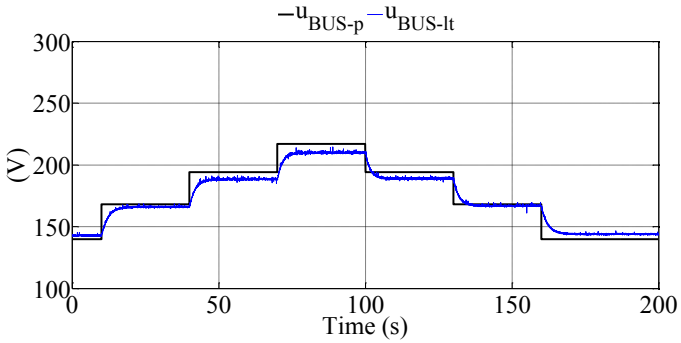

Figure 66: Experimental evolution of DC voltage for LT algorithm.

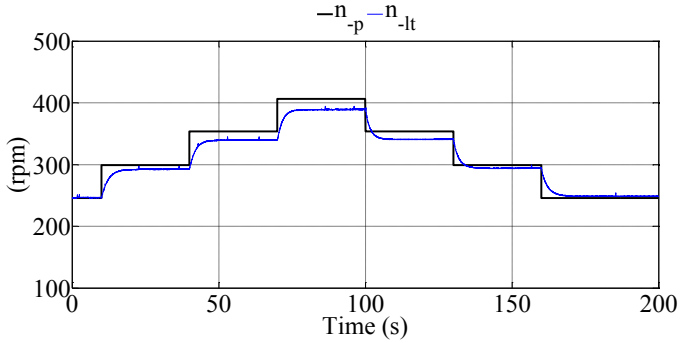

Figure 67: Experimental evolution of rotational speed for LT algorithm.

In this project, it can be intuitive to investigate capabilities of different MPPT algorithms.

First, it can be said that after wind speed jumps to a new steady value, all direct methods can arrive at the correct judgment about the direction of next perturbation.

Second, investigating the capability of rapid tracking and converging, when perturbation step-size is small as 2.5 V (Figure 53 to Figure 56), all direct methods cannot effectively get close to the maximum power point. Besides, when perturbation step-size is big enough such as 5 V and 10 V (Figure 57 to Figure 60 and Figure 61 to Figure 64), P&O-INR algorithm remarked with "-v" converges significantly around MPP; and for P&O-FL algorithms, the combination $\left(1/K_p = 10,\ \ 1/K_u = K_s = 5\right)$ has the best balance between converging and tracking.

Third, based on experimental evolutions for lookup table method (Figure 65 to Figure 67), it is obvious that its performance of tracking maximum power point is better than all direct methods. Because as mentioned in Chapter II.3 and the experimental results presented in Chapter IV.3, the rotational speed response respect to vary of u_{BUS} doesn't mislead the determination of lookup table algorithm, there is no information needed to be avoided. Furthermore, from the experimental evolutions of lookup table algorithm and it also can be assured based on the power distribution presented in Figure 30 that the operating points around MPP almost indicate close amount of power. So, even the actual operating point didn't stabilized exactly at the optimal one calculated by the data also from Figure 30, the actual output of electrical power p_{BUS} was still very close to the potential maximum power value.

Besides evolution curves above, the value of energy obtained by system is one important indicator of investigation. Table 5 presents values of energy for all MPPT algorithms and the difference from the potential value in form of percentage value.

Table 5 – Energy and difference from potential value for MPPT algorithms to Case 1

	Potential maximum power value	**P&O-F**			**P&O-INR**			**P&O-FL**									**LT**
	-	**Step-size**			**Maximum of step-size**			***1/Ku***									-
								2.5			5			10			
								1/Kp									
		2.5	5	10	2.5	5	10	2.5	5	10	2.5	5	10	2.5	5	10	
Energy (Wh)	16.88	15.70	16.16	16.54	15.20	16.16	16.39	15.61	15.88	15.40	16.26	16.39	16.15	16.67	16.58	16.65	16.83
Difference (%)	-	6.99	4.27	2.01	9.95	4.27	2.90	7.52	5.92	8.77	3.67	2.90	4.32	1.24	1.78	1.36	0.30

Comparing values of extracted energy of each method and the difference between the actual energy and the potential energy value of each method, large value of perturbation step-size always products more energy than small step-size. Overall, differences from potential value are small. The worst case could still products 90.05% of potential energy.

V.2.2.2. Case 2: triangle input of wind velocity

This experimental test is introduced to validate the capability of dynamic characteristics of four proposed MPPT algorithms.

Direct MPPT algorithms with 2.5 V fixed step-size or maximum limit of variable step-size:

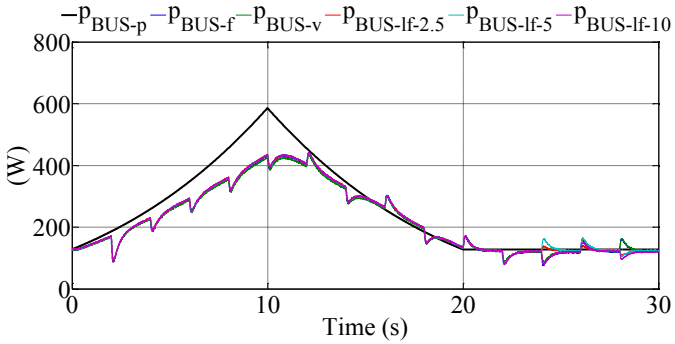

Figure 68: Experimental evolution of electrical powers with step-size maximum 2.5 V.

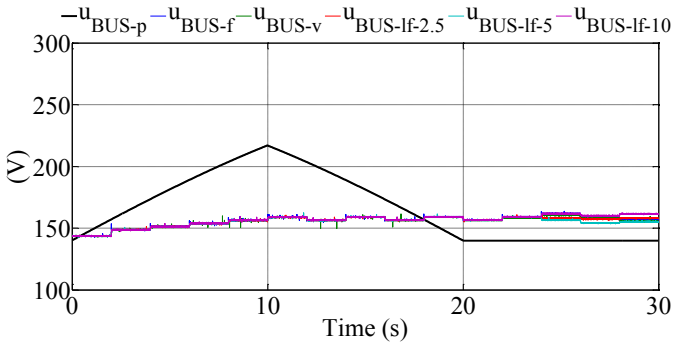

Figure 69: Experimental evolution of DC voltages with step-size maximum 2.5 V.

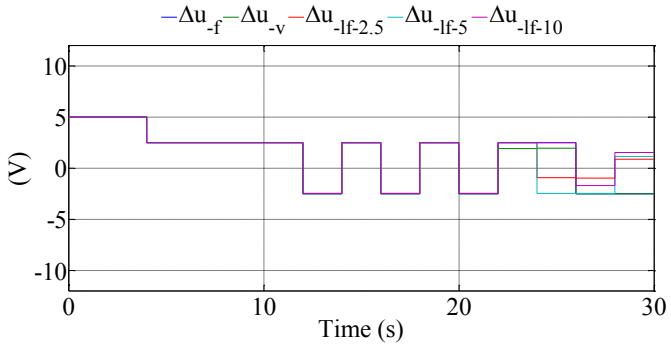

Figure 70: Experimental evolution of actual step size with maximum 2.5 V.

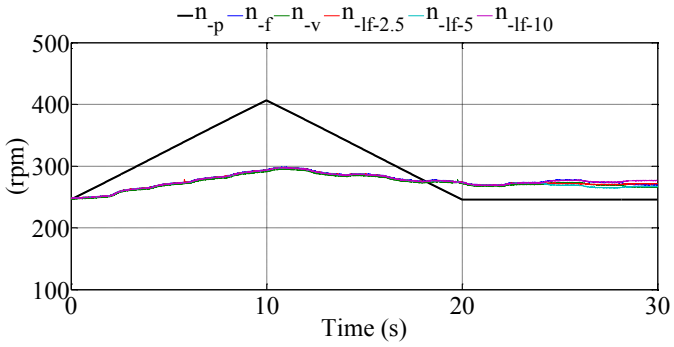

Figure 71: Experimental evolution of rotational speed with step-size maximum 2.5 V.

Direct MPPT algorithms with 5 V fixed step-size or maximum limit of variable step-size:

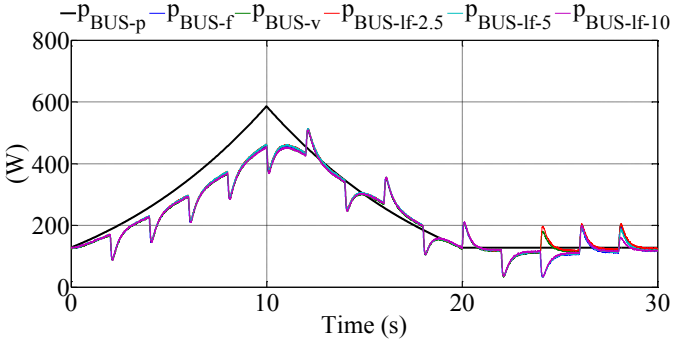

Figure 72: Experimental evolution of electrical powers with step-size maximum 5 V.

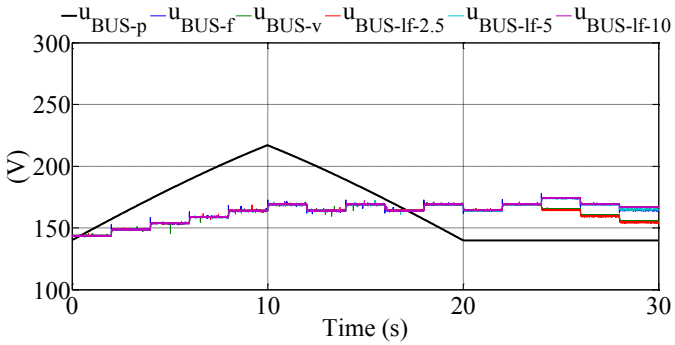

Figure 73: Experimental evolution of DC voltages with step-size maximum 5 V.

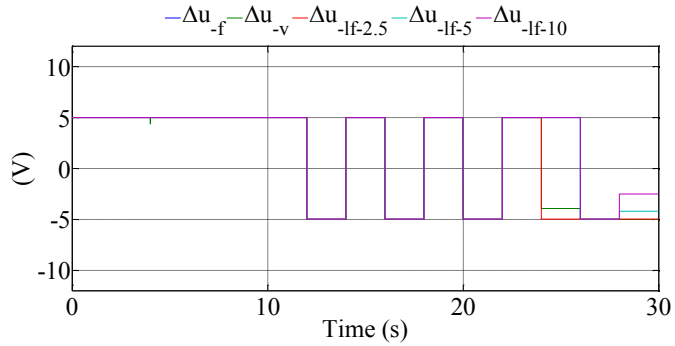

Figure 74: Experimental evolution of actual step size with maximum 5 V.

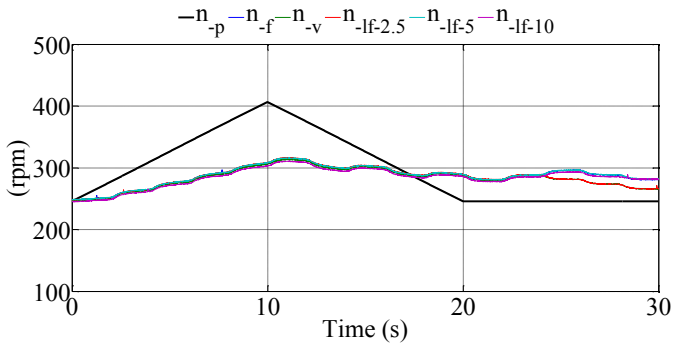

Figure 75: Experimental evolution of rotational speed with step-size maximum 5 V.

Direct MPPT algorithms with 10 V fixed step-size or maximum limit of variable step-size:

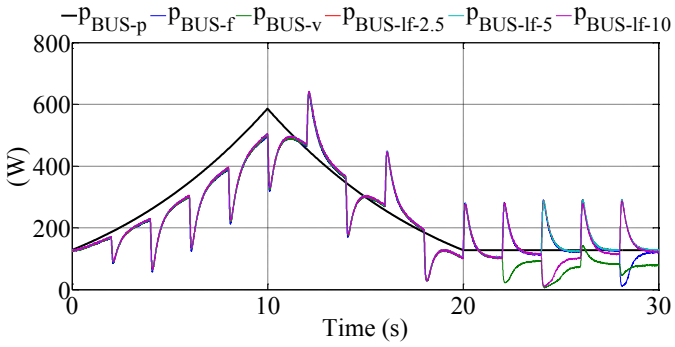

Figure 76: Experimental evolution of electrical powers with step-size maximum 10 V.

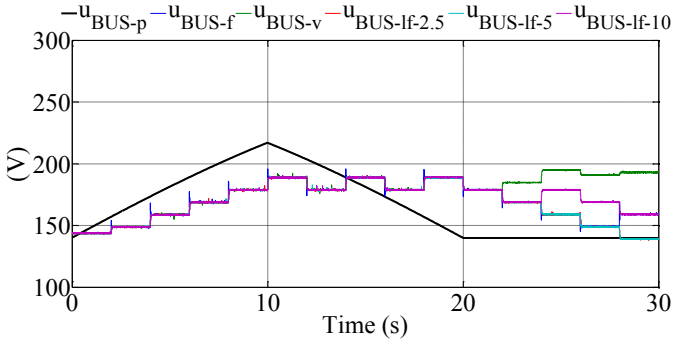

Figure 77: Experimental evolution of DC voltages with step-size maximum 10 V.

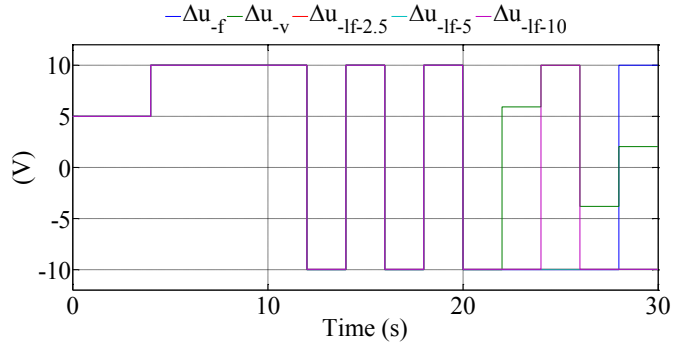

Figure 78: Experimental evolution of actual step size with maximum 10 V.

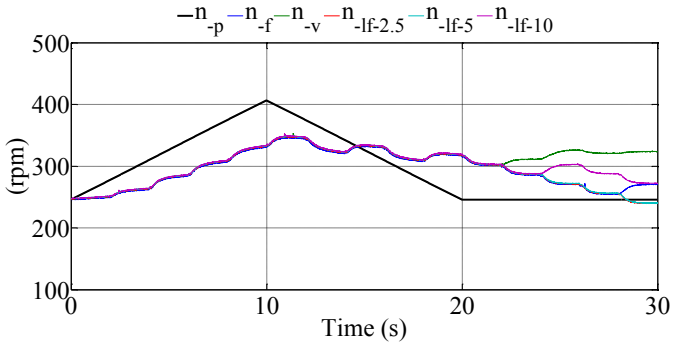

Figure 79: Experimental evolution of rotational speed with step-size maximum 10 V.

The proposed LT algorithm:

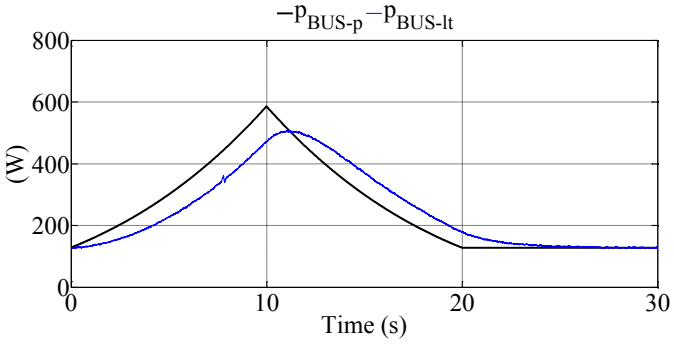

Figure 80: Experimental evolution of electrical power for LT algorithm.

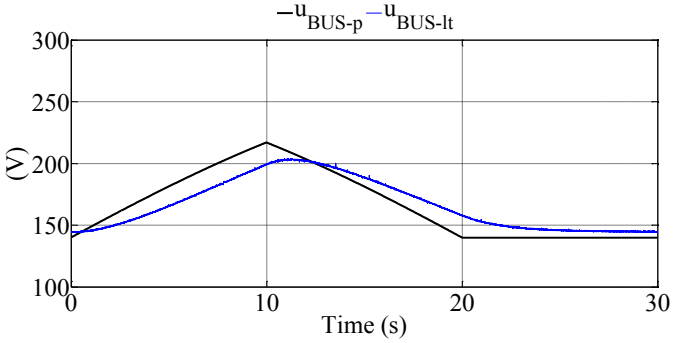

Figure 81: Experimental evolution of DC voltage for LT algorithm.

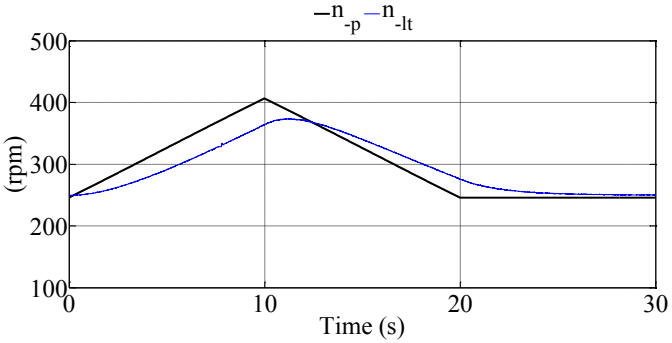

Figure 82: Experimental evolution of rotational speed for LT algorithm.

According to the information from Figure 68 to Figure 82, it is obvious that under the condition of rapid wind speed changes, evolutionary behaviors of variables for all direct methods are similar. Thus, P&O-INR method performed worse than P&O-F method, since it requires information more than one past step. With the inevitable observe time step, using more past information means that this algorithm responds more slowly to the wind speed change. Foreseeably, the energy differences between direct methods and indirect method are more significant than in Case 1.

Similar as Case 1, the energy extracted by each algorithm and the difference between their extracted energy and the potential reference are listed in Table 6.

Table 6 – Energy and difference from potential value for MPPT algorithms to Case 2

	Potential maximum power value	**P&O-F**			**P&O-INR**			**P&O-FL**									**LT**
								1/Ku									
	-	**Step-size**			**Maximum of step-size**			2.5			5			10			-
								1/Kp									
		2.5	5	10	2.5	5	10	2.5	5	10	2.5	5	10	2.5	5	10	
Energy (Wh)	2.13	1.86	1.88	1.95	1.85	1.90	1.80	1.89	1.89	1.87	1.93	1.90	1.88	2.02	2.02	1.96	2.09
Difference (%)	-	12.68	11.74	8.45	13.15	10.80	15.49	11.27	11.27	12.21	9.39	10.80	11.74	5.16	5.16	7.98	1.88

According to the result in Table 6, the effect of rapid change of wind velocity can be recognized. Comparing with proposed lookup table algorithm, the efficiency of extracting power for three direct MPPT algorithms reduced significantly. This proved the description that P&O algorithm works worse in the wind turbine system with medium and large mechanical inertia when wind changes rapidly [35].

V.2.2.3. Case 3: wind velocity profile based on recorded data

Different from the Case 1 and 2, the wind velocity profile implemented in this case includes random and huge vary about wind velocity. Under this condition, all proposed MPPT algorithms work in the condition close to the real environment.

Direct MPPT algorithms with 2.5 V fixed step-size or maximum limit of variable step-size:

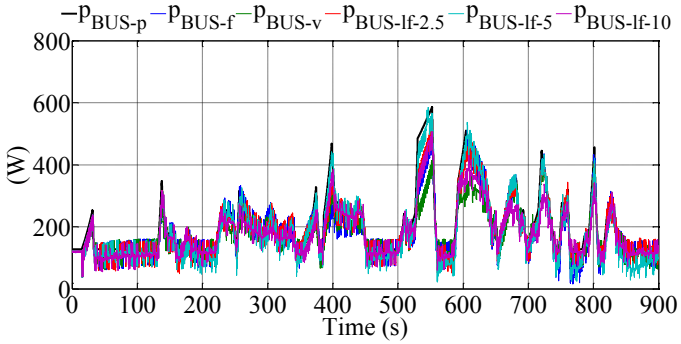

Figure 83: Experimental evolution of electrical powers with step-size maximum 2.5 V.

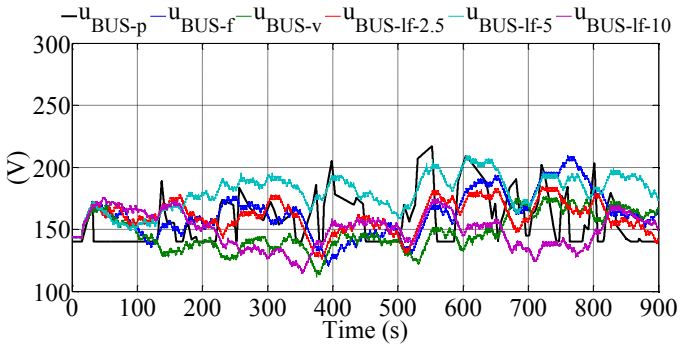

Figure 84: Experimental evolution of DC voltages with step-size maximum 2.5 V.

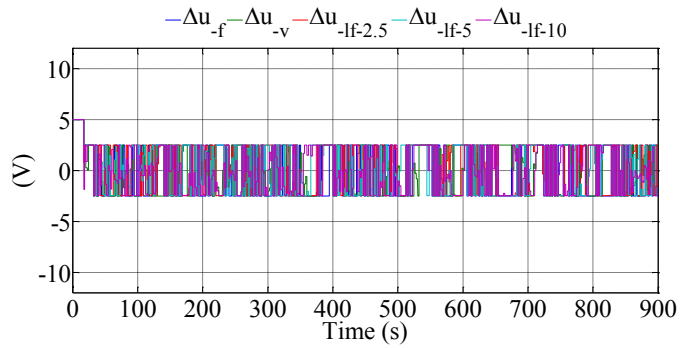

Figure 85: Experimental evolution of actual step size with maximum 2.5 V.

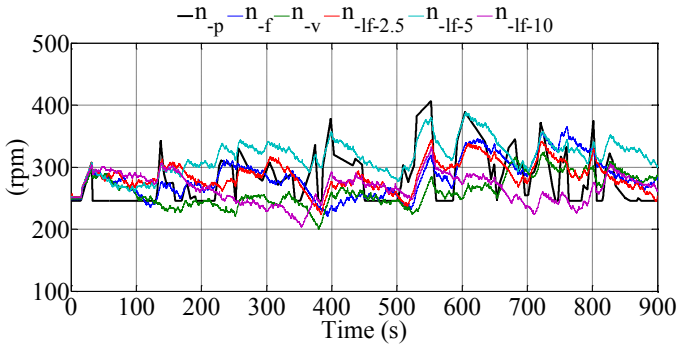

Figure 86: Experimental evolution of rotational speed with step-size maximum 2.5 V.

Direct MPPT algorithms with 5 V fixed step-size or maximum limit of variable step-size:

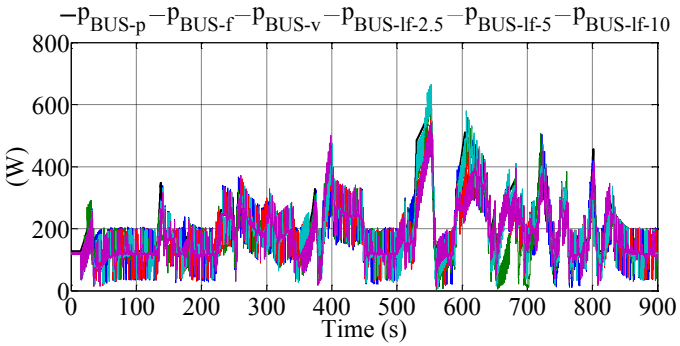

Figure 87: Experimental evolution of electrical powers with step-size maximum 5 V.

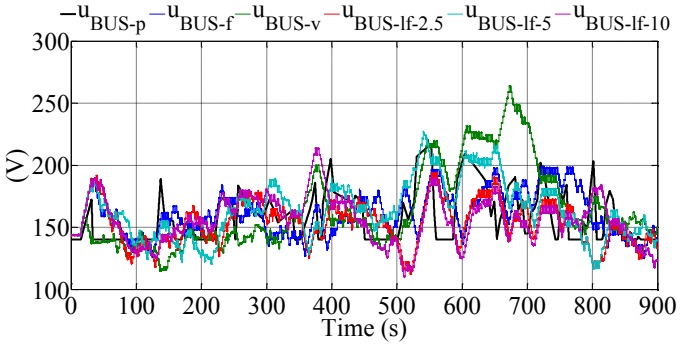

Figure 88: Experimental evolution of DC voltages with step-size maximum 5 V.

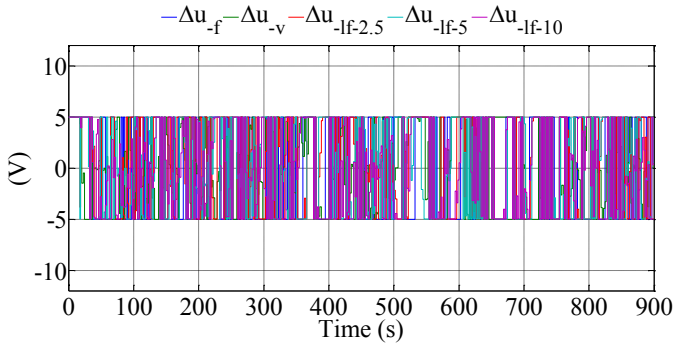

Figure 89: Experimental evolution of actual step size with maximum 5 V.

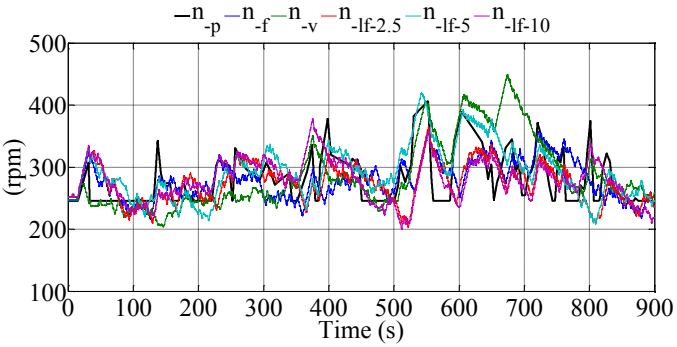

Figure 90: Experimental evolution of rotational speed with step-size maximum 5 V.

Direct MPPT algorithms with 10 V fixed step-size or maximum limit of variable step-size:

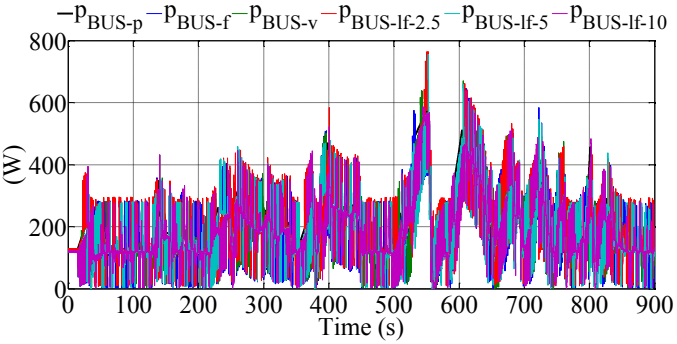

Figure 91: Experimental evolution of electrical powers with step-size maximum 10 V.

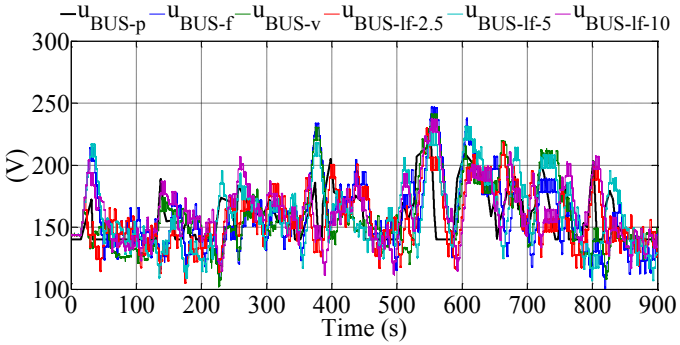

Figure 92: Experimental evolution of DC voltages with step-size maximum 10 V.

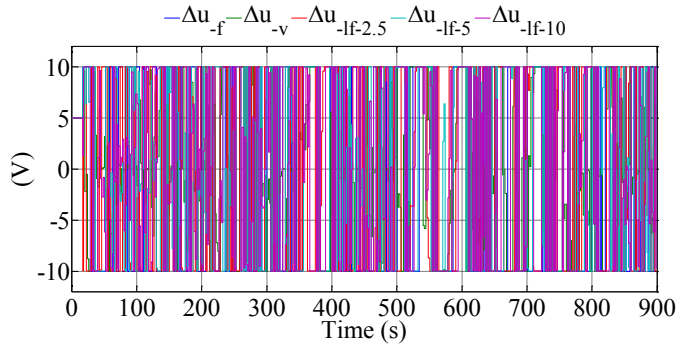

Figure 93: Experimental evolution of actual step size with maximum 10 V.

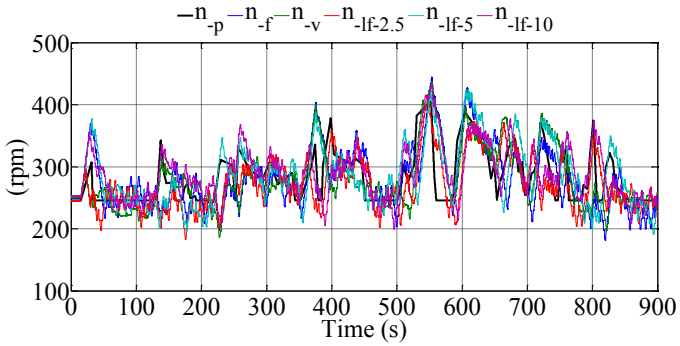

Figure 94: Experimental evolution of rotational speed with step-size maximum 10 V.

The proposed LT algorithm:

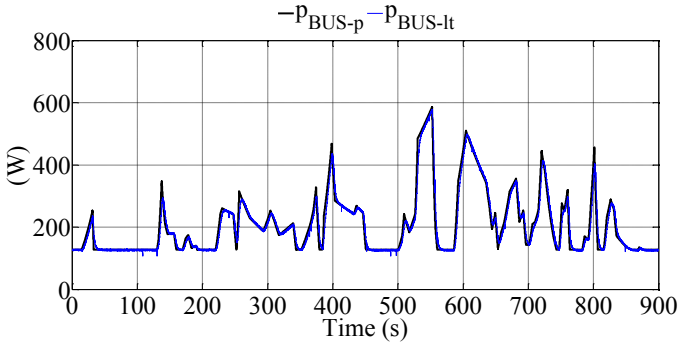

Figure 95: Experimental evolution of electrical power for LT algorithm.

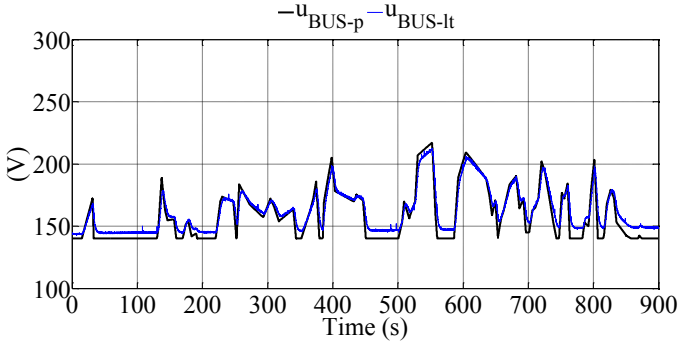

Figure 96: Experimental evolution of DC voltage for LT algorithm.

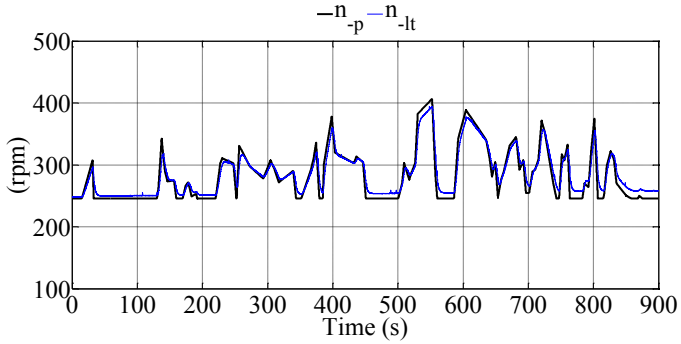

Figure 97: Experimental evolution of rotational speed for LT algorithm.

Following the same logic, the extracted energy and the efficiency of MPPT algorithms are calculated and list follow.

Summarizing these three cases, under complex wind speed variation, direct methods are disadvantageous: P&O is less performant under rapid variation of wind speed, knowing that mechanical inertia cannot be ignored. Concerning the production, energies extracted by direct methods are significantly affected by how fast the wind speed varies. On the other hand, lookup table method extracts about 98.82% of potential energy. Even though evolutions of u_{BUS} and Ω didn't match the curve optimal theoretical 100% as presented in Figure 66, Figure 67, Figure 81, Figure 82, Figure 96 and Figure 97, it is significantly better than the others.

Table 7 – Energy and difference from potential value for MPPT algorithms to Case 3

	Potential maximum power value	**P&O-F**			**P&O-INR**			**P&O-FL**									**LT**
								1/Ku									
	-	**Step-size**			**Maximum of step-size**			2.5			5			10			-
								1/Kp									
		2.5	5	10	2.5	5	10	2.5	5	10	2.5	5	10	2.5	5	10	
Energy (Wh)	52.28	46.06	46.22	46.01	44.36	45.45	46.69	47.08	45.79	45.07	46.29	47.57	46.27	48.95	46.50	46.87	51.66
Difference (%)	-	11.88	11.59	11.99	15.14	13.05	10.68	9.93	12.41	13.78	11.45	9.00	11.49	6.36	11.04	10.35	1.18

In addition, all implemented MPPT algorithms achieved the theoretical designed goals combining with the hysteresis control. For already designed profiles and real measurement data, indirect method performs great capabilities of tracking MPP and stabilizing around MPP. The performance of direct methods based on the principle of P&O is restricted by the sluggish mechanical inertia of the system and the existing of measurement noise, and whatever the ways of calculating the perturb step-size cannot solve this problem.

V.2.3. Conclusion

In all three cases, the indirect method extracted over 98% of potential theoretical energy with rapid wind speed tracking MPP and without oscillation of operating condition around MPP.

The direct methods based on P&O algorithm and the lookup table indirect method were performed independently but based on the same converter controller to track the given reference. Variable step-size P&O method, based on the slope of the DC bus voltage change with respect to the electrical power change, achieves the goal that step-size converges when operating point gets close to MPP; the step-size modified by fuzzy logic can also find acceptable combination of normalizing gain to obtain the same achievement. Nevertheless, the variable step-size methods cannot improve considerably the results.

Concerning the implementation of these MPPT, lookup table requires accurate knowledge of controlled system, which means that efforts of prior tests are indispensable to cover all the operating conditions; moreover, an expensive mechanical rotation speed sensor, even directly wind speed, is required. All of these requirements increase the cost and the complexity for implementing this method.

Contrariwise, commonly used electrical sensors are required to operate direct methods. P&O-F and P&O-INR request only basic tests to determine the parameters of P&O. Nevertheless, the determination of parameters of the P&O-FL requires that the designers need to have more experience in the application and have to do more experiments to validate their parameters identification.

V.3. Power limited control

V.3.1. Experiment design

With the experimental experiences obtained in the studies of MPPT topic, the basic functions of all proposed PLC algorithms can be easily judged to be successful. Hence, for PLC operating condition, the experimental test cases like Case 1 and 2 for MPPT topic had not been considered at the beginning for this stage of research.

In order to compare all proposed PLC algorithm, the real wind velocity data implemented in the Case 3 for MPPT experimental test is used to calculate one random power limited profile (p_{limit} presented in Figure 98). This calculation also is based on the physical minimum power of the experimental platform. Thus, the wind velocity profile displayed in Figure 51 and the limited power curve in Figure 98 determine the operating condition for the following experiments.

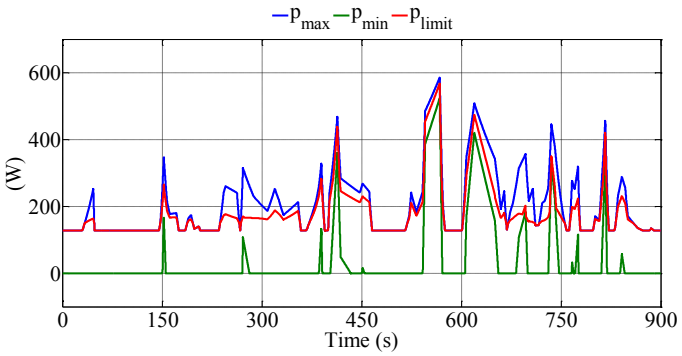

Figure 98: Profile of calculated limited power curve.

Similar as experiments for MPPT, several groups of tests are introduced.

P&O-F method: step-size respectively equals 2.5 V, 5 V, 7 V, and 10 V.

P&O-INR method: maximum value of step-size respectively equals 2.5 V, 5 V, 7 V, and 10 V.

P&O-FL method: the way to realize the modification of its parameters is similar as MPTT condition, but there are a few differences from the MPPT condition (as presented in Figure 99).

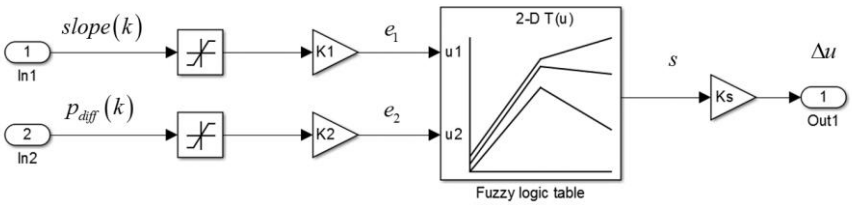

Figure 99: Structure used in Matlab®/Simulink® for normalization and anti-normalization.

The combination of parameters $\{1/K_1 \quad 1/K_2 \quad 1/K_s\}$ implemented in experimental test respectively equal: (4.5, 17.5, 7), (4.5, 17.5, 10), (5, 15, 7), (5, 15, 10), (5, 20, 7), (5, 20, 10), (10, 20, 7), and (10, 20, 10).

Online update lookup table Method based on indirect principle based on information of system measured on February 3, 2016. And all experimental were finished in February 24, 2016.

V.3.2. Evolution experimental and analysis

The results of these experimental tests are presented in following figures. Since, for each proposed PLC algorithm, there are much different step-sizes applied. And not like the MPPT condition, there are some selection of perturb step-size had been ignored for P&O-FL algorithm. Following the order of experimental results for MPPT condition to sort experimental results for PLC by step-size or maximum limit of step-size is not logical and appropriate. So, the more suitable order is to list the experimental results for each PLC algorithm together, then compare their characteristics by mathematic indicators. As the key variable, the evolution of p_{diff} is used to analyze characteristics of all regulating methods. Focusing on this variable, the efficiency of tracking the demanded power value for each proposed PLC algorithm are easy to be revealed, analyzed and compared.

V.3.2.1. P&O-F

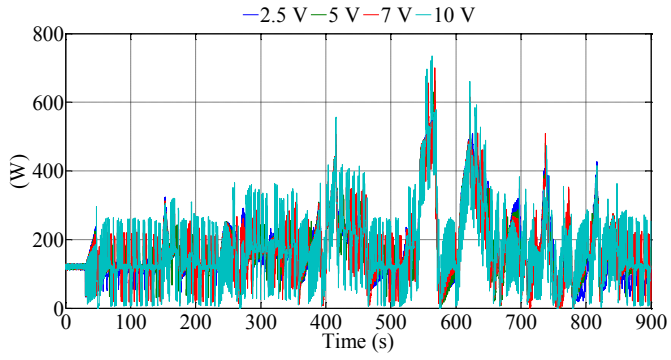

Figure 100: Evolution of p_{BUS}.

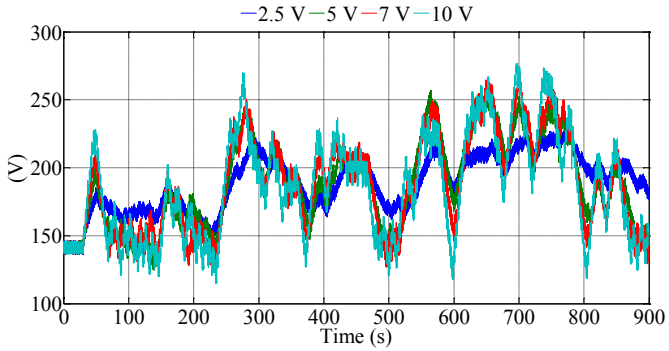

Figure 101: Evolution of u_{BUS} .

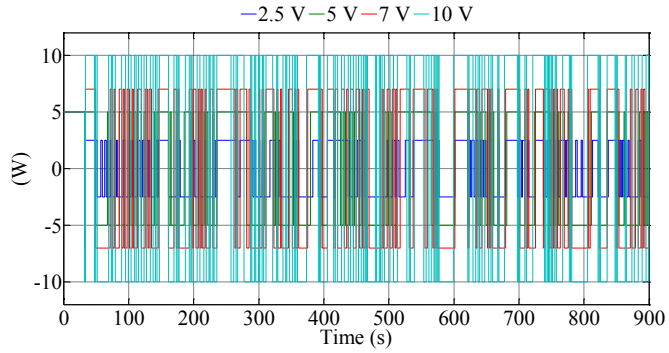

Figure 102: Evolution of Δu .

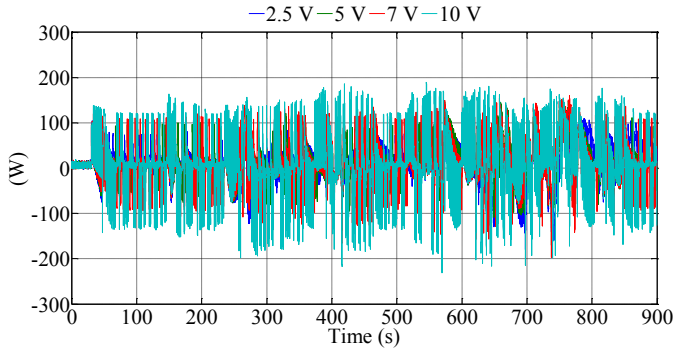

Figure 103: Evolution of p_{diff} .

As illustrated above, it is easy to be found that P&O-F applications with different fixed step-sizes succeed to follow the limited power command profile, while the sluggish mechanic inertia results in significant transition process. Large step-size can reduced the transition time but also led more peaks of dynamic process of each perturbation.

V.3.2.2. P&O-INR

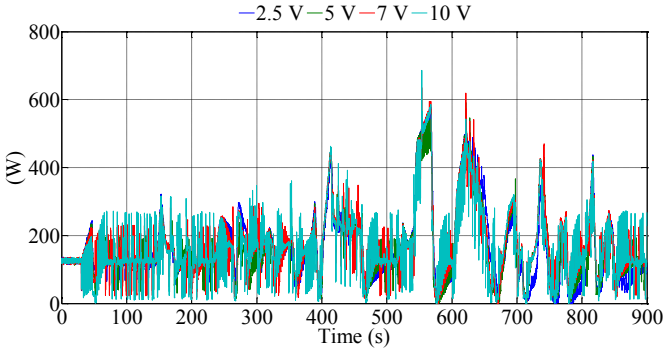

Figure 104: Evolution of p_{BUS} .

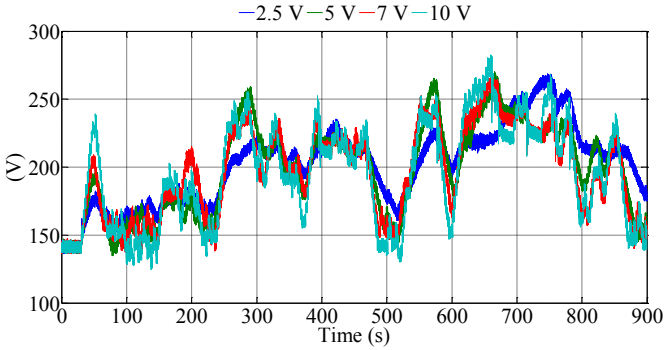

Figure 105: Evolution of u_{BUS} .

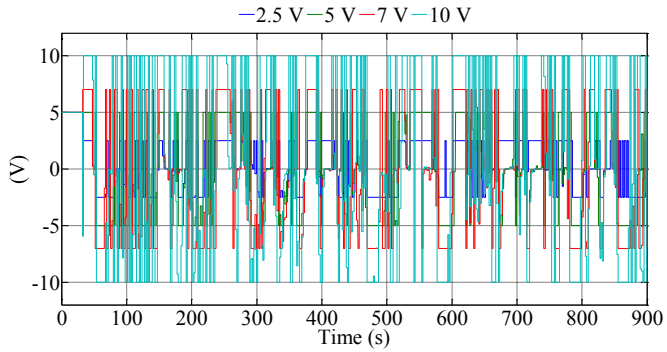

Figure 106: Evolution of Δu .

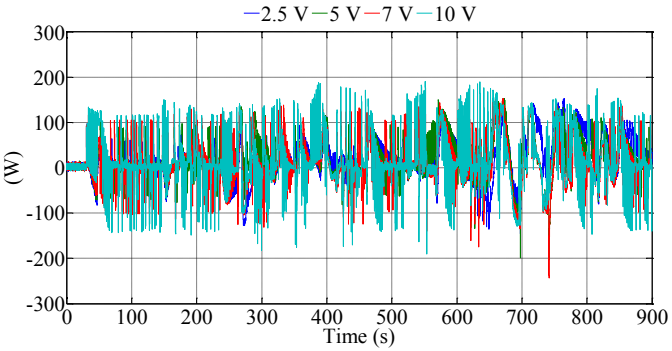

Figure 107: Evolution of p_{diff} .

Comparing results of P&O-INR and P&O-F, obviously, the dynamic process resulted by each perturbation had been suppressed, whatever analyzing the evolution of actual power p_{BUS} or the difference between limited value and actual value p_{diff} .

V.3.2.3. P&O-FL

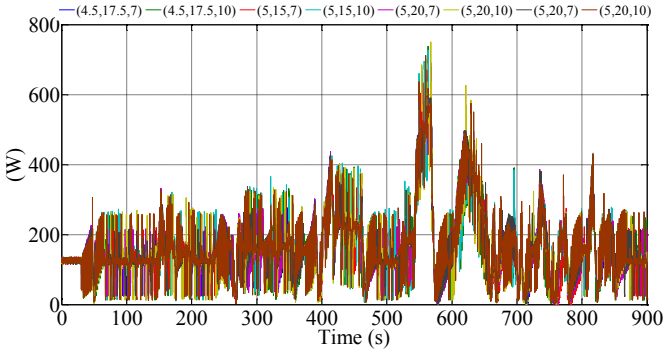

Figure 108: Evolution of p_{BUS} .

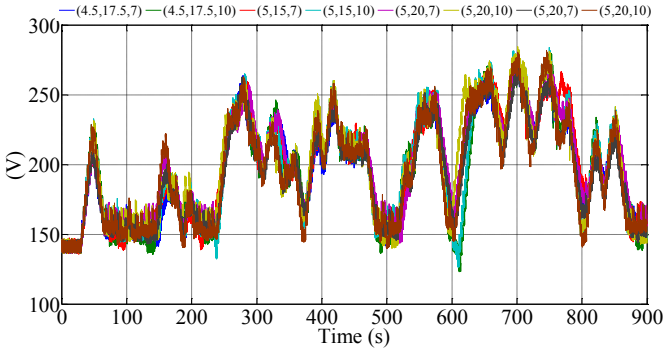

Figure 109: Evolution of u_{BUS} .

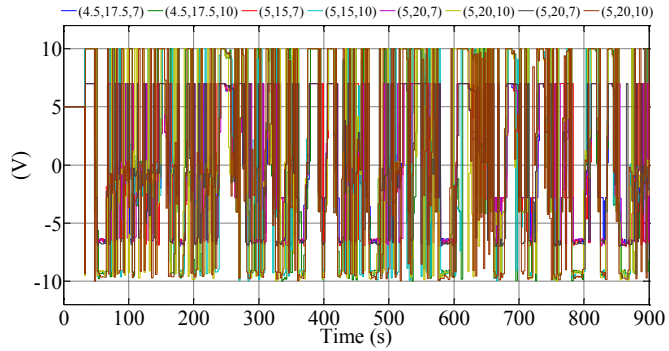

Figure 110: Evolution of Δu .

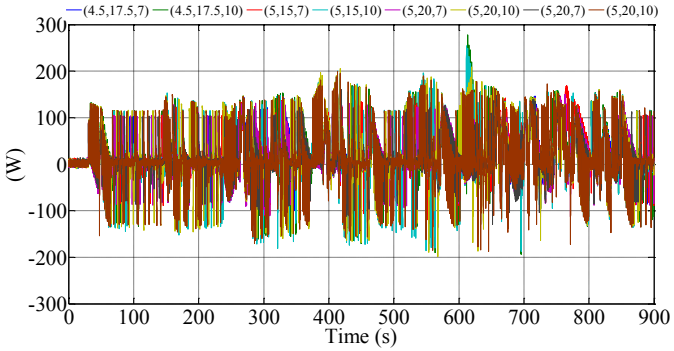

Figure 111: Evolution of p_{diff} .

For the P&O-FL algorithm, the modification of parameter set of $\{1/K_1 \quad 1/K_2 \quad K_s\}$ is similar the process of optimization. Briefly, even three parameters are isolated each other in physic sense, the coupling effect between them are still complex. So, the comparison research will be achieved based on mathematic indicators introduced after all results presented.

V.3.2.4. Online update lookup table algorithm

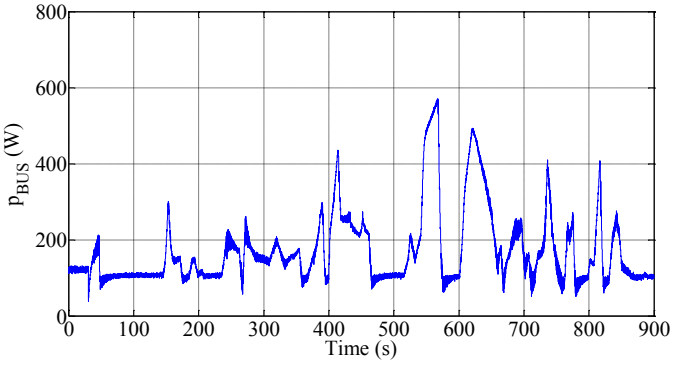

Figure 112: Evolution of p_{BUS} .

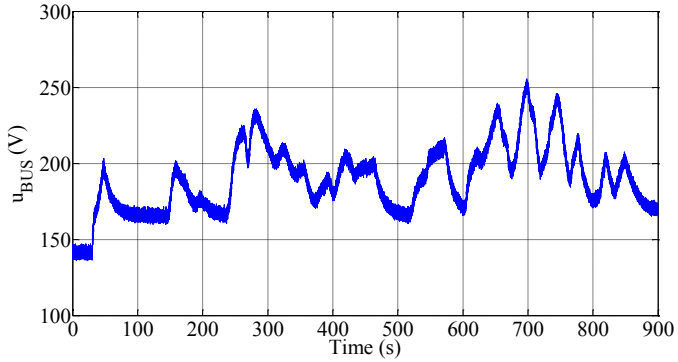

Figure 113: Evolution of u_{BUS} .

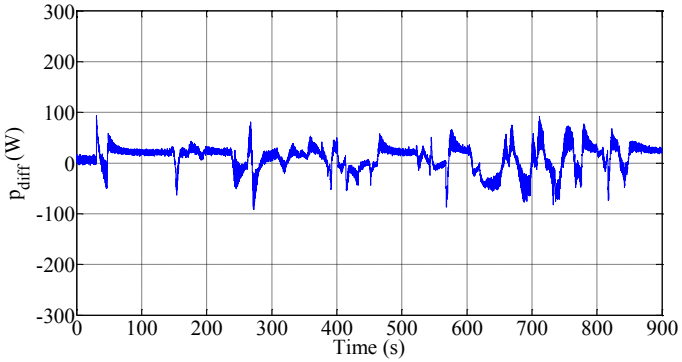

Figure 114: Evolution of p_{diff} .

Based on the experimental results for online update lookup table algorithm, it can be said with certainty that the response of electrical power of this algorithm contains less dynamic behaviors introducing noises into the variable p_{diff} . But, huge deviation of mean for some period of experiment existed. The cause is that this indirect method lies on the mathematic mode of studied system and almost follows the open loop control principle. So, in theory, it is sensitive about the parameter drift. But, the actual influences of parameter drift to the proposed online update lookup table still needs to be validated.

One small experiment was implemented to explore and explain this defect.

The experimental conditions of this test are as follow: p_{limit} is fixed at 250 W; wind velocity varies from 7 m/s (before 50 seconds) to 6.5 m/s (from 50 seconds to 90 seconds) then turns to 7 m/s, as presented in Figure 115.

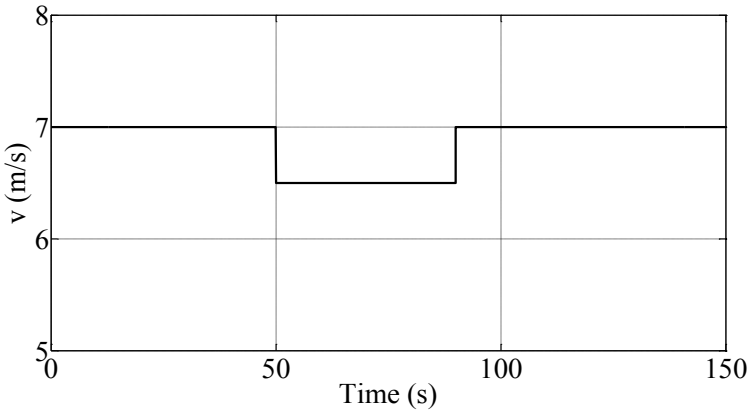

Figure 115: Wind velocity profile.

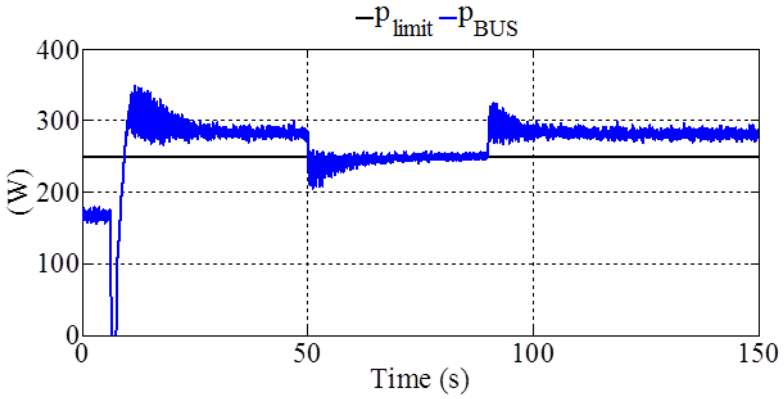

Figure 116: Profile of demanded power and evolution of actual electrical power.

Based on Figure 115 and Figure 116, it is necessary to notice that the 7 m/s is the chosen value of wind speeds to establish the online update lookup table method. However, it is clear that the online update lookup table method still introduce an error of p_{BUS}. Analyzing the theory of this method, when the parameters of system change, these parameter drifts result in the movement of relative curves of $u_{BUS} - n$ for different wind velocities, such as presented in Figure 117 and Figure 118.

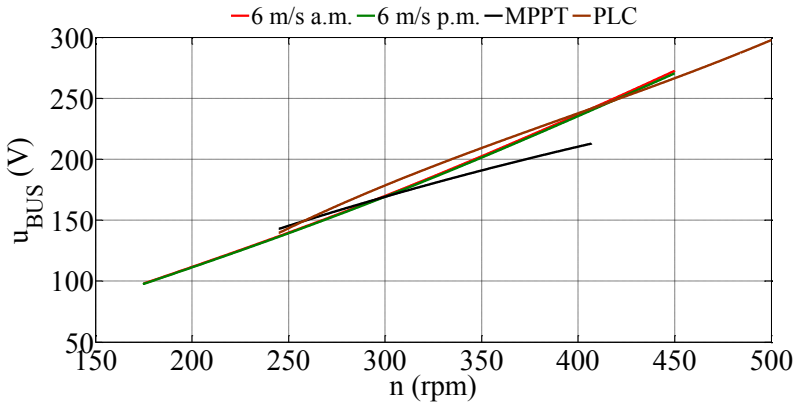

Figure 117: Parameter drift presented in $u_{BUS} - n$ space.

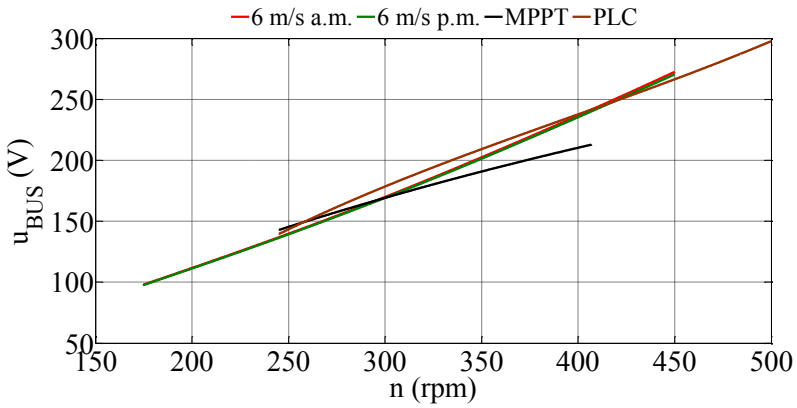

Figure 118: Zoom around cross points.

Based on measurements of u_{BUS} and n for 6 m/s, separately at morning (a.m.) and afternoon (p.m.) of 17th of December 2015, in Figure 117, $u_{BUS}-n$ curves representing MPPT case and 150W PLC case are presented: the curve marked 'MPPT' is the function used to realize MPPT case and the curve marked 'PLC' is for 150W power demand which is suitable for 6 m/s wind speed. Figure 118 presents a zoom to illustrate the following evidence: despite the fact that the distance between two $u_{BUS}-n$ curves of 6 m/s for both morning and afternoon is not significant, the cross points give big differences: the difference between the rotational speed n is near 10 rpm and the difference between the bus voltages u_{BUS} is around 5 V. Given the shape of the relationship between p_{BUS} and u_{BUS} around the MPP, the amount of this difference of u_{BUS} cannot introduce a huge impact of p_{BUS}. But, considering the increment of same curve around power limited operating points, same amount of difference of u_{BUS} will result in significant difference of p_{BUS}. In fact, these variations result from the change of temperature of system electrical equipment. Consequently, it seems that increasing amount of measurement of operating points can increase the precision of this online updating lookup table method. But, at the same time, more measurements mean that those measured data span more temperature range, since the temperature of the system is increasing when the system is running. Thus, there is one contradiction between the consistency of measured data with respect to temperature and the accuracy supplied by measured data for lookup table method. Furthermore, considering the effect resulting from these difference during the same day (presented in Figure 118), it is not feasible to find out one group of data based on which one given lookup table method can deal with all different environmental conditions.

V.3.3. Conclusion

Integrating all information about experiment for PLC condition, analysis of comprehensive comparison is described as follow. Referencing statistical concepts, regarding p_{diff} as a rodman variable, the mathematic mean, which is defined as average value, and the variance indicating the expected value of the squared deviation from the mean, are calculated to compare dynamic and steady-state characteristics of different regulating methods. At first, to all methods based on the P&O theory, a sampling method is a sampling time equals 2 s, is applied to filter the peak of each perturbation step of all algorithm based on P&O principle (marked as "Mean sampling" and "Variance sampling"). Then, the overall comparison (marked as "Mean overall" and "Variance overall") is presented in Table 8.

Table 8 – Means and variances for all PLC methods

Method	**Mean sampling**	**Variance sampling**	**Mean overall**	**Variance overall**
P&O-F 2.5 V	0.1075	21.6158	0.1116	20.0722
P&O-F 5 V	0.1285	17.4951	0.1318	19.4622
P&O-F 7 V	0.1353	17.9021	0.1360	26.1909
P&O-F 10 V	0.1383	14.9045	0.1347	39.5348
P&O-INR 2.5 V	0.1869	26.6797	0.1947	25.9007
P&O-INR 5 V	0.1788	24.0390	0.1866	25.0621
P&O-INR 7 V	0.1296	21.4507	0.1326	26.0033
P&O-INR10 V	0.1732	24.1157	0.1778	34.7039
P&O-FL (4.5,17.5,7)	0.1921	21.6994	0.1979	23.5178
P&O-FL (4.5,17.5,10)	0.2180	24.0726	0.2229	33.1278
P&O-FL (5,15,7)	0.2009	23.0639	0.2117	26.4571
P&O-FL(5,15,10)	0.1833	21.6108	0.1895	32.3361
P&O-FL (5,20,7)	0.1781	22.4394	0.1860	24.6240
P&O-FL(5,20,10)	0.1967	20.7878	0.2022	32.1932
P&O-FL(10,20,7)	0.1613	19.0379	0.1662	22.0579
P&O-FL(10,20,10)	0.1770	19.2552	0.1826	31.6463
Online update LT	0.2080	14.3937	0.2032	14.4115

Summarizing all presented results, under complex condition of wind velocity and power demands variation, the indirect regulating method and the direct regulating method present the opposite performance.

All three direct methods based on P&O theory perform less in the view of dynamic, resulting from the mechanical inertia which cannot be ignored; but, overall, their steady-state errors are less than the indirect method. Even for the P&O-FL method, if we find the suitable combination of parameters (such as (10, 20, 7) presented in Table 8), the value of mean of p_{diff} can be reduced to be lower than the LT method.

Relatively, the online update LT method has the biggest deviation of mean among all algorithms, whose value should be as smaller as possible; but it almost maintains the smallest variance (near 14.4) with and without the sampling method. This is benefited from that the chosen parameters, the rotational speed and the bus voltage, maintain the proportional relationship between them without information misleading the PLC algorithm.

Considering the priori work of implementing each regulating method, direct methods do not require the knowledge about the steady-state operating points of system, i.e. big data, and they demand commonly used electrical sensors. P&O-F and P&O-INR method request basic tests to determine the parameters of P&O. But the P&O-FL method ask rich experiences of application of designers and the determination of parameters of fuzzy logic need to be validated by many experiments. Contrariwise, the online update lookup table method requires accurate mathematic model of controlled system to cover all operating envelop. Furthermore, expensive mechanical sensors with high precision are required to measure the mechanical rotational speed or straight the wind velocity. All these demands increase the complexity and the cost of the application of this method. Combining the regulating effect, the time and resource devoted for the indirect method is too much.

Chapter VI. Conclusions and perspectives

This thesis presented concepts of small scale wind energy system fitting the demand of urban electric system; made a model of this system including a PMSM, a DC\DC convertor and the emulator of wind speed and blades; described the principles of proposed MPPT and PLC algorithms and designed several sets of experiments to validate those algorithms and compare their characteristics for matching power control objectives.

Four different methods of MPPT algorithm were presented and compared: P&O-F, P&O-INR, P&O-FL, and look-up table indirect method. Based on a test bench and three wind speed profiles, the obtained results showed that the indirect method gives the best performances in all three cases. However, the implementation implies requirements that increase the cost and the complexity. Regarding the direct methods, all algorithms achieved properly the fundamental theory of P&O, but for rapid variation of wind speed, the superiority of the variable step-size direct methods is not significant; this is due to the dynamic process of the perturbation that strongly weakens the effect of the MPPT algorithm. Solving this problem will be the subject of future studies.

Three PLC methods based on direct principle (P&O-F, P&O-INR, P&O-FL) and one PLC method based on the indirect principle (online update lookup table) have been studied, designed and then implemented into an experimental platform highlighting the sluggish mechanical inertia. The experimental test conditions are based on a real wind velocity profile and a calculated power limited

profile. Based on the experimental results, and using means and variances of all evaluations of p_{diff} have been calculated and analyzed. Integrating all the results, the online update lookup table method based on priori identification of system characteristics performs with good dynamic response and low steady-state precision. However, this kind of PLC method is sensitive to the difference between actual system and the pre-identified mathematic model. Correspondingly, three direct methods based on P&O principle present better steady state characteristics, but the dynamic characteristics are limited by the sluggish mechanical inertia and the control loop's capability.

In summary, the lookup table theory is not appropriate to the integrated MPPT and PLC cases, since its strong sensitivity to the parameter drift of the system requires to be covered by lots of preparatory work and more information to identify the operating status during its operating period. To direct methods, the future research direction is to improve the dynamic characteristics of the control loop, to suppressing the effect from the sluggish mechanical inertia. This can significantly improve the performance of direct methods based on perturb and observe theory. And, as presented in Chapter IV, used voltage closed-loop control method at the DC bus is the hysteresis algorithm which is robust and simple. However, some advanced control algorithms for the closed-loop, *i.e.* the sliding mode control, are interesting to be planned in the future work, because theoretically they have the potentiality to supply better performance, even though they would increase the complexity of application of whole system. Combining different voltage closed-loop control methods, the application of MPPT and PLC control strategies could present attractive results. From the point of view of the small scale wind turbine integration work, there are several works can be planned to achieved in future. The energy conversion structure used in this thesis is composed of the diode bridge and one DC-DC boost convertor, since its simplicity of application and low energy loss. So, as the contrast objective, the active energy conversion structure using a controllable rectifier is worth to be included to realize MPPT and PLC researches under the constraint from our lab's DC bus microgrid application environment. Being one part of the DC bus microgrid, after integration, the energy cost management research of whole microgrid including the studied wind turbine system naturally is going to be organized in the expected works.

Chapter VII. References

[1] P. Basak, S. Chowdhury, S. H. nee Dey, and S. Chowdhury, "A literature review on integration of distributed energy resources in the perspective of control, protection and stability of microgrid," *Renewable and Sustainable Energy Reviews*, vol. 16, no. 8, pp. 5545–5556, 2012.

[2] M. Sechilariu and F. Locment, *Urban DC Microgrid: Intelligent Control and Power Flow Optimization*. Elsevier Inc, 2016, ch. Connecting and Integrating Variable Renewable Electricity in Utility Grid, pp. 1–33.

[3] M. Sechilariu, "Urban dc microgrids for advanced local energy management with smart grid communication," in *3rd International Congress on Energy Efficiency and Energy Related Materials (ENEFM2015)*, Turkey, Springer, 2017, pp. 3–9.

[4] M. Sechilariu, B. C. Wang, F. Locment, and A. Jouglet, "DC microgrid power flow optimization by multi-layer supervision control. design and experimental validation," *Energy conversion and management*, vol. 82, pp. 1–10, 2014.

[5] J. F. Manwell, J. G. McGowan, and A. L. Rogers, "*Wind energy explained: theory, design and application*." John Wiley & Sons, 2010.

[6] H. Wu, M. Sechilariu, and F. Locment, "Impact of power converters' efficiency on building-integrated microgrid," in *2015 17th European Conference on Power Electronics and Applications (EPE'15 ECCE-Europe)*, Switzerland, Sept 2015, pp. 1–10.

[7] V. Fthenakis and H. C. Kim, "Land use and electricity generation: A life-cycle analysis," *Renewable and Sustainable Energy Reviews*, vol. 13, no. 6, pp. 1465–1474, 2009.

[8] J. Wilkes, J. Moccia, and M. Dragan, "Wind in power: 2011 European statistics," *EWEA, Brussels (BE)*, 2012.

[9] W. D. Musial, R. Sheppard, D. Dolan, and B. Naughton, "Development of offshore wind recommended practice for us waters: Preprint," National Renewable Energy Laboratory (NREL), Golden, CO., Tech. Rep., 2013.

[10] A.-J. Buchner, M. Lohry, L. Martinelli, J. Soria, and A. Smits, "Dynamic stall in vertical axis wind turbines: comparing experiments and computations," *Journal of Wind Engineering and Industrial Aerodynamics*, vol. 146, pp. 163–171, 2015.

[11] H. J. Sutherland, D. E. Berg, and T. D. Ashwill, "A retrospective of vawt technology," *Sandia Report No. SAND2012-0304*, 2012.

[12] N. A. Orlando, M. Liserre, R. A. Mastromauro, and A. Dell'Aquila, "A survey of control issues in PMSG-based small wind-turbine systems," *IEEE Transactions on Industrial Informatics*, vol. 9, no. 3, pp. 1211–1221, Aug 2013.

[13] Y. S. Park, S. M. Jang, M. M. Koo, J. Y. Choi, and S. Y. Sung, "Comparative investigation on integrated system of permanent magnet synchronous generator and power converter based on machine topology for small-scale wind power application," *IEEE Transactions on Magnetics*, vol. 49, no. 7, pp. 3846–3849, July 2013.

[14] A. Orrell, H. Rhoads-Weaver, M. Gagne, K. Sahl, B. Pro, R. Baranowski, L. Flowers, and J. Jenkins, "2012 market report on wind technologies in distributed applications," U.S. Department of Energy, Tech. Rep., 2013.

[15] C. Trust, "Small-scale wind energy: policy insights and practical guidance," Carbon Trust, Tech. Rep., 2008.

[16] Anon, "Solar and wind powered sign lighting," Energy Development Cooperative Ltd., Tech. Rep., 2013.

[17] P. Gipe, "*Wind Energy Basics: A Guide to Home and Community-Scale Wind-Energy Systems*." Chelsea Green Publishing, 2009.

[18] F. Bianchi, H. de Battista, and R. Mantz, *Wind Turbine Control Systems: Principles, Modelling and Gain Scheduling Design*, ser. Advances in Industrial Control. Springer London, 2009.

[19] F. Xu, J. Zhang, and M. Cheng, "Analysis of double objectives control for wind power generation system with frequency separation," in *Electric Utility Deregulation and Restructuring and Power Technologies (DRPT), 2011 4th International Conference on*, July 2011, pp. 1366–1371.

[20] A. Abdelli, “Optimisation multicritère d’une chane éolienne passive,” Ph.D. dissertation, Institut National Polytechnique de Toulouse, 2007.

[21] F. Locment, “Conception et modélisation d’une machine synchrone à 7 phases à aimants permanents et flux axial: commande vectorielle en modes normal et dégradé,” Ph.D. dissertation, Université des Sciences et Technologie de Lille-Lille I, 2006.

[22] R. L. Iglesias, R. L. Arantegui, and M. A. Alonso, “Power electronics evolution in wind turbines a market-based analysis,” *Renewable and Sustainable Energy Reviews*, vol. 15, no. 9, pp. 4982–4993, 2011.

[23] A. Chakraborty, “Advancements in power electronics and drives in interface with growing renewable energy resources,” *Renewable and Sustainable Energy Reviews*, vol. 15, no. 4, pp. 1816 – 1827, 2011.

[24] H. Wang, C. Nayar, J. Su, and M. Ding, “Control and interfacing of a grid-connected small-scale wind turbine generator,” *IEEE Transactions on Energy Conversion*, vol. 26, no. 2, pp. 428–434, June 2011.

[25] J. A. Baroudi, V. Dinavahi, and A. M. Knight, “A review of power converter topologies for wind generators,” *Renewable Energy*, vol. 32, no. 14, pp. 2369 – 2385, 2007.

[26] Z. Chen, J. M. Guerrero, and F. Blaabjerg, “A review of the state of the art of power electronics for wind turbines,” *IEEE Transactions on Power Electronics*, vol. 24, no. 8, pp. 1859–1875, Aug 2009.

[27] J.-C. Wu and Y.-H. Wang, “Power conversion interface for small-capacity wind power generation system,” *IET Generation, Transmission & Distribution*, vol. 8, no. 4, pp. 689–696, 2014.

[28] L. Santos, M. Sechilariu, and F. Locment, “Day-ahead microgrid optimal self-scheduling: Comparison between three methods applied to isolated dc microgrid,” in *IECON 2014 - 40th Annual Conference of the IEEE Industrial Electronics Society*, USA, Oct 2014, pp. 2010–2016.

[29] L. Santos, M. Sechilariu, and F. Locment, “Prediction-based economic dispatch and online optimization for grid-connected dc microgrid,” in *2016 IEEE International Energy Conference (ENERGYCON)*, Belgium, April 2016, pp. 1–6.

[30] L. Santos, M. Sechilariu, and F. Locment, “Prediction-based optimization for islanded microgrid resources scheduling and management,” in *2015 IEEE 24th International Symposium on Industrial Electronics (ISIE)*, Brazil, June 2015, pp. 760–765.

[31] H. Al-Ghossini, H. Liu, F. Locment, and M. Sechilariu, “Estimation of speed rotation for MPPT used by small scale wind generator integrated in dc microgrid experimental validation,” in *IECON 2014 - 40th Annual Conference of the IEEE Industrial Electronics Society*, USA, Oct 2014, pp. 2082–2088.

[32] H. Liu, F. Locment, and M. Sechilariu, “Maximum power point tracking method for small scale wind generator experimental validation,” in *2015 54th Annual Conference of the Society of Instrument and Control Engineers of Japan (SICE)*, China, July 2015, pp. 864–869.

[33] H. Al-Ghossini, F. Locment, and M. Sechilariu, “Experimental comparison of small wind turbine vector control with and without position sensor extended Kalman filter application,” in *2013 15th European Conference on Power Electronics and Applications (EPE)*, France, Sept 2013, pp. 1–9.

[34] A. Urtasun, P. Sanchis, I. San Martn, J. López, and L. Marroyo, “Modeling of small wind turbines based on PMSG with diode bridge for sensorless maximum power tracking,” *Renewable energy*, vol. 55, pp. 138–149, 2013.

[35] M. Abdullah, A. Yatim, C. Tan, and R. Saidur, “A review of maximum power point tracking algorithms for wind energy systems,” *Renewable and Sustainable Energy Reviews*, vol. 16, no. 5, pp. 3220 – 3227, 2012.

[36] M. Pucci and M. Cirrincione, “Neural MPPT control of wind generators with induction machines without speed sensors,” *IEEE Transactions on Industrial Electronics*, vol. 58, no. 1, pp. 37–47, 2011.

[37] R. Kot, M. Rolak, and M. Malinowski, “Comparison of maximum peak power tracking algorithms for a small wind turbine,” *Mathematics and Computers in Simulation*, vol. 91, pp. 29–40, 2013.

[38] Z. M. Dalala, Z. U. Zahid, W. Yu, Y. Cho, and J.-S. J. Lai, “Design and analysis of an MPPT technique for small-scale wind energy conversion systems,” *IEEE Transactions on Energy Conversion*, vol. 28, no. 3, pp. 756–767, 2013.

[39] C.-Y. Lee, P.-H. Chen, and Y.-X. Shen, “Maximum power point tracking (MPPT) system of small wind power generator using RBFNN approach,” *Expert Systems with Applications*, vol. 38, no. 10, pp. 12058–12065, 2011.

[40] K. S. M. Raza, H. Goto, H.-J. Guo, and O. Ichinokura, “A novel speed-sensorless adaptive hill climbing algorithm for fast and efficient maximum power point tracking of wind energy conversion systems,” in *2008 IEEE International Conference on Sustainable Energy Technologies*, Singapore, IEEE, 2008, pp. 628–633.

[41] Q. Wang and L. Chang, “An intelligent maximum power extraction algorithm for inverter-based variable speed wind turbine systems,” *IEEE Transactions on Power Electronics*, vol. 19, no. 5, pp. 1242–1249, Sept 2004.

[42] C. C. Hua, W. T. Chen, and Y. H. Fang, “Design and implementation of digital power converter for wind energy conversion system,” in *2013 1st International Future Energy Electronics Conference (IFEEC)*, Taiwan, Nov 2013, pp. 181–186.

[43] T. L. Tiang and D. Ishak, “Novel MPPT control in permanent magnet synchronous generator system for battery energy storage,” in Applied Mechanics and Materials, vol. 110. Trans Tech Publications, 2012, pp. 5179–5183.

[44] A. Soetedjo, A. Lomi, and W. P. Mulayanto, “Modeling of wind energy system with MPPT control,” in *2011 International Conference on Electrical Engineering and Informatics (ICEEI)*, Indonesia, July 2011, pp. 1–6.

[45] B. Neammanee, S. Sirisumranukul, and S. Chatratana, “Control performance analysis of feedforward and maximum peak power tracking for small-and medium-sized fixed pitch wind turbines,” in *2006 9th International Conference on Control, Automation, Robotics and Vision*, Singapore, Dec 2006, pp. 1–7.

[46] M. Kesraoui, N. Korichi, and A. Belkadi, “Maximum power point tracker of wind energy conversion system,” *Renewable Energy*, vol. 36, no. 10, pp. 2655 – 2662, 2011.

[47] R. M. Linus and P. Damodharan, “Maximum power point tracking method using a modified perturb and observe algorithm for grid connected wind energy conversion systems,” *IET Renewable Power Generation*, vol. 9, no. 6, pp. 682–689, 2015.

[48] K. Vijayakumar, N. Kumaresan, and N. Ammasaigounden, “Speed sensor-less maximum power point tracking and constant output power operation of wind-driven wound rotor induction generators,” *IET Power Electronics*, vol. 8, no. 1, pp. 33–46, 2015.

[49] S. M. R. Kazmi, H. Goto, H. J. Guo, and O. Ichinokura, “A novel algorithm for fast and efficient speed-sensorless maximum power point tracking in wind energy conversion systems,” *IEEE Transactions on Industrial Electronics*, vol. 58, no. 1, pp. 29–36, Jan 2011.

[50] C. T. Pan and Y. L. Juan, “A novel sensorless MPPT controller for a high-efficiency microscale wind power generation system,” *IEEE Transactions on Energy Conversion*, vol. 25, no. 1, pp. 207–216, March 2010.

[51] M.-K. Hong and H.-H. Lee, “*Adaptive Maximum Power Point Tracking Algorithm for Variable Speed Wind Power Systems*.” Berlin, Heidelberg: Springer Berlin Heidelberg, 2010, pp. 380–388.

[52] E. Koutroulis and K. Kalaitzakis, “Design of a maximum power tracking system for wind-energy-conversion applications,” *IEEE Transactions on Industrial Electronics*, vol. 53, no. 2, pp. 486–494, April 2006.

[53] K. S. M. Raza, H. Goto, H.-J. Guo, and O. Ichinokura, “Maximum power point tracking control and voltage regulation of a dc grid-tied wind energy conversion system based on a novel permanent magnet reluctance generator,” in *2007 ICEMS International Conference on Electrical Machines and Systems*, South Korea, Oct 2007, pp. 1533–1538.

[54] M. Narayana, G. Putrus, M. Jovanovic, P. Leung, and S. McDonald, “Generic maximum power point tracking controller for small-scale wind turbines,” *Renewable Energy*, vol. 44, pp. 72 – 79, 2012.

[55] A. I. Putri, M. Ahn, and J. Choi, “Speed sensorless fuzzy MPPT control of grid-connected PMSG for wind power generation,” in *2012 International Conference on Renewable Energy Research and Applications (ICRERA),* Japan, Nov 2012, pp. 1–6.

[56] A. M. Eltamaly and H. M. Farh, “Maximum power extraction from wind energy system based on fuzzy logic control,” *Electric Power Systems Research*, vol. 97, pp. 144 – 150, 2013.

[57] Q.-N. Trinh and H.-H. Lee, “Fuzzy logic controller for maximum power tracking in PMSG-based wind power systems,” in *Advanced Intelligent Computing Theories and Applications. With Aspects of Artificial Intelligence*. Springer, 2010, pp. 543–553.

[58] H. Q. Minh, N. Frédéric, E. Najib, and H. Abdelaziz, “Fuzzy control of variable speed wind turbine using permanent magnet synchronous machine for stand-alone system,” in *Sustainability in Energy and Buildings*. Springer, 2012, pp. 31–44.

[59] I. Houssamo, F. Locment, and M. Sechilariu, “Experimental analysis of impact of MPPT methods on energy efficiency for photovoltaic power systems,” *International Journal of Electrical Power & Energy Systems*, vol. 46, pp. 98–107, 2013.

[60] M. A. Abdullah, A. H. M. Yatim, and C. W. Tan, “A study of maximum power point tracking algorithms for wind energy system,” in *2011 IEEE First Conference on Clean Energy and Technology (CET),* Malaysia, June 2011, pp. 321–326.

[61] M. Pucci and M. Cirrincione, “Neural MPPT control of wind generators with induction machines without speed sensors,” *IEEE Transactions on Industrial Electronics*, vol. 58, no. 1, pp. 37–47, Jan 2011.

[62] S. M. R. Kazmi, H. Goto, H. J. Guo, and O. Ichinokura, “Review and critical analysis of the research papers published till date on maximum power point tracking in wind energy conversion system,” in *2010 IEEE Energy Conversion Congress and Exposition*, USA, Sept 2010, pp. 4075–4082.

[63] A. Urtasun, P. Sanchis, and L. Marroyo, “Small wind turbine sensorless MPPT: robustness analysis and lossless approach,” *IEEE Transactions on Industry Applications*, vol. 50, no. 6, pp. 4113–4121, 2014.

[64] A. B. Cuesta, F. J. Gomez-Gil, J. V. M. Fraile, J. A. Rodrguez, J. R. Calvo, and J. P. Vara, “Feasibility of a simple small wind turbine with variable-speed regulation made of commercial components,” *Énergies*, vol. 6, no. 7, pp. 3373–3391, 2013.

[65] K. N. Yu and C. K. Liao, “Applying novel fractional order incremental conductance algorithm to design and study the maximum power tracking of small wind power systems,” *Journal of applied research and technology*, vol. 13, no. 2, pp. 238–244, 2015.

[66] R. Bharanikumar, A. Yazhini, and A. N. Kumar, “Modeling and simulation of wind turbine driven permanent magnet generator with new MPPT algorithm,” *Asian Power electronics journal*, vol. 4, no. 2, pp. 52–58, 2010.

[67] M. López and J.-C. Vannier, “Stand-alone wind energy conversion system with maximum power transfer control/sistema aislado de conversión eólica con control de máxima transferencia de potencia,” *Ingeniare: Revista Chilena de Ingenieria*, vol. 17, no. 3, p. 329, 2009.

[68] J. S. Thongam and M. Ouhrouche, “*MPPT control methods in wind energy conversion systems*.” INTECH Open Access Publisher, 2011.

[69] C.-M. Hong, C.-H. Chen, and C.-S. Tu, “Maximum power point tracking-based control algorithm for pmsg wind generation system without mechanical sensors,” *Energy conversion and management*, vol. 69, pp. 58–67, 2013.

[70] K. Belmokhtar, M. Doumbia, and K. Agbossou, “Novel fuzzy logic based sensorless maximum power point tracking strategy for wind turbine systems driven DFIG (doubly-fed induction generator),” *Energy*, vol. 76, pp. 679–693, 2014.

[71] H. Zhao, Q. Wu, C. N. Rasmussen, and M. Blanke, “Adaptive speed control of a small wind energy conversion system for maximum power point tracking,” *IEEE Transactions on Energy Conversion*, vol. 29, no. 3, pp. 576–584, 2014.

[72] Z. Qi and E. Lin, “Integrated power control for small wind power system,” *Journal of Power Sources*, vol. 217, pp. 322 – 328, 2012.

[73] Z. M. Dalala, Z. U. Zahid, and J.-S. J. Lai, “New overall control strategy for small-scale WECS in MPPT and stall regions with mode transfer control,” *IEEE Transactions on Energy Conversion*, vol. 28, no. 4, pp. 1082–1092, 2013.

[74] X.-x. Yin, Y.-g. Lin, W. Li, H.-w. Liu, and Y.-j. Gu, “Output power control for hydro-viscous transmission based continuously variable speed wind turbine,” *Renewable Energy*, vol. 72, pp. 395–405, 2014.

[75] J. Chen, J. Chen, C. Gong, and X. Deng, “Energy management and power control for a stand-alone wind energy conversion system,” in *IECON 2012-38th Annual Conference on IEEE Industrial Electronics Society*, Canada, IEEE, 2012, pp. 989–994.

[76] J. Hui, A. Bakhshai, and P. Jain, “Power management supervisory control algorithm for standalone wind energy systems,” in *2014 IEEE 36th International Telecommunications Energy Conference (INTELEC)*, Canada, IEEE, 2014, pp. 1–6.

[77] D.-H. Tran, B. Sareni, X. Roboam, and C. Espanet, “Integrated optimal design of a passive wind turbine system: an experimental validation,” *IEEE Transactions on Sustainable Energy*, vol. 1, no. 1, pp. 48–56, 2010.

[78] M. Mohseni, S. M. Islam, and M. A. Masoum, “Enhanced hysteresis-based current regulators in vector control of DFIG wind turbines,” *IEEE Transactions on Power Electronics*, vol. 26, no. 1, pp. 223–234, 2011.

Appendices

Appendix I: parameters of industrial drive C3S063V2F10 from Parker

Appendix II: parameters of controller board DSPACE DS1103

Appendix III: parameters of PMSM

Appendix IV: parameters of programmable electric load PL-6000-A Puissance+

Appendix V: parameters of the diode bridge SMIKRON SKD 51/14

Appendix VI: parameters of the insulated gate bipolar transistor (IGBT) module SEMIKRON SKM100GB063D

Appendix VII: parameters of industrial driver (SEMIKRON SKHI22A) for IGBT

Appendix I. Parameters of industrial drive C3S063V2F10 from Parker

Common Specifications

Performance	**Torque Loop**	62.5 micro seconds
	Velocity Loop	125 micro seconds
	Position Loop	125 micro seconds
Command Inputs (T10 only)	**Velocity & Torque Mode**	14 bit, ±10 VDC analog
	Position Mode	Step & Direction; 5V or 24 V level (300 kHz input frequency); differential signal
Onboard Digital Inputs	**Type**	Sinking type, 24 V nom. @ 10 mA, high = 9-32 V, low <8 V
	Functions: **Ixx T10 (4 dedicated)** **Ixx T11 (8 dedicated)** **Ixx T30** (1) **Ixx T40** (1)	 Drive stage enable, control input enable, reset, motor brake open/close Motion interrupt, Start, Drive Stage enable + 5 motion profile select inputs (or 4 inputs with a home input) User definable via IEC61131-3 programming environment User definable via IEC61131-3 programming environment
Analog Inputs (T11, T30, T40)		Two (dedicated); 14 bit
Onboard Digital Outputs	**Type**	Sourcing type, rated for 24 V @ 100 mA, short-circuit protected
	Functions: **Ixx T10 (4 dedicated)** **Ixx T11 (4 dedicated)** **Ixx T30** (2) **Ixx T40** (2)	 No fault, drive enabled, in position window, at zero point No fault, position reached, power stage active, at zero point User definable via IEC61131-3 programming environment User definable via IEC61131-3 programming environment
	Encoder	Programmable up to 16,384 ppr (pre-quadrature)
	Relay	Normally closed, dry contact (switching current: 10-300 mA, switching voltage [AC/DC]: 100 mV-60 V)
Analog Outputs (T11, T30, T40)		Two (dedicated); 8 bit; software configurable as monitor outputs
Communi-cations	**Type**	RS232 (3-wire) on RS485 (2- or 4-wire); 8-bit word length, 1 stop bit, no parity
	Baud Rate	Fixed at 115.8 Kbaud for RS232; adjustable for RS485
	Multi-drop (RS485)	Up to 255 nodes
	Profibus (3)	DPV0 supported; selectable Baud rate, 12 Mbd maximum transmission speed
	CANopen (3)	DCiA, DS102 supported; selectable Baud rate, 1 Mbd maximum transmission speed
	DeviceNet (3)	Polled, C05/cyclic I/O and bit strobe; 500 kBit/second max speed
	Ethernet (3)	100 Mbit TCP/IP
	ETHERNET Powerlink (3)	100 Mbits , < 1us jitter, 1 ms cycle timeation
	ETHERCAT (3)	100 Mbits , < 1us jitter, 1 ms cycle timeation
Environmental	**Temperature**	Still air: 33-113°F (0-45°C); moving air: 33-122°F (0-50°C)
	Humidity	0-75%, non-condensing
	IP Class	IP 20
Protection	**Short Circuit**	Phase-to-phase, phase-to-ground
	Brownout	Below 70 VDC
	Over Voltage	Will shut down when power dissipation capacity is exceeded
	Over Temperature	Motor 330°F (170°C), Drive 221°F (105°C)
	I^2t	Error generated if peak current > 3 seconds
	Safety Isolation	VDE0160
Standards		UL, cUL, CE (EMC), CE (LVD)

Compax3 SXXX V2 Specifications		S025 V2	S063 V2	S100 V2	S150 V2
Drive Input Power	Voltage	80 – 253 VAC	80 – 253 VAC	80 – 253 VAC	80 – 253 VAC
	Phase	1Ø	1Ø	3Ø	3Ø
	Frequency	50/60 Hz	50/60 Hz	50/60 Hz	50/60 Hz
	24 VDC Logic Power (Req'd)	24 VDC ±15%	24 VDC ±15%	24 VDC ±15%	24 VDC ±15%
Drive Output Power	PWM (selectable)	16/32 kHz	16/32 kHz	16/32 kHz	8/16/32 kHz
	Continuous Current (RMS)	2.5 Amps	6.3 Amps	10 Amps	15 Amps
	Peak Current (RMS)	5 Amps	12.6 Amps	20 Amps	30 Amps
	Commutation	Sinusoidal	Sinusoidal	Sinusoidal	Sinusoidal
Internal Regeneration Capacities/Storable Energy		560 µF / 15Ws	1120 µF / 30Ws	780 µF / 21Ws	1,170 µF / 31Ws

Appendix II. Parameters of controller board DSPACE DS1103

DS1103 PPC Controller Board

Powerful controller board for rapid control prototyping

Highlights

- Single-board system with real-time processor and comprehensive I/O
- CAN interface and serial interfaces ideally suited to automotive applications
- High I/O speed and accuracy
- PLL-driven UART for accurate baud rate selection

Application Areas

The DS1103 controller board is designed to meet the requirements of modern rapid control prototyping and is highly suitable for applications such as:

- Automotive controllers
- Induction motor control
- Robotics
- Positioning systems and stepper motors
- Active vibration control

An integrated Infineon CAN microcontroller makes the board an attractive tool for automotive and automation applications.

Key Benefits

The DS1103 is an all-rounder in rapid control prototyping. You can mount the board in a dSPACE Expansion Box or dSPACE AutoBox to test your control functions in a laboratory or directly in the vehicle. Its processing power and fast I/O are vital for applications that involve numerous actuators and sensors. Used with Real-Time Interface (RTI, p. 56), the controller board is fully programmable from the Simulink® block diagram environment. You can configure all I/O graphically by using RTI. This is a quick and easy way to implement your control functions on the board.

Comprehensive Interfaces

The unparalleled number of I/O interfaces makes the DS1103 a versatile controller board for numerous applications. It provides a great selection of interfaces, including 50 bit-I/O channels, 36 A/D channels, and 8 D/A channels. For additional I/O tasks, a DSP controller unit built around Texas Instruments' TM320F240 DSP is used as a subsystem.

Recording and Output of I/O Values

The control of electrical drives requires accurate recording and output of I/O values. It is possible to synchronize the A/D channels and D/A channels, and the position of the incremental encoder interface, with an internal PWM signal or an external trigger signal. Also, the serial interface (UART) is driven by a phase-locked loop to achieve absolutely accurate baud rate selection.

Technical Details

Parameter		Specification
Processor	PowerPC Type	■ PPC 750GX
	CPU clock	■ 1 GHz
	Cache	■ 32 KB level 1 (L1) instruction cache ■ 32 KB level 1 (L1) data cache ■ 1 MB level 2 (L2)
	Bus frequency	■ 133 MHz
	Temperature sensor	■ Reads actual temperature at the PPC
Memory	Local memory	■ 32 MB application SDRAM as program memory, cached
	Global memory	■ 96 MB communication SDRAM for data storage and data exchange with host
Timer	2 general-purpose timers	■ One 32-bit down counter ■ Reload by software ■ 15-ns resolution
		■ One 32-bit up counter with compare register ■ Reload by software ■ 30-ns resolution
	1 sampling rate timer (decrementer)	■ 32-bit down counter ■ Reload by software ■ 30-ns resolution
	1 time base counter	■ 64-bit up counter ■ 30-ns resolution
Interrupt controller		■ 3 timer interrupts ■ 7 incremental encoder index line interrupts ■ 1 UART (universal asynchronous receiver and transmitter) interrupt ■ 1 CAN interrupt ■ 1 slave DSP interrupt ■ 2 slave DSP PWM interrupts ■ 1 host interrupt ■ 4 external interrupts (user interrupts)
A/D converter	Channels	■ 16 multiplexed channels equipped with 4 sample & hold A/D converters (4 channels belong to one A/D converter. 4 consecutive samplings are necessary to sample all channels belonging to one A/D converter.) ■ 4 parallel channels each equipped with one sample & hold A/D converter ■ Note: 8 A/D converter channels (4 multiplexed and 4 parallel) can be sampled simultaneously.
	Resolution	■ 16-bit
	Input voltage range	■ ±10 V
	Overvoltage protection	■ ±15 V
	Conversion time	■ Multiplexed channels: 1 µs[1)] ■ Parallel channels: 800 ns[1)]
	Offset error	■ ±5 mV
	Gain error	■ ±0.25%
	Offset drift	■ 40 µV/K
	Gain drift	■ 50 ppm/K
	Signal-to-noise ratio	■ >83 dB
D/A converter	Channels	■ 8 channels
	Resolution	■ 16-bit
	Output range	■ ±10 V
	Settling time	■ 5 µs (14-bit)
	Offset error	■ ±1 mV
	Gain error	■ ±0.5%
	Offset drift	■ 30 µV/K
	Gain drift	■ 25 ppm/K

Parameter		Specification
D/A converter	Signal-to-noise ratio	■ >83 dB
	I_{max}	■ ±5 mA
	C_{Imax}	■ 10 nF
Digital I/O	Channels	■ 32-bit parallel I/O ■ Organized in four 8-bit groups ■ Each 8-bit group can be set to input or output (programmable by software)
	Voltage range	■ TTL input/output levels
	$I_{out, max}$	■ ±10 mA
Digital incremental encoder interface	Channels	■ 6 independent channels ■ Single-ended (TTL) or differential (RS422) input (software programmable for each channel)
	Position counters	■ 24-bit resolution ■ Max. 1.65 MHz input frequency, i.e.,fourfold pulse count up to 6.6 MHz ■ Counter reset or reload via software
	Encoder supply voltage	■ 5 V/1.5 A ■ Shared with analog incremental encoder interface
Analog incremental encoder interface	Channels	■ 1 channel ■ Sinusoidal signals: 1 Vpp differential or 11 µApp differential (software programmable)
	Position counters	■ < 5° resolution ■ 32-bit loadable position counter ■ Max. 0.6 MHz input frequency, i.e., fourfold pulse count up to 2.4 MHz
	A/D converter performance	■ 6-bit resolution ■ 10 MSPS
	Encoder supply voltage	■ 5 V/1.5 A ■ Shared with digital incremental encoder interface
CAN interface	Configuration	■ 1 channel based on SAB 80C164 microcontroller ■ ISO DIS 11898-2 CAN high-speed standard
	Baud rate	■ Max. 1 Mbit/s
Serial interface	Configuration	■ TL6C550C single UART with FIFO ■ PLL-driven UART for accurate baud rate selection ■ RS232/RS422 compatibility
	Baud rate	■ Up to 115.2 kBd (RS232) ■ Up to 1 MBd (RS422)
Slave DSP	Type	■ Texas Instruments TMS320F240 DSP
	Clock rate	■ 20 MHz
	Memory	■ 64 Kx16 external code memory ■ 28 Kx16 external data memory ■ 4 Kx16 dual-port memory for communication ■ 32 KB flash memory
	I/O channels[1)]	■ 16 A/D converter inputs ■ 10 PWM outputs ■ 4 capture inputs ■ 2 serial ports
	Input voltage range	■ TTL input/output level ■ A/D converter inputs: 0 … 5 V
	Output current	■ Max. ±13 mA
Host interface		■ Plug & Play support ■ Requires a full-size 16-bit ISA slot
Physical characteristics	Physical size	■ 340 x 125 x 45 mm (13.4 x 4.9 x 1.77 in)
	Ambient temperature	■ 0 … 50 °C (32 … 122 °F)
	Cooling	■ Passive cooling
	Power supply	■ +5 V ±5%, 4 A ■ +12 V ±5%, 0.75A ■ -12 V ±5%, 0.25A

Order Information

Product	Order Number
DS1103 PPC Controller Board	■ DS1103

Relevant Software and Hardware

Software		Order Number
Included	■ DS1103 Real-Time Library	–
	■ Experiment and Platform Manager for hardware management	–
Required	■ Real-Time Interface (RTI) (p. 56)	■ RTI
	■ Microtec C Compiler for PowerPC (p. 94)	■ CCPPPC
Optional	■ Real-Time Interface CAN Blockset (p. 68)	■ RTICAN_BS
	■ Real-Time Interface CAN MultiMessage Blockset (p. 70)	■ RTICANMM_BS
	■ ControlDesk® Next Generation (p. 102)	See p. 102
	■ Platform API Package (p. 168)	■ PLATFORM_API
	■ MotionDesk (p. 134)	■ MotionDesk

Hardware		Order Number
Optional	■ Connector Panel (p. 326)	■ CP1103
	■ Connector/LED Combi Panel (p. 326)	■ CLP1103
	■ Set of adapter cables for DS1103	■ ADP_CAB1103

Appendix III. Parameters of PMSM

BRUSHLESS MOTORS
NX430EAJ
ELECTRONIC DRIVE (1)
DIGIVEX 7.5/15 et DIGIVEX 8/16
(230 V) (400 V)

PARVEX SSD DRIVES

Torque at low speed	M_o	Nm		5.5	
Permanent current at low speed	I_o	A_{rms}		5.24	
Peak torque	M_p	Nm		18.8	
Current for the peak torque	I_p	A_{rms}		21	
Back emf constant at 1000 rpm (25°C)*	Ke	V_{rms}		65.6	
Torque sensitivity	Kt	Nm/A_{rms}		1.05	
Winding resistance (25°C)*	Rb	Ω		2.33	
Winding inductance*	L	mH		10.9	
Rotor inertia	J	kgm^2x10^{-5}		42.6	
Thermal time constant	Tth	min		18	
Motor mass	M	kg		4.8	
Voltage of the mains	UR1 UR2 UR3	V_{rms}	230	400	480
Rated speed	Nn1 Nn2 Nn3	rpm	3200	5500	6200
Rated torque	Mn1 Mn2 Mn3	Nm	4.68	3.35	2.82
Rated current	In1 In2 In3	A_{rms}	4.53	3.31	2.83
Rated power	Pn1 Pn2 Pn3	W	1570	1930	1830

All data are given in typical values under standard conditions

** Phase to phase* *(1) Please check the availability of this drive with 480 V*

Voltages and currents are given in rms values

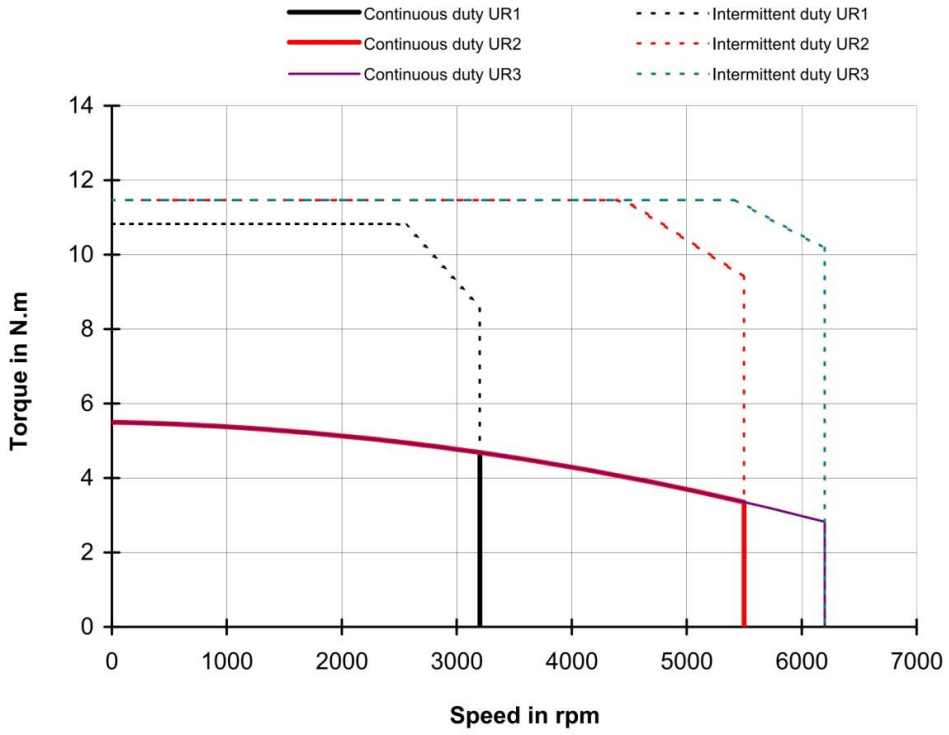

Characteristics are given for an optimal drive of the motor FICHE-009

Création: 11 mai 2000	Edition:	10/févr/2005	NX430EAJ	. -

Appendix IV. Parameters of programmable electric load PL-6000-A Puissance+

GENERAL SPECIFICATIONS:

INPUT RATING

Voltage range:	230V+6%/-10%
Frequency range:	47-65Hz

PROGRAMMATION VALUE

Voltage accuracy:	0.05%FS+0.05%V
Voltage resolution:	12 bits
Current accuracy:	0.01%FS+0.01%V
Current resolution:	12 bits
Power accuracy:	0.05%FS+0.05%V
Power resolution:	12 bits

REGULATION

Voltage line regulation:	0.01%
Voltage load regulation:	0.05%
Current line regulation:	0.1%
Current load regulation:	0.05%
Power line regulation:	0.5%
Power load regulation:	0.1%
Sense:	2V

DYNAMIC MODE

Bandwidth:	2kHz
Rise & fall time:	<20µs
Overshoot:	<5%
Recovery time:	<20 µs

SIGNAL QUALITY

Voltage Ripple & Noise (rms)	0.2%
Voltage Ripple & Noise (Pk-Pk)	2%
Current Ripple & Noise (rms)	0.2%
Current Ripple & Noise (Pk-Pk)	2%

MEASUREMENT

Voltage accuracy:	0.1%FS
Current accuracy:	0.1%FS

PROTECTION

Over voltage/Over current/Over temperature/Reverse current

ISOLATION

Line/output:	100 MΩ @ 500Vdc
Output to case:	10 MΩ @ 500Vdc

DIELECTRIC

Line to output:	2500Veff-50Hz
Line to case:	1500Veff

ENVIRONMENT

Operating temperature:	-10°C/40°C
Storage temperature:	-25°C/80°C
Humidity:	10-90%
Protection:	IP30

CONFORMITY

CE

STANDARD REMOTE CONTROL

HMI:	touchscreen display Waveform storage
ANALOG	
ETHERNET	
RS232	

OPTION

Power analyzer	POW-ANA-PL
Specific range	SR-PL
Double range	DR-PSA
10kHz bandwidth	WBW-PL
Control Resistance	CR-PL
IEEE remote control	IEEE
Last configuration data save	MEM
MASTER configuration	PSAM
SLAVE configuration	PSAS

SOFTWARE option

Arbitrary function generator	OPS1
Advanced Sequence	OPS4
MPP tracking	MPP

Appendix V. Parameters of the diode bridge SMIKRON SKD 51/14

SKD 51

V_{RSM} V	V_{RRM}, V_{DRM} V	I_D = 50[1] A (full conduction) (T_c = 127 °C)
500	400	SKD 51/04
900	800	SKD 51/08
1300	1200	SKD 51/12
1500	1400	SKD 51/14
1700	1600	SKD 51/16
1900	1800	SKD 51/18

Power Bridge Rectifiers

SKD 51

Features

- Glass passivated silicon chips
- Fast-on terminals for pcb solder or plug on connections
- Sturdy insulated metal base plate
- Low thermal impedance through use of direct copper bonded aluminum substrate
- Blocking voltage up to 1800V
- High surge currents
- UL recognized, file no. E63 532

Typical Applications*

- Three phase rectifier for power supplies
- Input rectifier for variable frequency drives
- Rectifier for DC motor field supplies
- Battery charger rectifiers
- Recommended snubber network: RC: 0.1 µF, 50 Ω (P_R = 1 W)

1) For solder connection. Permissible current for plug connection see DIN IEC 760E and DIN 46249 part 1
2) Freely suspended or mounted on an insulator
3) Mounted on a painted metal sheet of min. 250 x 250 x 1 mm

Symbol	Conditions	Values	Units
I_D	T_c = 127 °C	50	A
	T_a = 45 °C; isolated [2]	7	A
	T_a = 45 °C; chassis [3]	18	A
	T_a = 45 °C; R4A/120	27	A
	T_a = 45 °C; P5A/100	31	A
I_{FSM}	T_{vj} = 25 °C; 10 ms	775	A
	T_{vj} = 150 °C; 10 ms	700	A
i^2t	T_{vj} = 25 °C; 8,3 ... 10 ms	3000	A^2s
	T_{vj} = 150 °C; 8,3 ... 10 ms	2450	A^2s
V_F	T_{vj} = 25 °C; I_F = 75 A	max. 1,45	V
$V_{(TO)}$	T_{vj} = 150 °C	max. 0,8	V
r_T	T_{vj} = 150 °C	max. 8,5	mΩ
I_{RD}	T_{vj} = 25 °C; V_{DD} = V_{DRM}; V_{RD} = V_{RRM}	max. 0,2	mA
	T_{vj} = 150 °C; V_{RD} = V_{RRM}	4	mA
t_{rr}	T_{vj} = 25 °C; I_F = I_R = 1A	5	µs
$R_{th(j-c)}$	per diode	1,1	K/W
	total	0,183	K/W
$R_{th(c-s)}$	total	0,1	K/W
$R_{th(j-a)}$	isolated [2] (chassis [3])	9 (3,15)	K/W
T_{vj}		- 40 ... +150	°C
T_{stg}		- 40 ... +125	°C
V_{isol}	a. c. 50 Hz; r.m.s.; 1 s / 1 min.	3600 (3000)	V
M_s	to heatsink	4,5 ± 15 %	Nm
M_t			
m		97	g
Case		G 51	

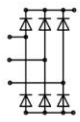

SKD

Appendix VI. Parameters of the insulated gate bipolar transistor (IGBT) module SEMIKRON SKM100GB063D

SKM 100GB063D

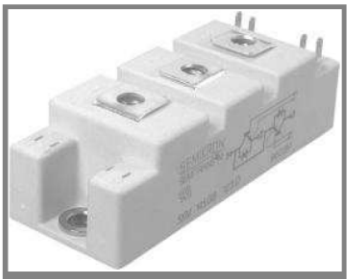

SEMITRANS® 2

Superfast NPT-IGBT Module

SKM 100GB063D

Features

- N channel, homogeneous Silicon structure (NPT- Non punch through IGBT)
- Low tail current with low temperature dependence
- High short circuit capability, self limiting if term. G is clamped to E
- Pos. temp.-coeff. of V_{CEsat}
- Very low C_{ies}, C_{oes}, C_{res}
- Latch-up free
- Fast & soft inverse CAL diodes
- Isolated copper Bonding Technology without hard mould
- Large clearance (10 mm) and creepage distances (20 mm)

Typical Applications*

- Switching (not for linear use)
- Switched mode power supplies
- UPS
- Three phase inverters for servo / AC motor speed control
- Pulse frequencies also above 10 kHz

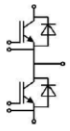

GB

Absolute Maximum Ratings T_c = 25 °C, unless otherwise specified

Symbol	Conditions		Values	Units
IGBT				
V_{CES}	T_j = 25 °C		600	V
I_C	T_j = 150 °C	T_{case} = 25 °C	130	A
		T_{case} = 70 °C	100	A
I_{CRM}	I_{CRM}=2xI_{Cnom}		200	A
V_{GES}			± 20	V
t_{psc}	V_{CC} = 300 V; $V_{GE} \leq$ 20 V; V_{CES} < 600 V	T_j = 125 °C	10	µs
Inverse Diode				
I_F	T_j = 150 °C	T_{case} = 25 °C	100	A
		T_{case} = 80 °C	75	A
I_{FRM}	I_{FRM}=2xI_{Fnom}		200	A
I_{FSM}	t_p = 10 ms; sin.	T_j = 150 °C	720	A
Module				
$I_{t(RMS)}$			200	A
T_{vj}			- 40 ... + 150	°C
V_{isol}	AC, 1 min.		2500	V

Characteristics T_c = 25 °C, unless otherwise specified

Symbol	Conditions		min.	typ.	max.	Units
IGBT						
$V_{GE(th)}$	V_{GE} = V_{CE}, I_C = 2 mA		4,5	5,5	6,5	V
I_{CES}	V_{GE} = 0 V, V_{CE} = V_{CES}	T_j = 25 °C		0,1	0,3	mA
V_{CE0}		T_j = 25 °C		1,05		V
		T_j = 125 °C		1		V
r_{CE}	V_{GE} = 15 V	T_j = 25°C		10,5		mΩ
		T_j = 125°C		14		mΩ
$V_{CE(sat)}$	I_{Cnom} = 100 A, V_{GE} = 15 V	T_j = 25°C$_{chiplev.}$		2,1	2,5	V
		T_j = 125°C$_{chiplev.}$		2,4	2,8	V
C_{ies}	V_{CE} = 25, V_{GE} = 0 V	f = 1 MHz		5,6		nF
C_{oes}				0,6		nF
C_{res}				0,4		nF
Q_G	V_{GE} = 0V - +15V			240		nC
R_{Gint}	T_j = °C			0		Ω
$t_{d(on)}$	R_{Gon} = 10 Ω	V_{CC} = 300V		50		ns
t_r		I_C= 100A		40		ns
E_{on}		T_j = 125 °C		4		mJ
$t_{d(off)}$	R_{Goff} = 10 Ω	V_{GE} = ±15 V		300		ns
t_f				35		ns
E_{off}				3		mJ
$R_{th(j-c)}$	per IGBT				0,27	K/W

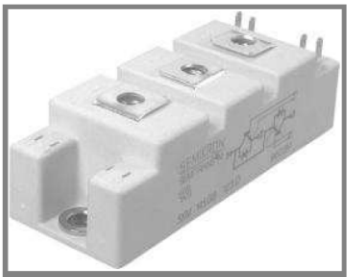

SEMITRANS® 2

Superfast NPT-IGBT Module

SKM 100GB063D

Characteristics

Symbol	Conditions		min.	typ.	max.	Units
Inverse Diode						
$V_F = V_{EC}$	I_{Fnom} = 100 A; V_{GE} = 0 V	T_j = 25 °$C_{chiplev.}$		1,55	1,9	V
		T_j = 125 °$C_{chiplev.}$		1,55		V
V_{F0}		T_j = 125 °C			0,9	V
r_F		T_j = 125 °C		8	10	mΩ
I_{RRM}	I_F = 100 A	T_j = 125 °C		44		A
Q_{rr}				6		µC
E_{rr}	V_{GE} = -15 V; V_{CC} = 300 V					mJ
$R_{th(j-c)D}$	per diode				0,6	K/W
Module						
L_{CE}					30	nH
$R_{CC'+EE'}$	res., terminal-chip	T_{case}= 25 °C		0,75		mΩ
		T_{case}= 125 °C		1		mΩ
$R_{th(c-s)}$	per module				0,05	K/W
M_s	to heat sink M6		3		5	Nm
M_t	to terminals M5		2,5		5	Nm
w					160	g

Appendix VII. Parameters of the industrial driver SEMIKRON SKHI22A for IGBT

SKHI 22 A / B (R) ...

SEMIDRIVER™

Hybrid Dual IGBT Driver

SKHI 22 A / B (R)

Features

- Double driver for halfbridge IGBT modules
- SKHI 22A is compatible to old SKHI 22
- SKHI 22B has additional functionality
- CMOS compatible inputs
- Short circuit potection by V_{CE} monitoring and switch off
- Drive interlock top / bottom
- Isolation by transformers
- Supply undervotage protection (13 V)
- Error latch / output

Typical Applications

- Driver for IGBT modules in bridge circuits in industrial applications

1) see fig. 6

2) At R_{CE} = 18 kΩ, C_{CE} = 330 pF

Absolute Maximum Ratings

Symbol	Conditions	Values	Units
V_S	Supply voltage prim.	18	V
V_{iH}	Input signal volt. (High) SKHI 22A	V_S + 0,3	V
	SKHI 22B	5 + 0,3	V
$Iout_{PEAK}$	Output peak current	8	A
$Iout_{AVmax}$	Output average current	40	mA
f_{max}	max. switching frequency	50	kHz
V_{CE}	Collector emitter voltage sense across the IGBT	1200	V
dv/dt	Rate of rise and fall of voltage secondary to primary side	50	kV/µs
V_{isolIO}	Isolation test voltage input - output (2 sec. AC)	2500	Vac
V_{isol12}	Isolation test voltage output 1 - output 2 (2 sec. AC)	1500	V
R_{Gonmin}	Minimum rating for R_{Gon}	3	Ω
$R_{Goffmin}$	Minimum rating for R_{Goff}	3	Ω
$Q_{out/pulse}$	Max. rating for output charge per pulse	4[1)]	µC
T_{op}	Operating temperature	- 40 ... + 85	°C
T_{stg}	Storage temperature	- 40 ... + 85	°C

Characteristics T_a = 25 °C, unless otherwise specified

Symbol	Conditions	min.	typ.	max.	Units
V_S	Supply voltage primary side	14,4	15	15,6	V
I_{SO}	Supply current primary side (no load)		80		mA
	Supply current primary side (max.)			290	mA
V_i	Input signal voltage SKHI 22A on/off		15 / 0		V
	SKHI 22B on/off		5 / 0		V
V_{IT+}	Input threshold voltage (High) SKHI 22A			12,5	V
	SKHI 22B			3,9	V
V_{IT-}	Input threshold voltage (Low) SKHI 22A	4,5			V
	SKHI 22B	1,5			V
R_{in}	Input resistance SKHI 22A		10		kΩ
	SKHI 22B		3,3		kΩ
$V_{G(on)}$	Turn on gate voltage output		+ 15		V
$V_{G(off)}$	Turn off gate voltage output		- 7		V
R_{GE}	Internal gate-emitter resistance		22		kΩ
f_{ASIC}	Asic system switching frequency		8		MHz
$t_{d(on)IO}$	Input-output turn-on propagation time	0,85	1	1,15	µs
$t_{d(off)IO}$	Input-output turn-off propagation time	0,85	1	1,15	µs
$t_{d(err)}$	Error input-output propagation time		0,6		µs
$t_{pERRRESET}$	Error reset time		9		µs
t_{TD}	Top-Bot Interlock Dead Time SKHI 22A		4,3		µs
	SKHI 22B	no interlock		4,7	µs
V_{CEsat}	Reference voltage for V_{CE}-monitoring		5[2)]	10	V
C_{ps}	Coupling capacitance primary secondary		12		pF
MTBF	Mean Time Between Failure T_a = 40°C		2,0		10^6 h
w	weight		45		g